

**This dissertation has been
microfilmed exactly as received 67-9487**

**GOLDMAN, Michael Arthur, 1937-
LUMINOSITY DECAY ALONG A GAS FOCUSED
ELECTRON BEAM.**

**The University of Oklahoma, Ph.D., 1967
Physics, electronics and electricity**

University Microfilms, Inc., Ann Arbor, Michigan

THE UNIVERSITY OF OKLAHOMA

GRADUATE COLLEGE

LUMINOSITY DECAY ALONG A GAS FOCUSED
ELECTRON BEAM

A DISSERTATION

SUBMITTED TO THE GRADUATE FACULTY

in partial fulfillment of the requirements for the
degree of
DOCTOR OF PHILOSOPHY

BY

MICHAEL ARTHUR GOLDMAN

Norman, Oklahoma

1967

LUMINOSITY DECAY ALONG A GAS FOCUSED
ELECTRON BEAM

APPROVED BY

R. B. Fowler

Chun C. Li

R. B. Hara

Robert M. St. John

Sybrand Moorme

DISSERTATION COMMITTEE

ACKNOWLEDGEMENTS

The author wishes to express his appreciation to Professor Richard G. Fowler for suggesting the present research problem and for guiding the research investigation.

Thanks are due to Dr. Sidney J. B. Corrigan, Dr. Robert M. St. John and Dr. Chun C. Lin for the loan of electronic instruments used in the investigation.

The author wishes to acknowledge the fine work of Rev. Norman Alexandre in constructing the glass vacuum system and electron gun envelope used in the experiment.

Thanks are due to instrument makers James Hood and John Edmondson for machining electron gun structures and auxillary apparatus and to Mr. Gary E. Copeland for assistance in taking of data.

I wish to thank my parents, Mr. and Mrs. Harry M. Goldman for their encouragement and counsel during the work.

TABLE OF CONTENTS

	Page
LIST OF FIGURES	iv
LIST OF TABLES.	v
LIST OF SYMBOLS	vi
CHAPTER	
I. INTRODUCTION.	1
II. APPARATUS	19
III. EXPERIMENTAL OBSERVATIONS	41
IV. DISCUSSION OF OBSERVATIONS, CONCLUSIONS	74
APPENDICES.	83
LIST OF REFERENCES.	98

LIST OF FIGURES

Figure	Page
1. Diagram of Experiment	20
2.1-2.2 The Collision Tube	21,22
3. Anode-Cathode Assembly.	23
4. Vacuum System of Experiment	26
5. Collision Tube Circuit.	27
6. Optical Detection System.	30
7. Photomultiplier Connections	31
8. Photodiode Trigger for Signal Averaging Computer.	36
9. Tuned Amplifier Output Versus Electrometer Output	38
10.1-10.3 Unfiltered Light Intensity Near Beam Entrance into the Drift Tube Versus Beam Potential.	43-45
11.1-11.9 Light Intensity Versus Distance Along the Beam.	51-59
12. Luminosity Decay Cross Section in Helium Versus Beam Energy	60
13. Luminosity Decay Cross Section in Neon Versus Beam Energy	61
14. The Electron Beam in Neon	62

Figure	Page
15.1-15.6 Luminosity Decay of Spectral Lines in Helium.	63-68
16.1-16.5 Luminosity in Mercury Versus Distance	69-73
17. Equivalent Circuit of the VTE-2 Electrometer.	91
18. Chopper Modulated Signal.	92

LIST OF TABLES

Table	Page
I. Positive Real Solutions of $y^3 + 2y^2 + y - z = 0$	85
II. Transverse Potentials Across the Beam, Calculated from the Theory of Frenkel and Bobkovsky	86
III. Intensity Versus Distance Along the Beam, Data.	94

LIST OF SYMBOLS

- A = target gas atomic weight,
- A_{ij} = Einstein coefficient for spontaneous emission of radiation from state i to state j of emitting atom,
- $A_j = \sum_{\substack{k \\ E_j > E_k}} A_{jk}$,
- e = electronic charge,
- $e\phi$ = kinetic energy of injected beam electron,
- J = electron beam current density at beam entry,
- I = electron beam current,
- $i, j, k =$ indices labelling atomic states of target gas,
- $I_{jk}(x) =$ power radiated per unit volume of gas located at position x along the beam, in a transition from state j to state k of gas atom,
- $P_{jk} =$ power radiated by the beam, as a whole, in the transition between atomic states j and k ,
- $n(x) =$ concentration, number per unit volume, of primary beam electrons at distance x along the beam,
- $n_0 = n(x = 0)$,
- $N =$ number of ground state gas atoms per unit volume,
- $Q_j(v) =$ atom cross section for excitation of gas atom from the ground state to state j , by collision with an electron of speed v ,
- $Q(v) = \sum_j Q_j(v)$, excitation cross section of gas atom,
- $L = [N Q(v)]^{-1}$

$Q_I(v)$ = cross section for ionization of gas by an electron of speed v ,
 θ = angle to beam axis at which a scattered electron is assumed to move,
 P = pressure of gas,
 T = temperature of gas,
 x = coordinate of longitudinal position along the beam, electrons enter the drift tube at $x = 0$,
 r = radial cylindrical coordinate of distance from the beam axis,
 $\rho(x)$ = space charge density within luminosity radius of beam,
 $\rho_-(x)$ = magnitude of negative space charge density due to primary beam electrons,
 R = radius of visible luminosity of beam,
 cR = inside radius of drift tube containing beam,
 S = chopping wheel period,
 $S(x)$ = peak to peak output voltage of signal averaging computer,
 t = signal integrating time of signal averaging computer,
 t_N = noise integrating time of signal averaging computer,
 $U_{jk}(x)$ = detected optical signal from beam, per unit current, corrected for noise,
 ν = number of ions produced per second by a primary beam electron,
 V = transverse potential across the luminosity radius of the beam,
 V_w = maximum estimated potential difference between beam and wall of drift tube,
 Z = peak to peak noise voltage output of signal averaging computer,
 i_b = electron beam current (reference to Figure 17),
 i_m = electrometer panel meter current (reference to Figure 17),
 R_{in}, R_m = internal resistors in electrometer (reference to Figure 17).

LUMINOSITY DECAY ALONG A GAS FOCUSED
ELECTRON BEAM

CHAPTER I
INTRODUCTION

The subject of investigation of this study is the visible radiation produced along the length of an electron beam projected into an atomic gas or vapor. Radiation of individual spectral transitions and also broadband visible radiation is measured as a function of beam energy and gas density at varying positions along the beam. Information obtained about radiation intensity along the beam is used to test measurements by Koppius and Duffendack^{1,2} and Fowler^{3,4,5} of cross sections for the process of atomic elation by monoenergetic electrons. The primary objective of the present study was to test the assumptions of the density saturation method of measuring total cross sections for atomic elation by electrons, as developed by Koppius and Duffendack and Fowler. Fowler defines elation as production of ionization or atomic excitation by inelastic electron collisions of the first kind. The testing is done by using an experimental procedure complementary to the density saturation method. Total elation cross sections taken together with information available on cross sections for detailed excitation and ionization processes would provide information about the relative size contributions

to the process of atomic excitation by low energy electrons due to excitation of low lying energy states and of high lying states near the ionization energy. A secondary objective of the study was an examination of the mechanisms responsible for the gas focusing of low energy electron beams.

The density saturation method of studying elation cross sections, as employed by Koppius in a study of radiation from mercury, consisted of his measuring spectral intensities emitted throughout the volume of a discharge tube excited by an electron stream issuing from a thermionically emitting cathode to a planar anode. Light intensity emitted in individual ultraviolet transitions from the 6^3P state of mercury was measured as a function of mercury vapor density in the discharge tube. The electron energy employed was 30 electron volts, the anode-to-cathode spacing was 3 centimeters, vapor pressures were between .2 and 3.6 millitorr, corresponding to vapor temperatures from 0°C to 34°C . Under the assumption that energetic 30 volt electrons could have no more than one inelastic collision of the first kind in passage across the discharge tube, Koppius was able to fit his experimental data to a curve of the form,

$$W_{jk} = cI[1 - \exp(-QNd)] \quad (1.1)$$

where

W_{jk} is the intensity of a given atomic transition, between states j and k , due to emission throughout the entire space between cathode and anode,

I is the beam current,

N is the gas atom concentration,

d is the emitting beam path length,

Q is the elation cross section, that is the cross section for all excitation and ionization processes of the first kind,

c is a constant which depends upon the transition observed.

The observed elation section was of the order $150 \times 10^{-16} \text{ cm}^2$.

A theory of the radiative processes along an initially mono-energetic electron beam travelling along a linear path, whose electrons are capable of having only a single inelastic collision has been given by Fowler⁴. Fowler indicates that the first primary component of the beam, that is those electrons having the full energy at which they entered the beam, decays along the beam being degraded to lower energy secondary electrons not having inelastic collisions. The primary current density, J_p , decays as

$$J_p = J \exp(-NQx) \quad (1.2)$$

and the power radiated per unit volume in a transition between states j and k of the gas atoms is given by the relation

$$I_{jk}(x) = F_{jk} h\nu_{jk} Q_j \frac{J}{e} N \exp(-NQx) \quad (1.3)$$

where J is the current density at beam entrance, F_{jk} depends upon the spontaneous emission coefficients of the radiating gas,⁴ $h\nu_{jk}$ is the energy quantum of the transition, e is the electronic charge, Q_j is the cross section for excitation of state j from the ground state and x is

the distance along the beam measured from beam entry into the gas. The radiated power is, integrated over the entire beam length d ,

$$P_{jk} = F_{jk} h\nu_{jk} \frac{Q_j I}{Q_e} [1 - \exp(-NQd)] \quad . \quad (1.4)$$

The theory assumes that elastic scatter does not cause loss of beam electrons. At $x = 0$,

$$I_{jk}(x = 0) = F_{jk} h\nu_{jk} Q_j \frac{JN}{e} \quad (1.5)$$

and the emitted power per unit volume in the transition from state j to state k is proportional to the cross section for excitation of state j from the ground state of the atom, appropriate to the energy of the beam electrons entering the gas.

In Koppius' experiment the claim is made that the radiation observed is due to single collisions of monenergetic electrons. The energy at which the experiment was conducted was sufficiently large however, to allow multiple inelastic collisions of a single electron to occur, an energy of 30 electron volts. At the higher vapor densities employed in Koppius' experiment the data presented of light intensity versus mercury vapor pressure lead to a mean free path for elation of approximately one fifth of the cathode-to-anode spacing of the experiment tube. Thus it would be expected a-priori that multiple inelastic collisions would occur during an electron's passage across the tube, based upon the energy available to the primary electrons. By a probe analysis of the electron energy distribution,

Koppius concluded that stage exciting or ionizing collisions did not, in fact, occur. The measured elation cross section was, however, several times larger than the total collision cross section of mercury as measured by Brode and other experimenters.⁶

For 70 volt primary electrons in helium, Fowler claims an elation cross section of $8 \times 10^{-17} \text{ cm}^2$. Fowler claimed that there is little or no reason to believe that elastic scattering of electrons contributes to the size of the cross sections measured by the density saturation method. This is not entirely clear in Koppius' experiment. In that experiment a planar diode geometry was used; electrons were accelerated from a filament to a plane anode three centimeters distant. A 30 volt electron scattered elastically from the electron stream at large angles might be lost at the walls of the container bounding the stream without causing radiative collisions. In Fowler's experiment an annular cylindrical geometry was used, the cathode and anode being concentric cylinders. The saturation light intensity was not sensitive to the length of electron trajectory in the collision space and the light intensity was independent of the elastic scattering at gas pressure sufficiently low that the elastic scattering mean free path is large compared to the cathode-to-anode spacing. In the annular geometry an elastically scattered electron had a small solid angle to escape from the collision region to the end walls of the cylinder. An elation cross section was derived from the low pressure and high pressure saturation light intensities independent of the elastic scatter cross section.

The motivation for the present experiment was a desire to test the assumptions of the density saturation theory, in particular equation (1.3), for a linear beam of electrons of energy sufficiently low that an electron was capable of experiencing no more than one inelastic collision which could produce radiation in the spectral range to be observed.

In helium and neon, electrons having energy less than two times the lowest excitation energy of the gas can have only single inelastic collisions. To obtain a collimated beam it was thought desirable that the primary electron energy be greater than the ionization energy of the gas. The ionization potential of mercury is greater than twice its lowest excitation potential, but equation (1.3) may be tested in a limited energy range above the ionization energy provided visible region spectral transitions are observed. The ionization potential of mercury is 10.4 volts, the lowest excitation potential is 4.66 volts, visible spectral transitions originate on levels at or above 7.69 volts. Thus an electron possessing between 10.4 and 12.4 electron volts energy is capable of having no more than one inelastic collision which produces visible radiation.

The assumptions of the density saturation theory indicate that the number of fast primary electrons and the optical power emitted per length of beam for all optical transitions decay exponentially with length along the beam and furthermore have the same characteristic decay length. The characteristic decay length is allegedly inversely proportional to the elation cross section of the target gas atoms.

The means chosen to test equation (1.3) is to measure luminosity of selected spectral transitions as a function of electron energy and of distance along the length of a narrow, well collimated low energy electron beam at low target gas pressures. If equation (1.3) is valid in its implications, one expects a common exponential decay for the observed spectral lines in the beam energy range between gas ionization energy and twice the lowest excitation energy in the gases neon and helium.

Effect of Cascade Processes On Expected Luminosity Decay. Decay to be Expected Along the Beam in the Absence of Large Angle Elastic Scatter and Convective Transport of Excitation

In the following section an electron having initial beam energy will be referred to as a primary electron, an electron having had exactly one inelastic collision will be referred to as a secondary electron, an electron having had more than one inelastic collision but also having energy sufficient to experience another inelastic collision will be referred to as a tertiary electron and an electron of energy insufficient to cause inelastic collisions will be referred to as an ultimate electron.

In the following analysis it will be tentatively assumed that primary electron loss due to large angle scatter from the beam is negligible and the elastic scatter of the primary electrons is mainly at small angles to the beam direction. In practice, at the pressures and currents employed in the experiment, a net positive space charge along the beam

will hold the electrons, elastically scattered at small angles to the beam, along the beam. This will be discussed at length later in the chapter. The pressures at which the experiment are run are chosen so that the mean free paths of the primary electrons for elastic scatter are of order of the optically scanned length of electron beam, the paths being estimated from total collision cross sections determined from Ramsauer type experiments.^{7,8} Transfer of excited state atoms longitudinally along the beam will be assumed small, luminosity of individual atoms in excited states decaying within a few beam widths of the point of excitation. Longitudinal transfer of atomic excitation by diffusion of radiation along the beam is assumed small. The beam current is steady, the radiated power is independent of time. Let

x = coordinate of position along the beam,

$n(x)$ = number concentration of primary electrons per unit volume at position x along the beam,

n_0 = $n(x = 0)$, the primary electron concentration at beam entry,

N = number concentration of neutral gas atoms per unit volume,

v = speed of primary electrons,

A_{ij} = Einstein coefficient for spontaneous emission of radiation in a transition between states i and j of a target gas atom,

A_j = $\sum_k A_{jk}$, sum of Einstein coefficients for transitions starting at state j and ending on states of lower energy,

$Q_j(v)$ = cross section for elation of a gas atom from the ground state to state j by collision with an electron of speed v ,

$$1/L = N \sum_{\substack{j \\ E_j > 0}} Q_j(v) = N Q$$

Assuming loss of primary electrons by inelastic collision only, the convective loss of primary electrons is

$$v \frac{dn}{dx} = - \sum_j N n v Q_j(v) \quad (2.1)$$

with initial condition $n(x=0) = n_0$ and solution

$$n = n_0 \exp(-x/L) \quad (2.2)$$

The time rate of change of population density of excited radiative states due to direct electronic excitation, de-excitation by radiation and cascading is,

$$\frac{\partial n_j}{\partial t} = -A_j n_j + \sum_{\substack{i \\ E_i > E_j}} A_{ij} n_i + N Q_j(v) n v \quad (2.3)$$

+ contributions to excitation by inelastic collisions of secondary and tertiary electrons.

The contribution by secondary and tertiary electrons vanishes if the primary electron energy is less than twice the first excitation energy of the gas. Electron collisions with excited atoms are assumed improbable. If such collisions occurred they would be detected by a quadratic dependence of spectral line intensity with beam current.

Under steady state conditions, $\partial n_j / \partial t = 0$ and if the primary electron energy is less than twice the lowest excitation energy,

$$A_j n_j - \sum_{\substack{i \\ (i,j \text{ radiative}) \\ E_i > E_j}} A_{ij} n_i = n N v Q_j(v) \quad . \quad (2.4)$$

Equation (2.4) may be written in matrix notation as

$$[H_{ji}] \left[\frac{n_i(x)}{n(x)} \right] = N v [Q_j(v)] \quad (2.5)$$

where $\left[\frac{n_i(x)}{n(x)} \right]$ and $[Q_j(v)]$ are column matrices and $[H_{ji}]$ is an upper triangular matrix with positive diagonal elements, A_j . The coefficients in the set of linear equations for $n_i(x)/n(x)$ are position independent and the $Q_j(v)$ are position independent. A unique solution is expected which is linear in the $Q_j(v)$ and vanishes only when all $Q_j(v)$ vanish. Nominally the number of radiative states is infinite, but is actually some large finite number argues Fowler.³ Under the assumption that the system of equations (2.5) truncates, the matrix $[H_{ji}]$ is invertible and

$$\left[\frac{n_i(x)}{n(x)} \right] = N v [G_{ij}] [Q_j(v)] \quad (2.6)$$

where the matrix $[G_{ij}]$ is the inverse of the H matrix and depends upon the radiative emission coefficients of the gas atoms and not on position.

Thus,

$$n_i(x) = n_0 N v \exp(-x/L) \sum_j G_{ij} Q_j(v) \quad (2.7)$$

(i,j radiative states)

and

$$I_{jk}(x) = A_{jk} h\nu_{jk} \frac{J}{e} N \exp(-x/L) \sum_i G_{ji} Q_i(v) \quad (2.8)$$

(i,j radiative)

and cascading from higher states is expected to change neither the exponential decay of luminosity nor to change the common decay length of the optical transitions for beams of energy in the range between ionization energy and twice lowest excitation energy of the gas. The coefficients $A_{jk} \sum_i G_{ji} Q_i$ are different than the $F_{jk} Q_j$ in equation (1.3) defined by Fowler who does not consider cascade from higher states in his analysis. The present calculation assumes that the excited atoms radiate before they have travelled any appreciable distance along the beam.

If the differential cross section for elastic scatter is not strongly peaked in the forward direction, primary electrons may be lost from the beam by scatter to the walls of the chamber containing the beam. If there is a potential energy well across the beam, of depth eV , it may hold those electrons having energy transverse to the beam less than eV along the beam. Those electrons elastically scattered with transverse energy such greater than eV may be lost at a nearby wall of the chamber containing the beam. A primary electron of kinetic energy $e\phi$ moving initially parallel to the direction of the beam, which

is elastically scattered at an angle θ to the beam axis will be given a transverse energy $e\phi\sin^2\theta$. The electron will be lost from the beam if $e\phi\sin^2\theta \gg eV$ or $\sin\theta \gg \sqrt{\frac{V}{\phi}}$. If electron loss from the beam is due primarily to elastic scatter to the walls it would be expected a-priori that a luminous skirt of scattered electrons would form about the beam and a sharp luminosity radius would not characterize the beam. Decay of luminosity with distance along the beam due to elastic scatter of primary electrons to the walls is expected to be independent of the spectral transition of the observed light. Unfortunately no provision was made with the presently available apparatus, for a separate determination of the elastically scattered component from the beam. The author was led into believing, by the sharply defined luminosity boundary of the experimentally produced beams, that elastic scatter was not an appreciable source of loss of primary electrons. Whether this is actually the case is not determined in the present measurements, which measure the loss of primary electrons along the beam. It is hoped that at some future time such a determination will be made.

Related Measurements

Electrical, as opposed to optical, measurements of total cross sections for excitation of helium and neon by electrons having energies near the ionization energy have been made by Maier-Leibnitz⁹ and have been critically examined by Chantry, Phelps and Schulz.¹⁰ Measurements of total excitation cross sections of helium and neon have been made by McClure¹¹ in the electron energy range between the gas ionization energy

and twice the lowest excitation energy. McClure made his measurements by observation of the total ionization produced when primary electrons were stopped in the gas. He obtained total excitation cross sections of $1.5 \times 10^{-17} \text{ cm}^2$ for helium and $2.1 \times 10^{-17} \text{ cm}^2$ for neon in this energy range. Maier-Leibnitz experiment gives elation cross sections of $2 \times 10^{-17} \text{ cm}^2$ in neon for 24 volt electron energy and $2 \times 10^{-17} \text{ cm}^2$ in helium for 24 volt electron energy and $2 \times 10^{-17} \text{ cm}^2$ in helium for 28 volt electrons. Maier-Leibnitz' results indicate that at these energies the elation cross sections are increasing with increasing electron energy.

Ornstein and Elenbaas¹² have made measurements of the decay of luminosity of an electron beam at 30, 36 and 76 volts potential in helium at a gas pressure of 100 millitorr, over path lengths of 1.5 and 2.8 centimeters. Measurements were made of the decay of twelve prominent spectral lines by photographic photometry. The cross section determined from the decay of luminosity was not markedly dependent upon the particular spectral line observed for a 30 to 36 volt beam but showed some variation for a 76 volt beam. When the decay was averaged over the spectral lines a mean free path was found of .7 cm for 36 volt electrons. This corresponds to a cross section for decay of luminosity of approximately $4 \times 10^{-16} \text{ cm}^2$ at each of these beam potentials. In this experiment an initial exponential decay of luminosity was found, the decay gradually becoming less rapid with increasing distance along the beam. The deviation from exponential decay was attributed to back reflection of electrons from the collecting electrode of the relatively short beam.

Absolute measurements of electron excitation functions of low lying energy states of helium with principal quantum numbers $n = 3$ to $n = 6$ have been made by St. John, Miller and Lin.¹³ Excitation cross sections of 2^1S , 2^3S , 2^3P helium states have been measured by Holt and Krotkov.¹⁴ Cross sections for ionization of helium and other gases have been measured by several investigators, the results have been compiled and critically examined by Kieffer and Dunn.¹⁵ Published measurements are not presently available for the 2^1P excitation cross section of helium, but the cross section has been calculated by Vainshtein and Dolgov.¹⁶

The sums of the peak cross sections for low lying state excitations taken together with the ionization cross section and a power law extrapolation of higher lying states' peak contributions to the total excitation cross section provides an upper bound estimate of the excitation cross section of helium.

The Electron Beam

In the 1920's and early 1930's Johnson, Buchta, Ende and other experimenters learned how to produce long and apparently collimated low energy electron beams in argon, hydrogen and mercury vapor.¹⁸⁻²⁰ The beams were long and narrow and the visible radiation from the beams was sharply defined. Buchta, using mercury vapor at room temperature observed a 1 mm diameter beam 30 cm long at 30 volts potential, in marked contrast to beam behavior in vacuum where a 30 volt beam will spread

due to its own negative space charge. Buchta found that to form a good beam one needed a well shielded space for the beam to drift in so wall charges do not prevent beam formation, high electron emission and a small, well enclosed space between hot cathode and anode to prevent arc formation. Johnson explained the beam collimation as being caused by a positive ion core holding the beam together. As the beam traverses the gas present it ionizes some gas atoms, slow ultimate electrons produced in the ionization are thrown far beyond the limits of the luminous beam pencil, while the positive ions, because of their large masses and low velocities, accumulate along the primary electron path forming a stable positive ion core to the beam. Ende has experimentally verified the existence of the positive ion core by placing a sequence of parallel plate capacitors along the beam, with their charge spatially alternated, and observing the deflection of beam luminosity as the beam traversed the region of spatially alternating electric field.

Frenkel and Bobkovsky²¹ have made a theoretical study of the beam collimation. They examine beam collimation as a function of beam current, beam energy, beam radius and initial divergence angle at entry into the gas, gas pressure and ionization cross section. A small initial divergence angle is favorable to collimation as is a large ionization cross section, large ion mass and high pressure up to a limit. Frenkel and Bobkovsky calculate the radial potential variation across the beam under the assumption that primary electrons and positive ions are uniformly distributed across the cross sectional area of the beam.

The potential difference, V , between the beam center and luminosity edge of the beam is calculated, in Gaussian units, to be

$$V = \pi \rho R^2 \quad (3.1)$$

where R is the luminosity radius of the beam, ρ is the density of electric space charge in the beam. The space charge density in the beam is determined in terms of the electronic charge, e , the magnitude of the space charge density of the primary electrons in the beam, $\rho_- = n e$, the ionic mass, M , and the number of ions produced per second by a primary electron, ν , by the relation

$$\left(\frac{\rho}{\rho_-}\right)^3 + 2\left(\frac{\rho}{\rho_-}\right)^2 + \left(\frac{\rho}{\rho_-}\right) - \frac{M\nu^2}{2\pi e\rho_-} = 0 \quad (3.2)$$

The relation is obtained by equating the removal rate of positive ions, accelerated from the beam by the positive net beam charge, with the formation rate of positive ions along the beam. Near the beam entrance into the gas, under the assumption that the beam current is carried by primary electrons, the constant $\frac{M\nu^2}{2\pi e\rho_-}$ in the cubic equation can be calculated in terms of measurable beam parameters. These are the beam luminosity radius, beam current and potential, target gas temperature, gas atomic weight and cross section for ionization by electrons. If the ideal gas law is assumed to relate the temperature, pressure and density of the gas and primary electrons are assumed to be uniformly distributed over the luminosity radius of the beam,

$$\frac{M\nu^2}{2\pi e\rho_-} = 1.632 \times 10^{-2} \frac{A\phi^{3/2}}{I} \left[\left(\frac{273.2}{T + 273.2} \right) Q_{I,PR} \right]^2 \quad (3.3)$$

where I is the beam current in microamperes, ϕ is the beam potential in volts, A is the atomic weight of the gas, Q_I is the gas cross section for ionization in units of πa_0^2 at the primary electron energy where a_0 is Bohr's hydrogenic radius, R is the beam luminosity radius in millimeters, P is the gas pressure in millitorr and T is the gas temperature in degrees centigrade.

Equation (3.2) has been solved in terms of the parameter $\frac{Mv^2}{2\pi e\rho}$ and solutions are tabulated in Appendix A, Table I. Transverse beam potentials are computed from equations (3.1) through (3.3) in terms of assumed beam parameters and are tabulated in Appendix A, Table II. Ionization cross sections are available in the compilation by Kieffer and Dunn.¹⁵ The size of the potential transverse to the beam is relevant to the determination of the fractions of elastically scattered primary electrons trapped along and lost from the beam. The relevance of the computed transverse beam potentials to the experimental observations is discussed in chapter IV. The theory is not expected to be valid for beam energies near the ionization energy, that is in the limit of vanishing ionization cross section the space charges along the beam should become negative and the assumptions of uniform ion and primary electron distribution across the luminous beam area may no longer be reasonable.

Statement of the Problem

The problem to be studied is the measurement of the decay of light intensity along the length of a gas focused electron beam traversing helium, neon and mercury. The nature of the decay with distance

along the beam and its dependence upon the spectral transition of the light observed is examined in helium. The relation cross section in helium as determined from the decay is to be compared with the results of related electrical and optical measurements. The relation cross section as determined from light decay in mercury is to be compared with the cross section obtained by Koppius and Duffendack. Inferences as to the validity of the density saturation method of measuring cross sections with a linear beam are to be made.

CHAPTER II

APPARATUS

The Electron Gun

The electron gun consists of a planar indirectly heated mixed oxide cathode, a perforated double anode which both accelerates and collimates the electron beam, a focusing ring, a shielded drift tube and a collecting cup electrode. The gun structures are shown in Figures 1 through 3.

The cathode is a cup of commercially pure nickel, .128" inside diameter by .20" long by .012" wall thickness, coated on its end surface with a mixed calcium, barium, strontium carbonate paste which decomposes to the oxides on activation. The heater is a Semicon Inc. type STD-120 filament heater which fits inside the cathode cup. The cup is mounted inside a cylinder of number 304 stainless steel, .5" long, .25" inside diameter, .016" wall, by nickel tabs spot welded between the cylinder and cathode cup. The cylinder is mounted by friction fit onto a boron nitride mount piece shoulder which serves to center and to space the cathode above the anode collimating apertures. Two .060" diameter tungsten rods enter the cylinder axially through holes in the boron nitride mount. The heater is spot welded between the rods. The rods are connected, by flexible tabs of sheet nickel spot welded onto

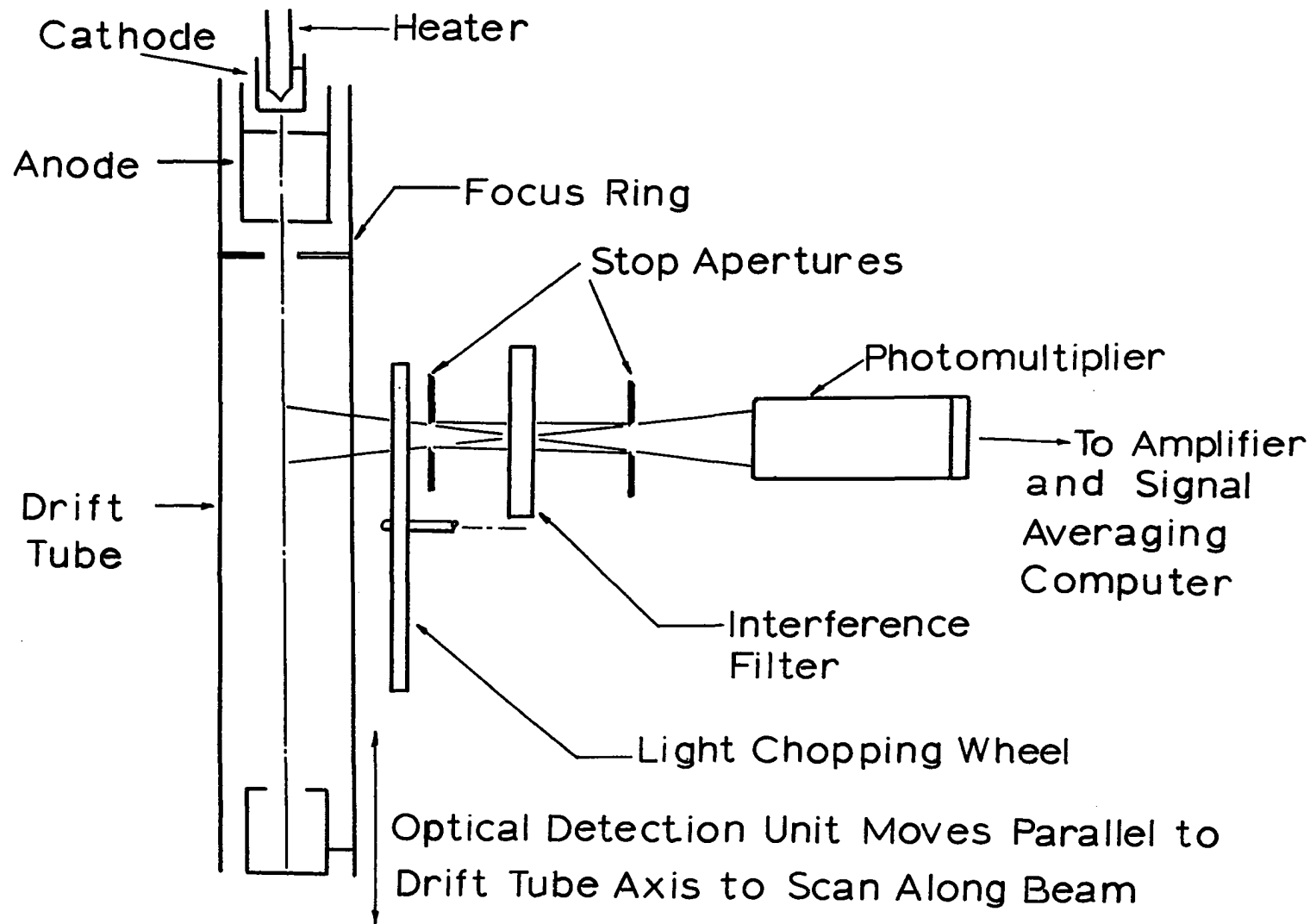


FIGURE 1. DIAGRAM OF THE EXPERIMENT.

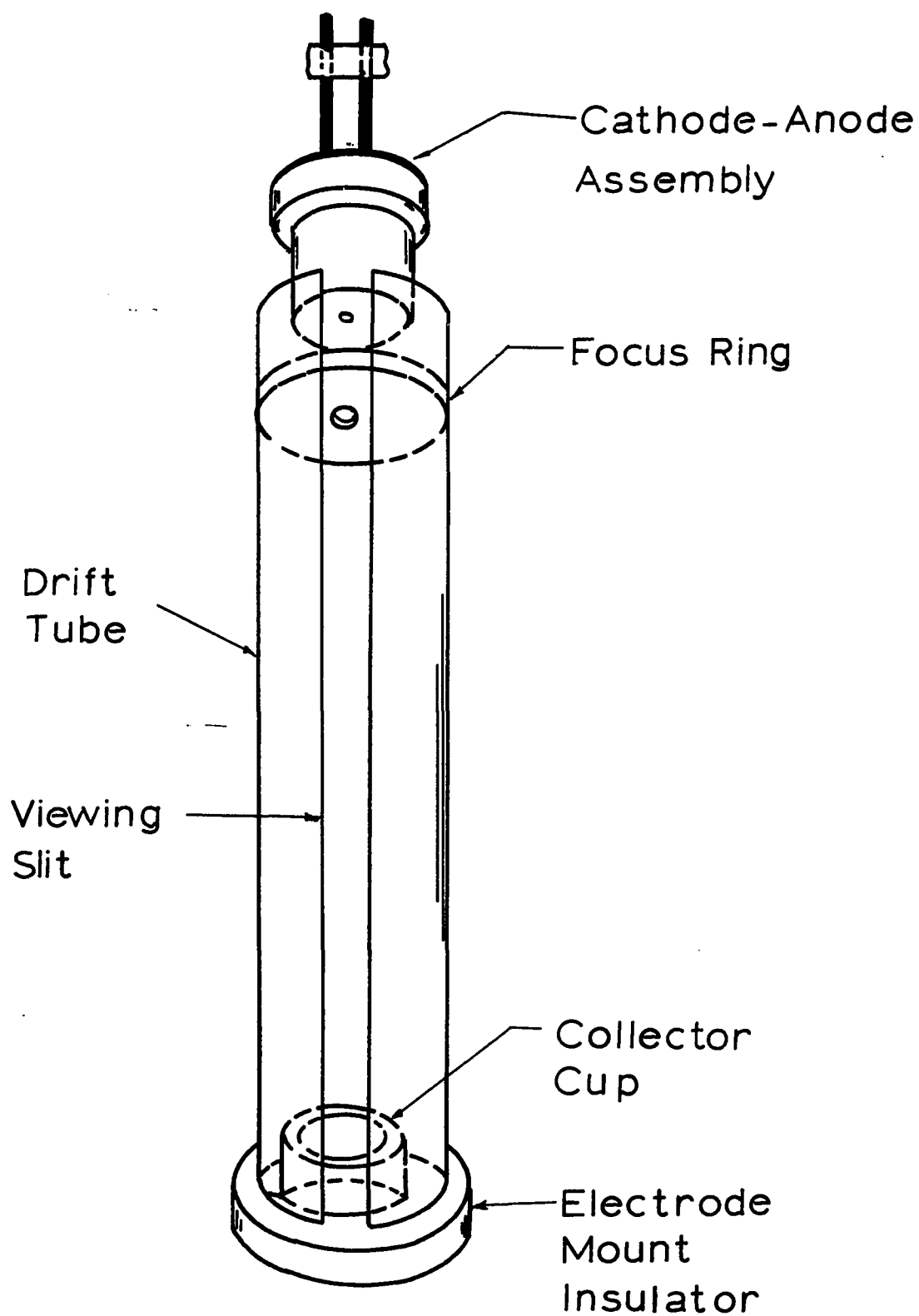


FIGURE 2.1. THE COLLISION TUBE.

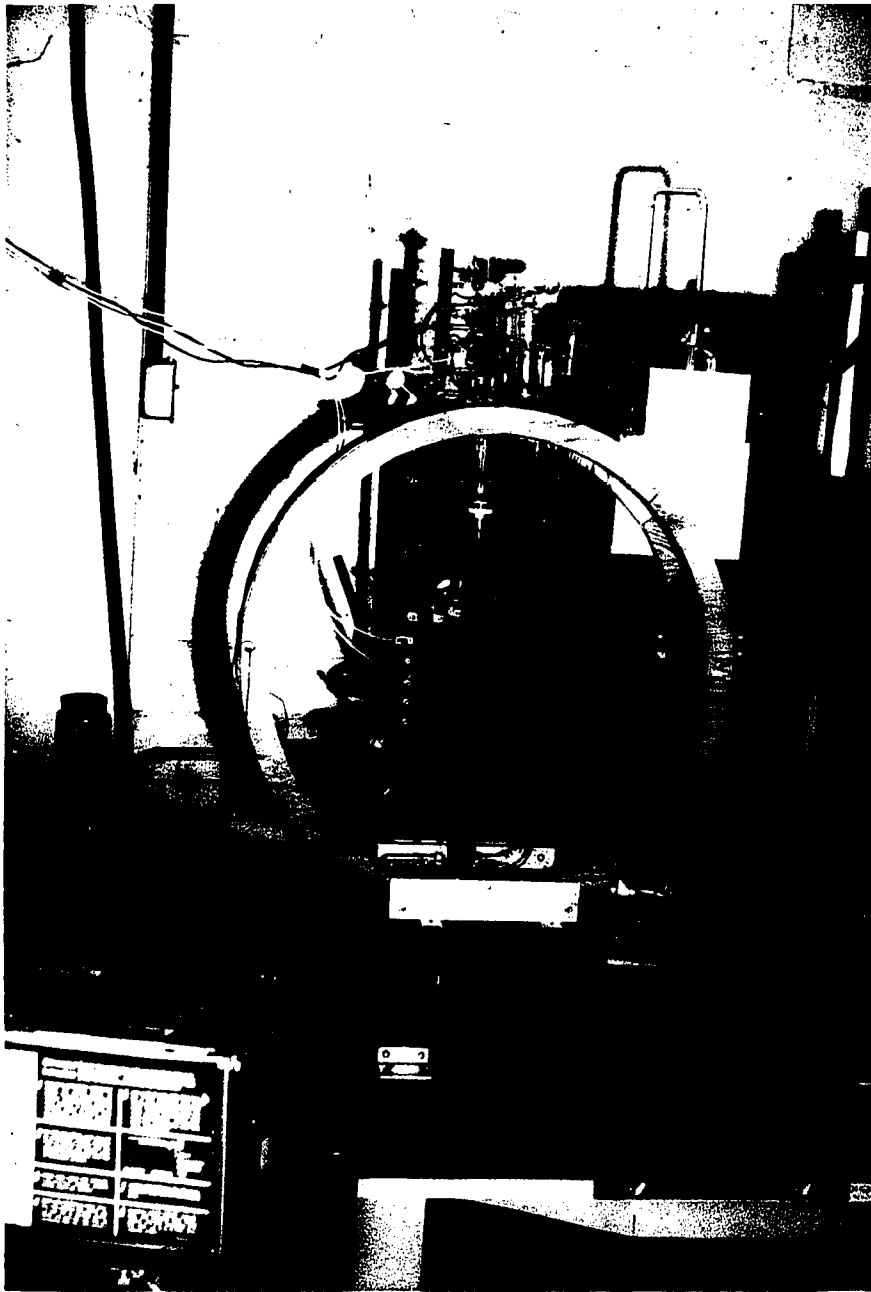
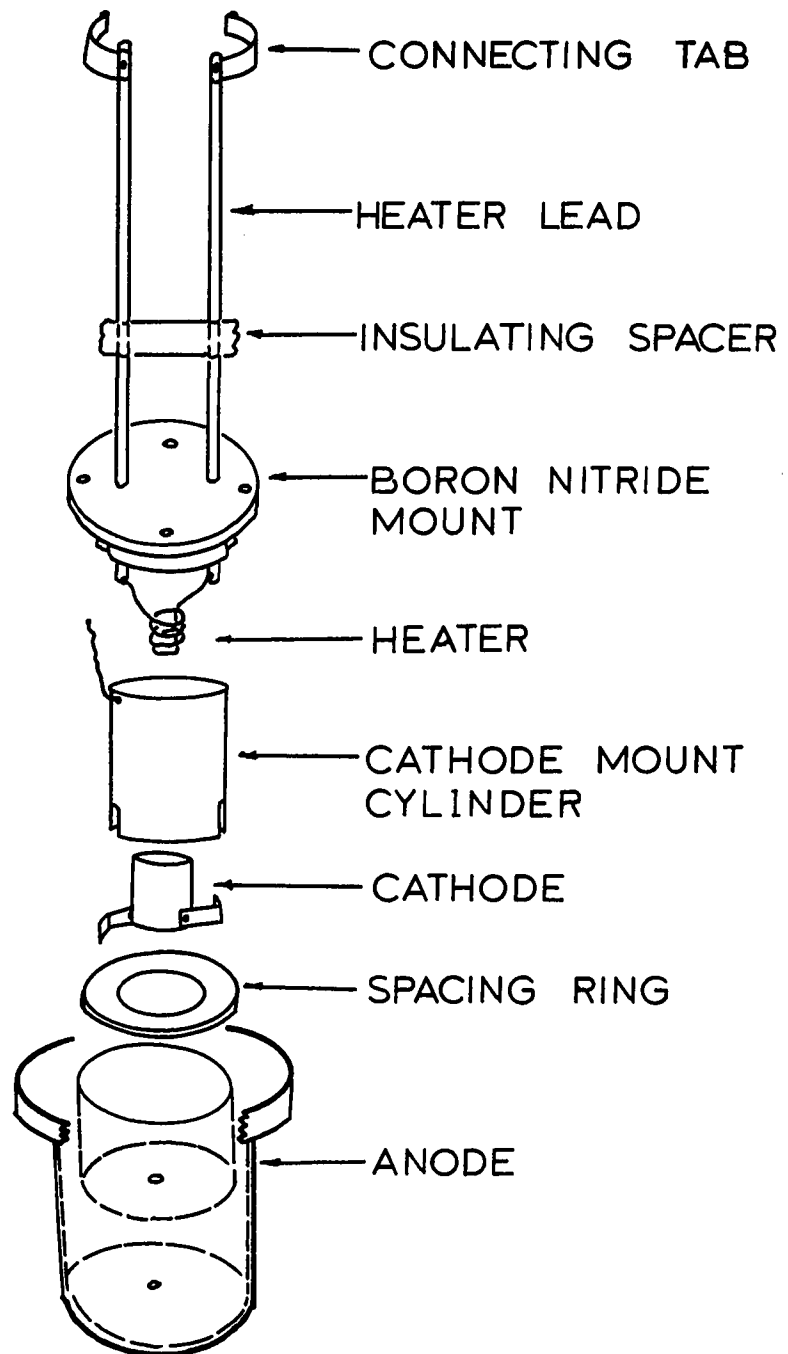


FIGURE 2.2. THE COLLISION TUBE.



CATHODE - ANODE ASSEMBLY

FIGURE 3.

them, to feed through electrodes sealed into the glass wall of the gun envelope. Vent holes are drilled into the boron nitride mount and into the side wall of the double anode to allow evacuation of the cathode region of the gun.

The anode is a double cup of molybdenum. It seats on a shoulder of the boron nitride mount piece holding the cathode structure, thereby locating and centering the cathode relative to the anode. The anode-cathode structure is a planar diode, with perforated anode. The cathode is spaced 2.7 mm from the anode and separated from it by a boron nitride spacing ring. Electrons from the cathode accelerating to the anode may pass through a first aperture in the anode, of diameter .026", and are collimated by passage through a second .026" aperture located .50" from the first one.

The drift tube is a slit cylinder of molybdenum 18.3" long, 1.18" inner diameter. The slit, of width .41", runs the length of the cylinder. The cylinder is coated with dag colloidal suspension to blacken its surface, lowering its optical reflectivity. The suspension was painted onto the metal and the drift tube cylinder was vacuum baked at 360°C overnight to remove organic binder and water vapor and was stored under vacuum until ready for installation.

The focusing ring is a circular disc of .015" thick molybdenum with a central aperture .125" in diameter. It is spot welded to an inconel holding ring 1.3" in diameter which is held by friction inside the drift tube cylinder and is electrically connected to the cylinder. The plane of the disc is normal to the cylinder axis. The disc is centered axially and is mounted at a distance of .5" from the second anode aperture.

The molybdenum collector cup is electrically connected to the drift tube. The anode is centered and located relative to the drift tube by mount rings of boron nitride. The electrode structure is mounted in a pyrex glass cylindrical envelope, 45 mm outer diameter, 24.8" length having .060" diameter connections to the tube electrodes. The tube is mounted with its axis and shield slot edges vertical so that the electron beam is projected vertically down the tube.

Before tube assembly the nickel and stainless steel electrodes are anodically electropolished in a 60 per cent phosphoric acid, 20 per cent sulphuric acid, 20 per cent distilled water electrolyte, followed by a rinse in distilled water and then acetone. The molybdenum electrodes, apart from the drift tube, were boiled in a 20 per cent potassium hydroxide solution followed by a rinse in distilled water and drying with a heat gun. After assembly of the gun and sealing of the tube onto the vacuum system, the electron gun, traps, glass vacuum lines and McLeod gauge are baked for several hours with heating tapes while under evacuation. The tube electrodes are then induction heated to red heat by an induction furnace. The cathode is activated and current is drawn under vacuum at 300 volt anode potential and cathode temperature above normal operating temperature for several hours before any runs are made.

The Vacuum System

Forepumping is done by a Welch Duo Seal mechanical pump rated at 58 liter/minute followed by an Eck and Krebs mercury diffusion pump.

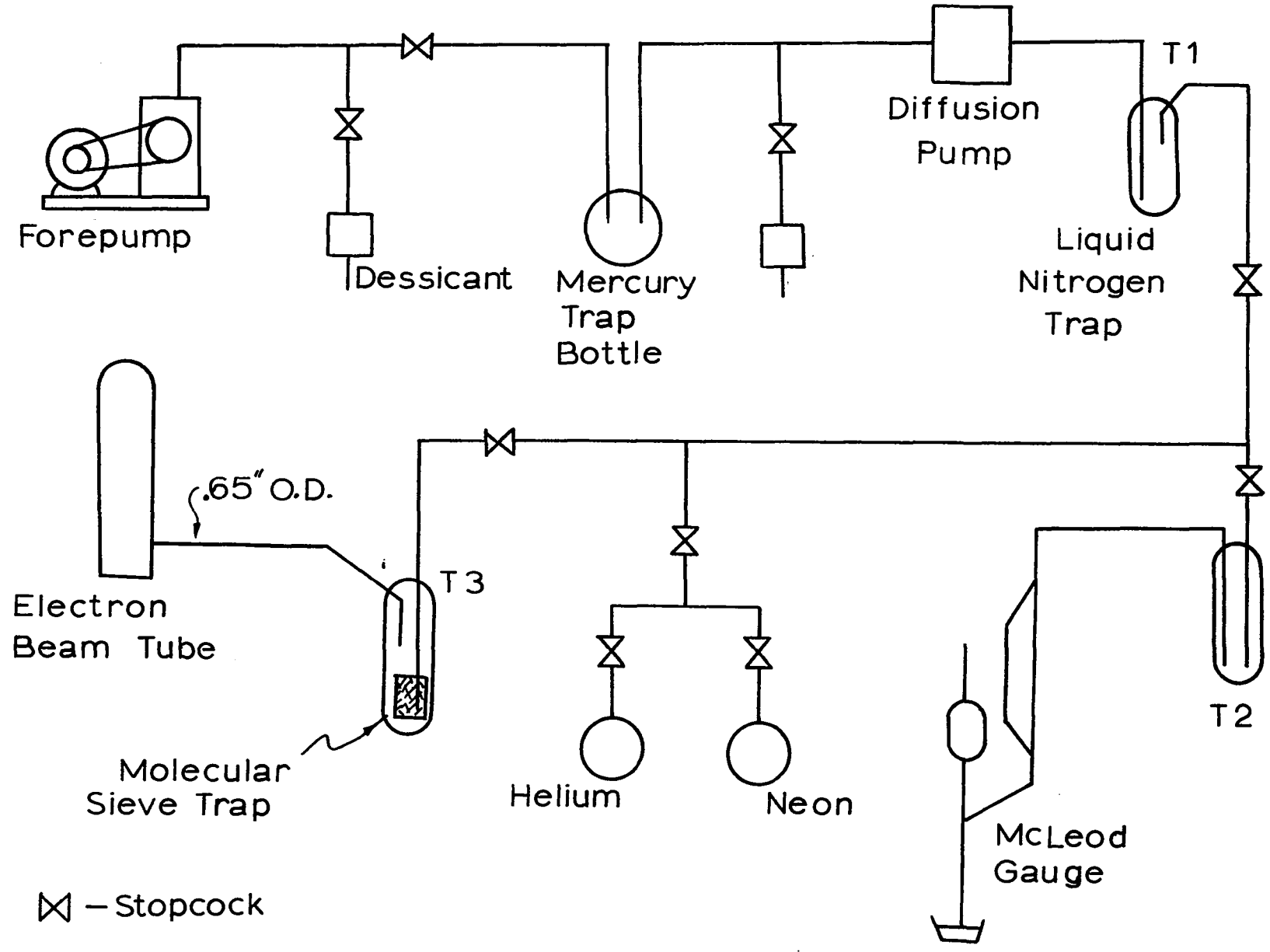


FIGURE 4. VACUUM SYSTEM OF THE EXPERIMENT.

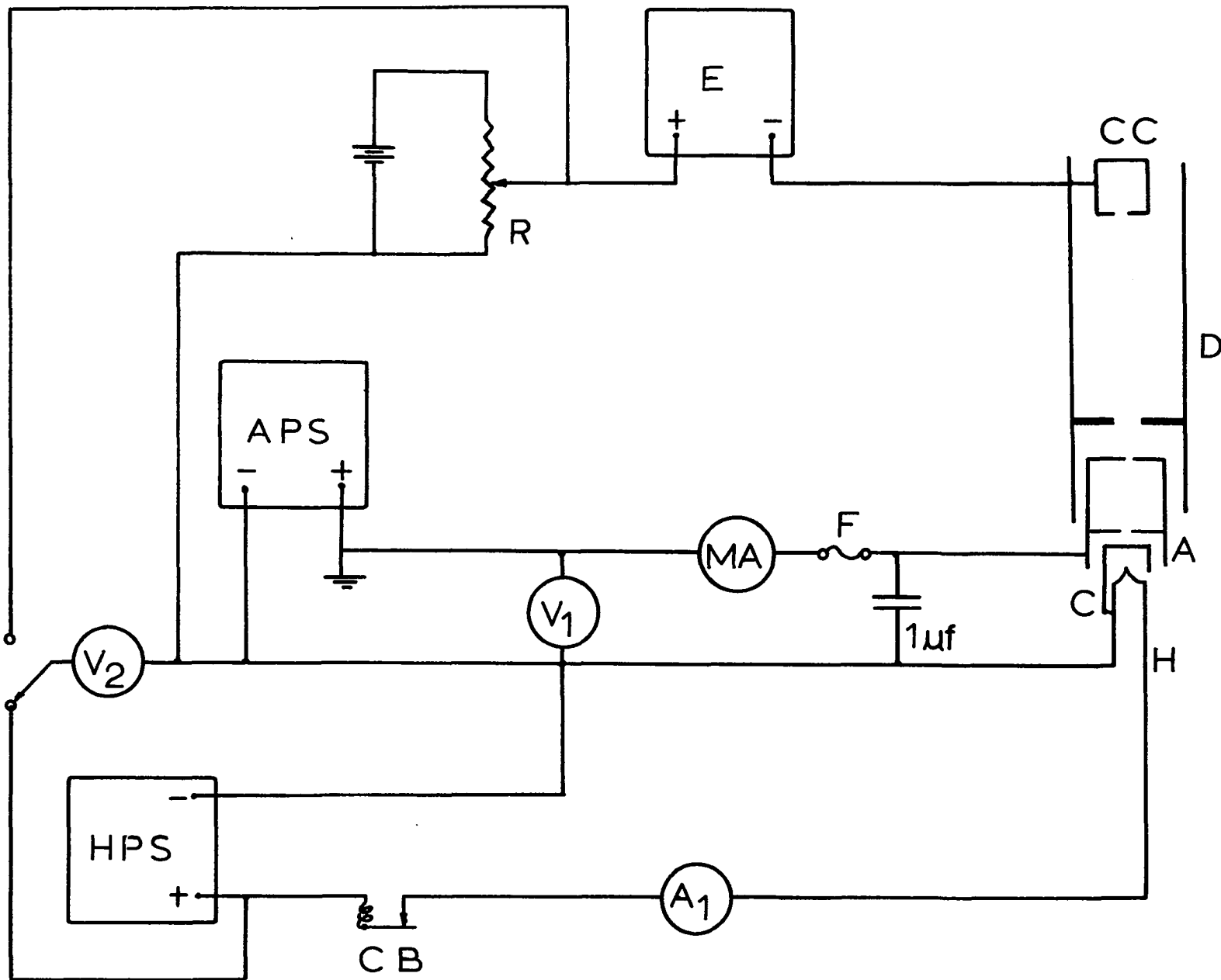


FIGURE 5. THE COLLISION TUBE CIRCUIT.

The diffusion pump is connected through a 20 mm hollow bore glass stopcock to a liquid nitrogen trap. Following the trap is a feeder line from reservoir bottles of Linde spectroscopic grade neon and helium, isolated by 4 mm glass vacuum stopcocks. A parallel connection leads to a 4 mm stopcock followed by a second nitrogen trap and a McLeod gauge. In a second parallel connection with the first trap is another nitrogen trap and zeolite trap of Linde type 5A molecular sieve, followed by the electron gun. The vacuum system is shown in Figure 4. During running of the experiment in helium and neon the McLeod gauge is isolated from the electron beam tube by two cold traps and the molecular sieve trap. The gauge was read with a cathetometer while the electron beam is in operation, both near the beginning and near the end of an experimental run. Little change is noted in the readings. It is felt that there is an appreciable source of error in the pressure measurements in helium and neon. Work by Ishii and Nakayama and Meineke and Reich^{22,23} indicates that the pressure measurements using a cold trapped McLeod gauge may be too high by approximately 15 per cent in neon and 6 per cent in helium. This may produce an error in the size of the cross sections obtained but will not affect relative measurements of luminosity versus length or luminosity decay cross section versus beam potential or spectral transition. The pressure measurements have not been corrected for this effect, of mercury migration from the gauge to the trap causing a pressure differential in the system.

A Fenwal type GA52J2 bead thermistor was mounted on fine wire inside the pyrex electron gun envelope, at a distance of approximately

1" from the cathode heater and above the anode. During the operation of the gun with helium or neon in the tube a rise of less than 10°C in temperature was indicated at this point. The temperature rise at this position was greater than in the drift tube which lay vertically below the heater and was not subject to convective heating and was surrounded by the large heat capacity double anode, focusing ring and drift tube wall. No correction was made for temperature rise above ambient room temperature in computing cross sections. The thermistor calibration was checked when the gun was dismantled to check that its calibration had not changed during sealing of the gun onto the vacuum system.

The Optical Detection System

Light output along the beam is monitored with an EMI type 9526B multiplier phototube, an eleven stage tube having a 30 mm diameter quartz end window, box and grid dynodes and a 23 mm diameter cesium-antimony cathode with S-13 spectral response. The phototube is mounted with its axis normal to the plane of the drift tube slit in the electron beam tube and is constrained to move in a vertical direction parallel to the edges of the drift tube slit. The phototube is electrostatically shielded, dynode voltages are obtained from a chain of dropping resistors fed from a regulated power supply (John Fluke model 405B). The multiplier is shielded magnetically by three layers of magnetically soft foil (Co-Netic foil obtained from the Perfection Mica Company) wrapped around a cylindrical brass case which housed the photomultiplier. The arrangement of the detector is shown in Figures 1 and 6, the photomultiplier connections are shown in Figure 7.

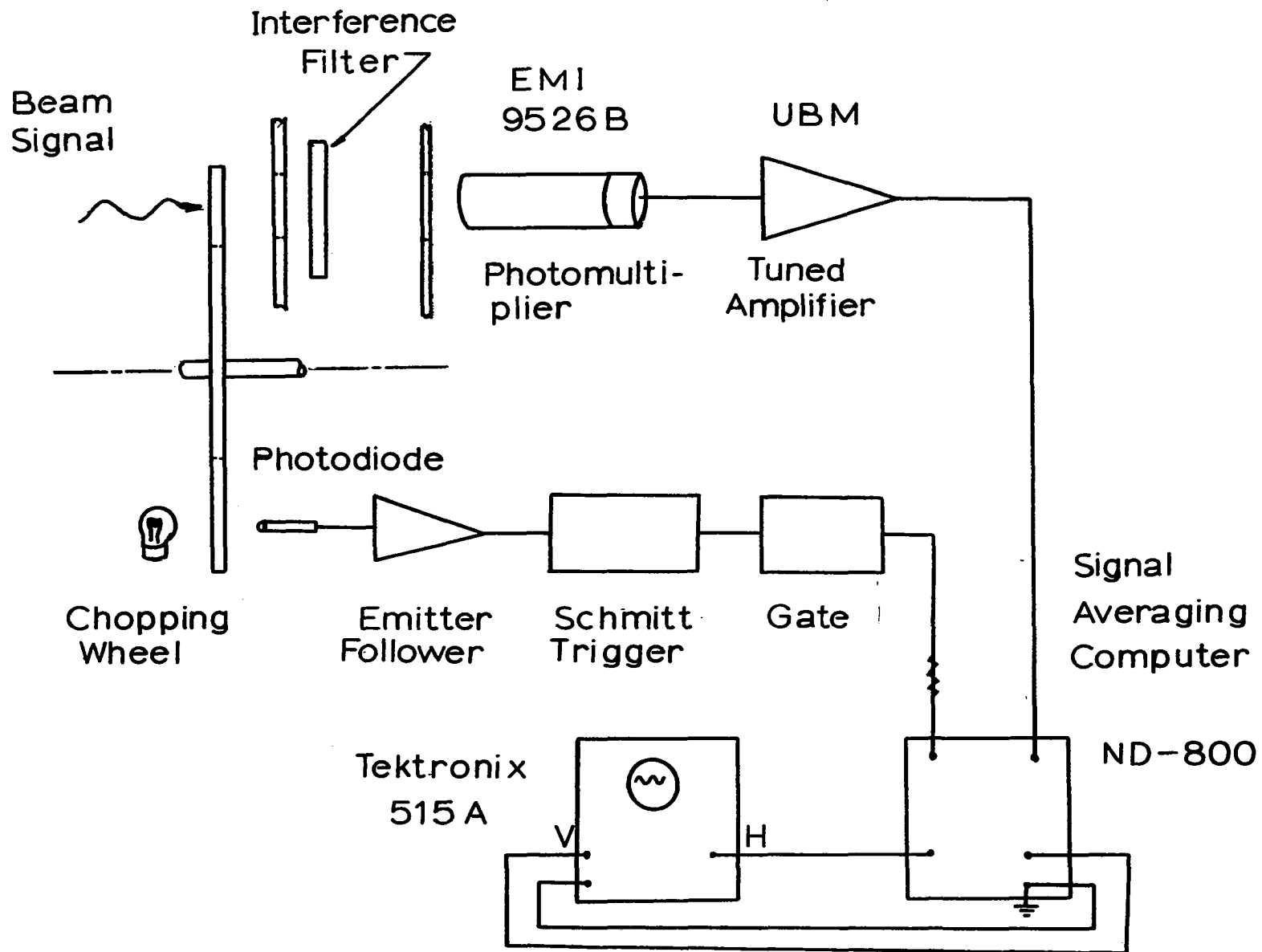


FIGURE 6. OPTICAL DETECTION SYSTEM.

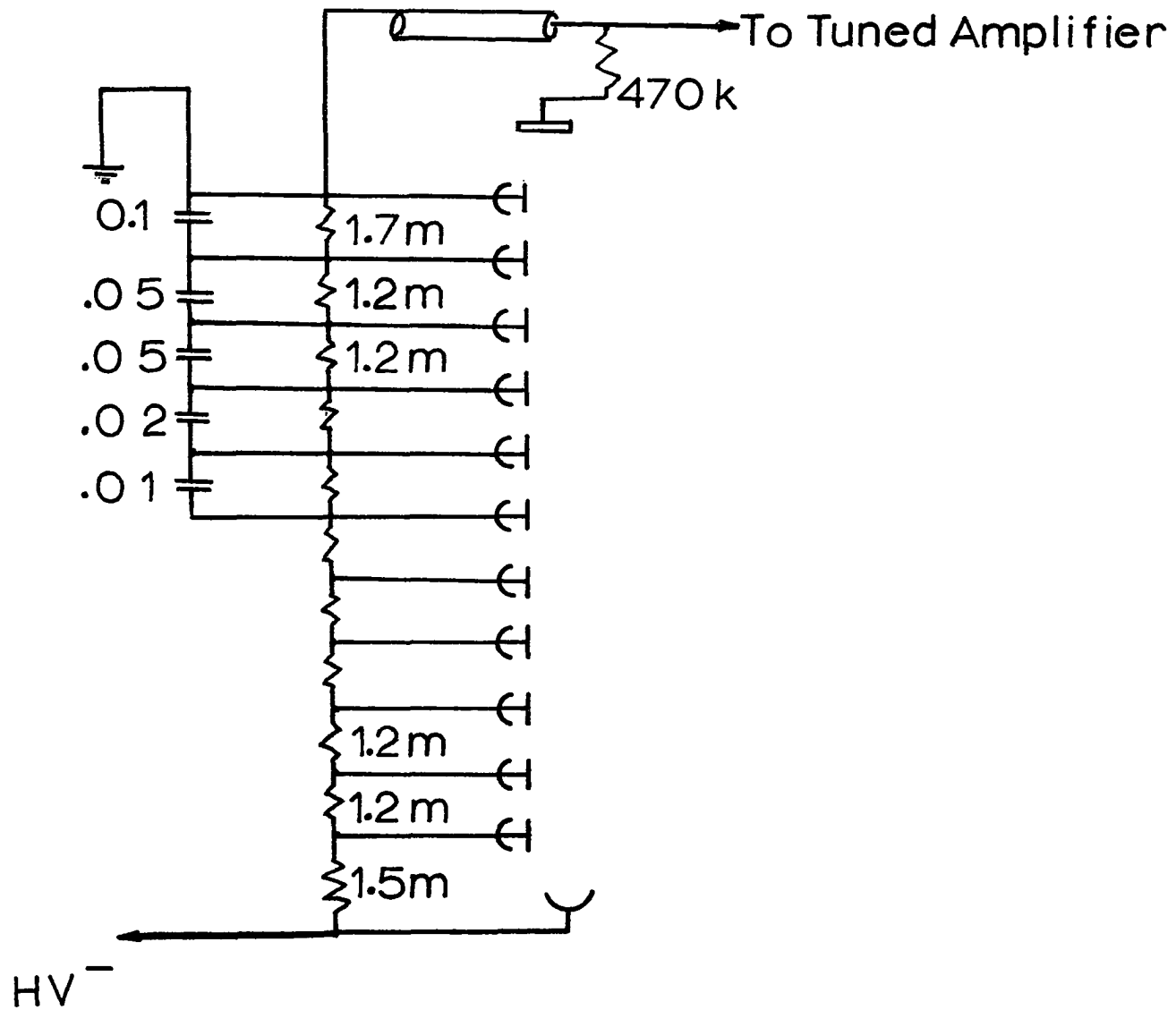


FIGURE 7. PHOTOMULTIPLIER CONNECTIONS.

The phototube end face is located 12 to 13" from the center of the drift tube. Rectangular stop apertures $3/16$ " wide by $3/4$ " long were mounted 2" and 7" in front of the phototube end window, with their long dimension horizontal and perpendicular to the electron beam. This arrangement allows light from a 1.5 cm length of beam to be scanned. Light emitted within that length of beam which is also emitted laterally between the edges of the drift tube slit in a ray bundle of fixed geometry can reach the multiplier's photocathode. The photocathode acts as the limiting stop determining the horizontal, that is lateral, extent of the detected ray bundle. The rectangular apertures limit the vertical extend of the detection ray bundle. No lens system was used in the present measurement to increase the light gathering ability of the optical detector. Convergent optics were omitted so that the detection system would be insensitive to a change of position of a millimeter or two in the location of the beam in the drift tube. The variation of light gathering power optical aperture with such a change of position is small with the present arrangement.

A filter holding box mounted between the aperture stops allows Wratten filters or 2 x 2" interference filters to be interposed between the electron beam and the phototube. The filters are mounted normal to the photomultiplier axis. The geometry of the aperture system is such that rays from the electron beam passing through the aperture stops and reaching the photocathode will traverse the filter within an angle of 6 degrees to the normal to the plane of the filter. The photomultiplier, stop apertures and filter are mounted as a unit on a platform which can

be moved vertically on laboratory jacks. The detector is located vertically by a set of machined spacing rings.

The light signal from the electron beam is mechanically chopped at 320 cycles per second by a ten slot aluminum wheel driven by a belt and pulley drive from an 1800 RPM synchronous motor. The photomultiplier output signal is fed into a Rhode and Schwartz model UBM tunable amplifier, tuned to the chopping frequency. The amplifier output is either observed on a General Radio Model MEDS-37 vacuum tube voltmeter or is placed into a Nuclear Data Inc. model ND-800 Enhancetron. The former detector was used in measurements of unfiltered light decay in neon and helium, the latter was used in measurements of decay of filtered helium light and of mercury light.

The Enhancetron is a 1024 channel pulse height analyzer, used as a storage device, triggered in synchronism with the signal chopping wheel. For improvement of signal-to-noise, the periodic signal output of the amplifier is accumulated, by many relatively rapid scans of the signal, in the analyzer memory so that the signal scans add coherently whereas the noise adds randomly. The peak to peak signal stored in the memory increases linearly with the number of scans while the peak to peak noise output increases as the square root of the number of scans. In observation of light filtered through a narrowband interference filter the coherent chopped background light is small when the electron beam is off and the noise is generated in the photomultiplier and tuned amplifier. If the chopper rotation speed is constant the number of computer sweeps is directly proportional to the signal integrating time.

Let,

$S(x)$ = peak to peak output voltage of the signal averaging computer, signal originating at position x along the beam,

t = signal averaging time,

Z = peak-to-peak noise output voltage of signal averaging computer, measured with electron beam signal turned off,

t_N = integrating time of noise measurement with beam signal off,

I = beam current,

$U_{jk}(x)$ = signal per unit current at position x along the beam filtered to observe transition j to k of target gas.

Under conditions of constant chopper speed, steady current and signal and noise being generated in the electronic circuit,

$$S(x) = I U_{jk}(x) t + c\sqrt{t}$$

and

(4.1)

$$Z = c\sqrt{t_N}$$

so that

$$U_{jk}(x) = \frac{1}{I} \left(\frac{S(x)}{t} - \frac{Z}{\sqrt{t} t_N} \right) \quad . \quad (4.2)$$

$U_{jk}(x)$ is taken as the observed light intensity and is taken to be proportional¹ to $I_{jk}(x)$. Integrating times are typically from 30 seconds to 2 minutes, the scan time is .032 second. With a chopping

frequency of 320 cps, a scan encompasses 10 cycles and the computer performs from 800 to 3000 scans in determining the signal. Integrating times were measured with a stopwatch.

The signal averaging computer requires an input trigger pulse synchronous with the chopper signal to recycle the signal scan. The trigger needed is of 3 to 10 volt amplitude and of .2 microsecond maximum rise time. The triggering system is shown in Figure 8. A collimated signal from a light bulb is chopped by the rotating wheel and detected by a 1 mm diameter photodiode (Texas Instruments type H-38 dual photodiode). The photodiode output feeds an emitter follower whose output trips a Schmitt trigger which produces a rectangular pulse of approximately 7 volt amplitude and 10^{-5} second rise time. The Schmitt trigger output is used to trigger a thyatron gate circuit which produces the desired fast rise time pulse. The gate circuit has been described by Fowler.¹⁷

The synchronous motor turning the chopping wheel drives an inertial load. When the motor is first started the O-ring belt drive will slip against the drive pulley keyed to the chopping wheel shaft, until the wheel reaches synchronous speed. Time is allowed for the chopper to reach synchronous speed before optical measurements are made.

Operation of the Gun

The electrical connections of the gun are shown in Figure 5. The anode, A, is operated at a potential of 130 ± 15 volts positive to the cathode, C, typically drawing an emission current of 3 to 6

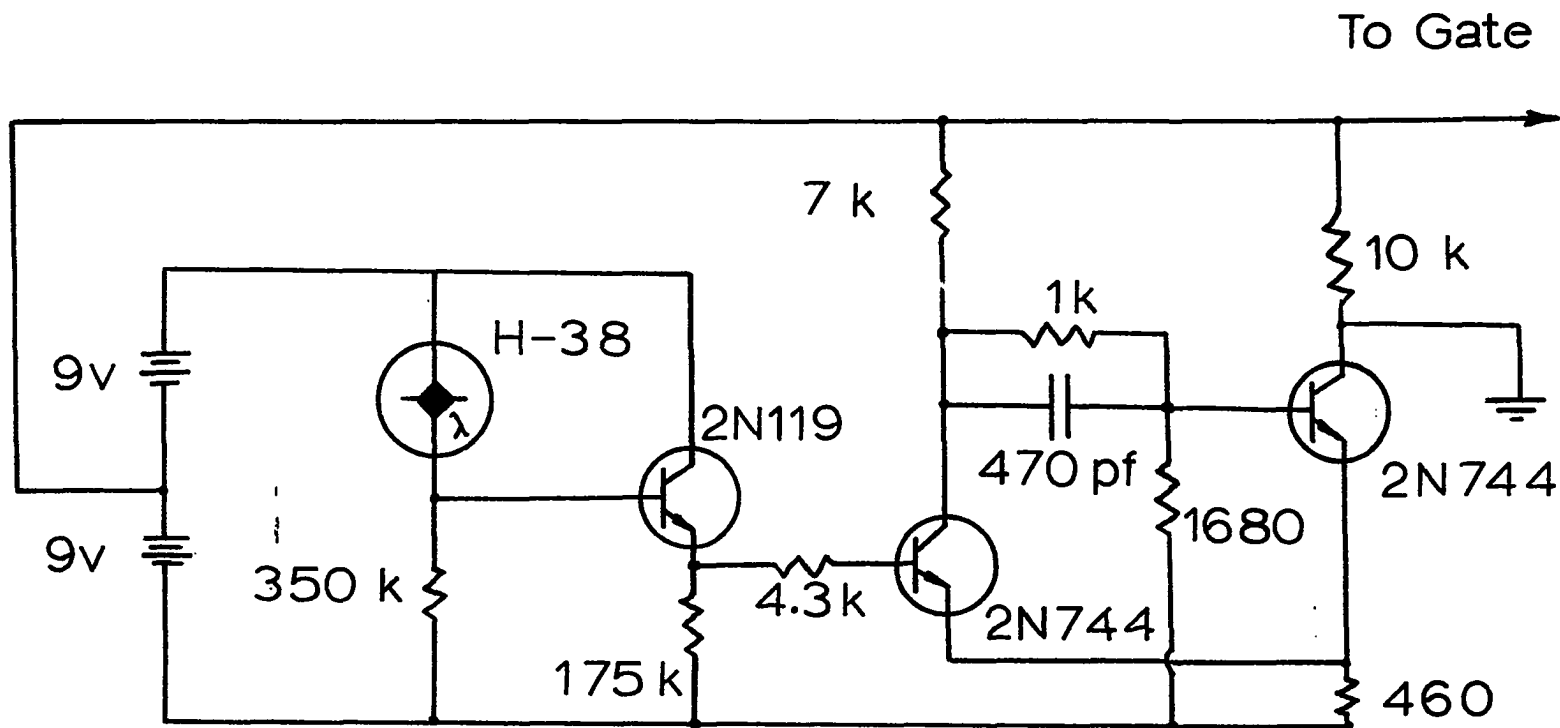


FIGURE 8. PHOTODIODE TRIGGER FOR SIGNAL AVERAGING COMPUTER.

milliamperes. When a beam is formed, a current, typically from 3 to 15 microamperes in size, reaches the drift tube. The size of the current is varied by varying either the heater current or anode potential. The drift tube potential to cathode determines the beam energy. The drift tube is operated at a potential below that of the anode and the combination of anode and focusing ring apertures' fields acts as a converging lens for those electrons which pass through the second anode aperture. When helium and neon are used in the experiment and the drift tube is at a potential between one and two times the lowest excitation potential of the gas, an electron having an inelastic collision with a gas atom before entering the drift tube region beyond the focusing ring will have insufficient energy to travel more than a few focus ring aperture diameters into the drift space. Those electrons which enter the drift space have not experienced inelastic collisions before their entry at these beam energies.

Beam current is measured on a Victoreen VTE-2 electrometer, E in Figure 5, placed in series with the drift tube and the gun cathode. The electrometer provides a series connection of small impedance to the beam current. The operation of the electrometer is discussed in appendix B. The response of the electrometer, photomultiplier and tuned amplifier was tested by monitoring the amplifier output with the vacuum tube voltmeter. The amplifier output was measured as the anode voltage was varied, causing concomitant variation of the beam current at a constant beam potential. Over a decade range the amplifier output was directly proportional to the beam current reading on the electrometer to

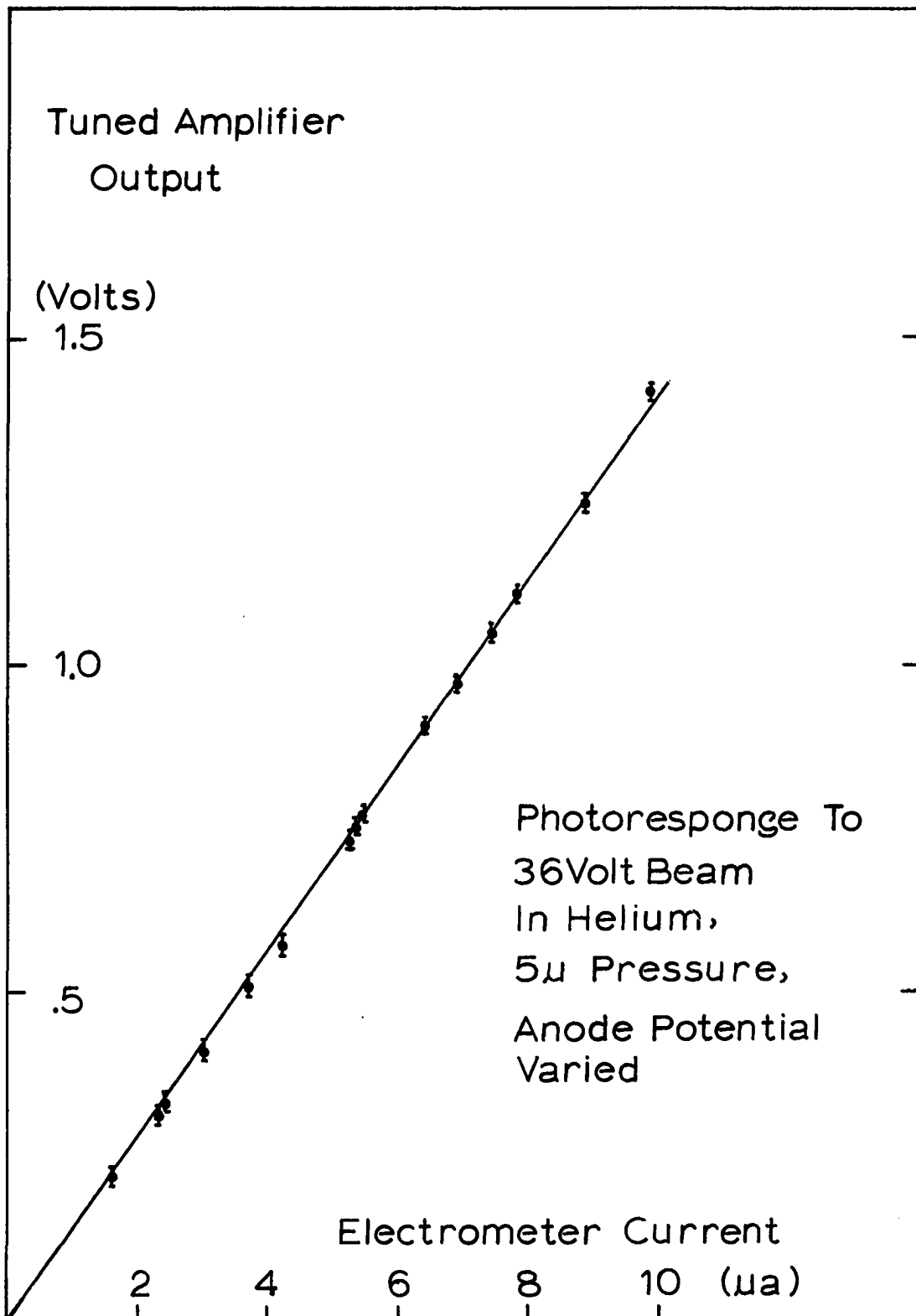


FIGURE 9. TUNED AMPLIFIER OUTPUT VERSUS
ELECTROMETER CURRENT.

within three per cent. Results of one test, made in helium with unfiltered light, detector located near beam entry into the drift tube, are shown in Figure 9. The error bars indicate noise fluctuation in the photomultiplier and amplifier.

Beam potential is supplied by B-batteries placed across a 10 turn potentiometer, R in Figure 5, allowing adjustment within 1/10 volt. The anode potential supply (APS) is a Kepco model ABC 200M regulated voltage supply. Emission current is measured with a Sensitive Research Corporation model S milliammeter (mA). Anode voltage is measured with a Weston model 45 direct current voltmeter (V_1) and beam voltage is measured with a model 901 Weston direct current voltmeter (V_2).

The electron gun is mounted vertically between a pair of 46 turn, 23" diameter coils. The coils are coaxially mounted in parallel vertical planes, with their common axis horizontal, oriented so as to cancel the horizontal component of the earth's magnetic field. The circular coils are shown in Figure 2.2. The beam can be steered down the drift tube by adjustment of the coil current. During the running of the experiment the coil current is adjusted to cancel bending of the scanned portion of the beam at the lowest beam energies used. Straightness of the optically scanned portion of the beam is checked at all energies run, both before and after each measurement. This check is important because beam bending into the drift tube wall might be observed as a spurious fast decay. For this reason the full length of available beam was not used in measurement as complete cancellation of the horizontal magnetic field over the entire tube length was not achieved and

the lower end of the beam showed bending deflection at the lower electron energies used. In practice the length of beam scanned was approximately half the beam length available in the tube.

CHAPTER III
EXPERIMENTAL OBSERVATIONS

Qualitative Observation of the Beam

Collimated thread-like beams were observed in helium and neon at pressures between 3 and 25 millitorr and in mercury at a pressure of 2 millitorr. The luminous width of the beams was of order 1 millimeter. The beams run at higher pressure in helium and neon were brighter than beams of the same current and voltage run at low pressure. A 30 volt beam in neon at 2.5 millitorr pressure, 13 microamperes current was faint even to a dark adapted eye while a beam of the same current and voltage in neon at 23 millitorr pressure was visible in a dimly lighted room, provided the beam tube was shielded from direct room light. The beam width decreased with increasing pressure in helium and neon in this pressure range. A 45 volt, 14 microampere beam in neon at 23 millitorr appeared to have a width of approximately one half millimeter.

The brightness of the beam entering the drift space through the focus ring aperture markedly decreased in each of the three gases studied as the beam potential was lowered to the ionization potential of the gas. Measurements of unfiltered light intensity observed near beam entry into the drift tube, normalized to constant current, versus beam potential are shown in Figures 10.1 through 10.3.

The observed beam was sharp and bright compared to any diffuse glow about the beam for electrons having energy below 50 electron volts in helium and neon. In helium, at a pressure of 17 millitorr, the glow is much fainter than the beam below 40 electron volts energy; as the beam energy increases to 75 electron volts the glow becomes brighter compared to the beam but the beam is still well defined and brighter than the glow around it. At energies two or more electron volts above ionization potential no skirt of scattered electrons was observed in neon at 23 millitorr or about the beam in mercury at a pressure corresponding to a mercury reservoir temperature of 26.5°C.

At the lower pressures at which the measurements were taken and at beam potentials within a couple of volts of the ionization potential, the beam would enter the drift space as a collimated column, proceed in collimation for some distance down the drift space and then broaden. The point at which broadening started could be moved down the drift space, increasing the length of narrow collimated beam, by increasing the beam energy. With sufficient increase of beam energy the entire available beam length would become collimated. The phenomenon was observed in helium, neon and mercury, being most pronounced in helium. At 3.8 millitorr pressure, 27 volt beam potential, 14 microampere current this beam bursting was observed in neon. In neon at 2.6 millitorr pressure the collimation markedly improved as the beam potential, that is the drift tube potential, was raised from 19 to 30 volts; at 40 volts a 20 centimeter length of beam was collimated. At 5 millitorr pressure, 20 microamperes current, beam bursting was observed in helium within a

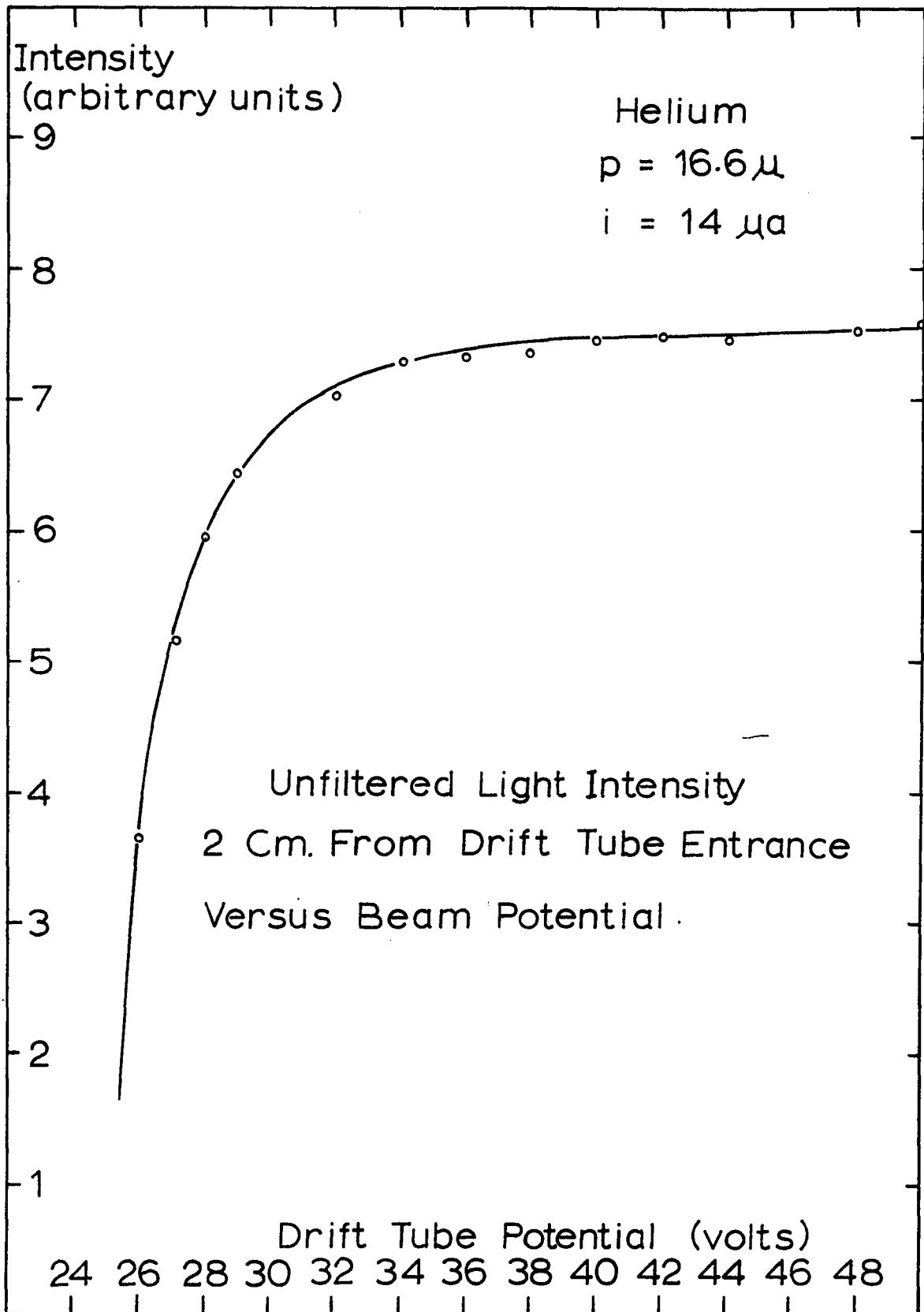


FIGURE 10.1.

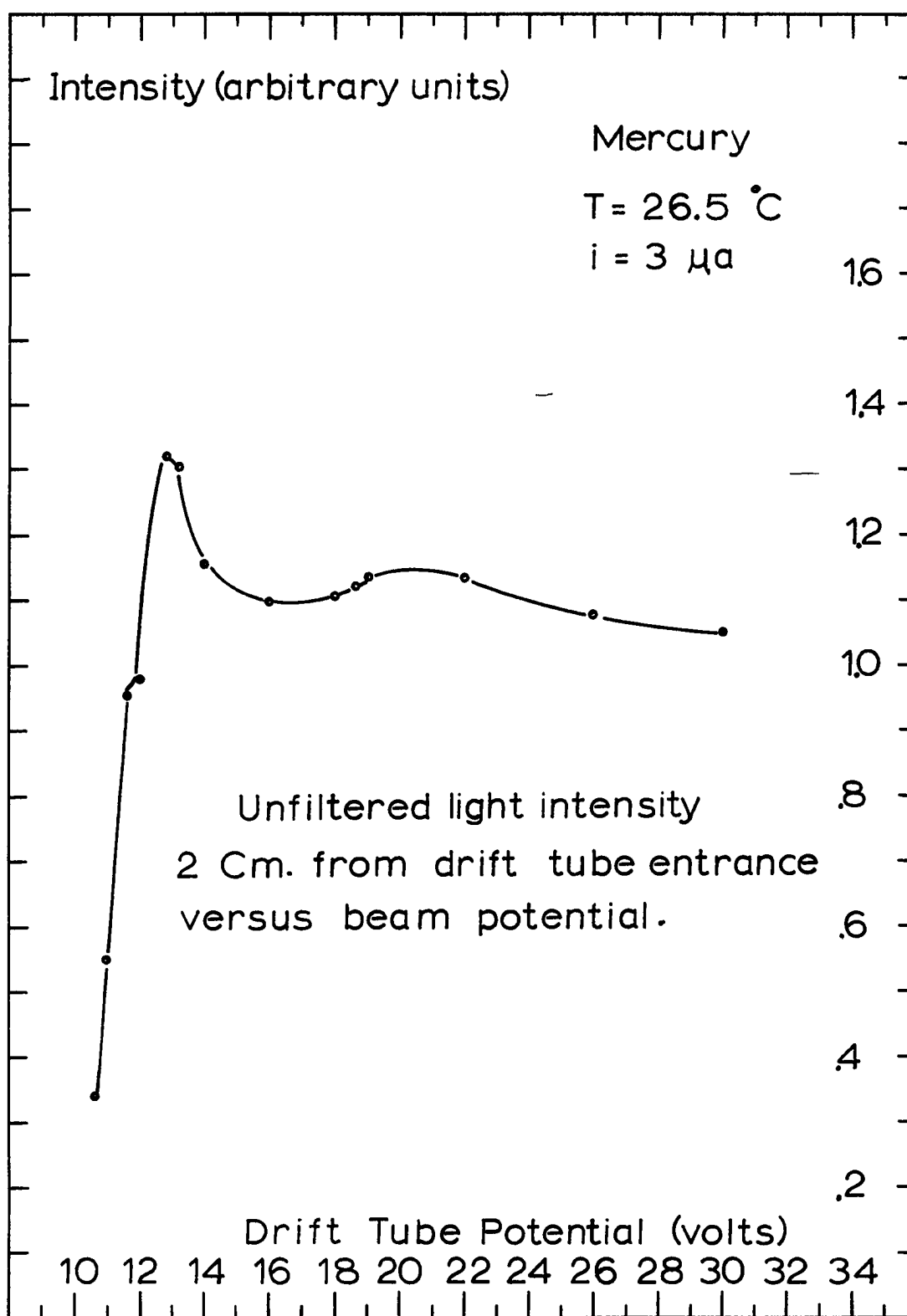


FIGURE 10.2.

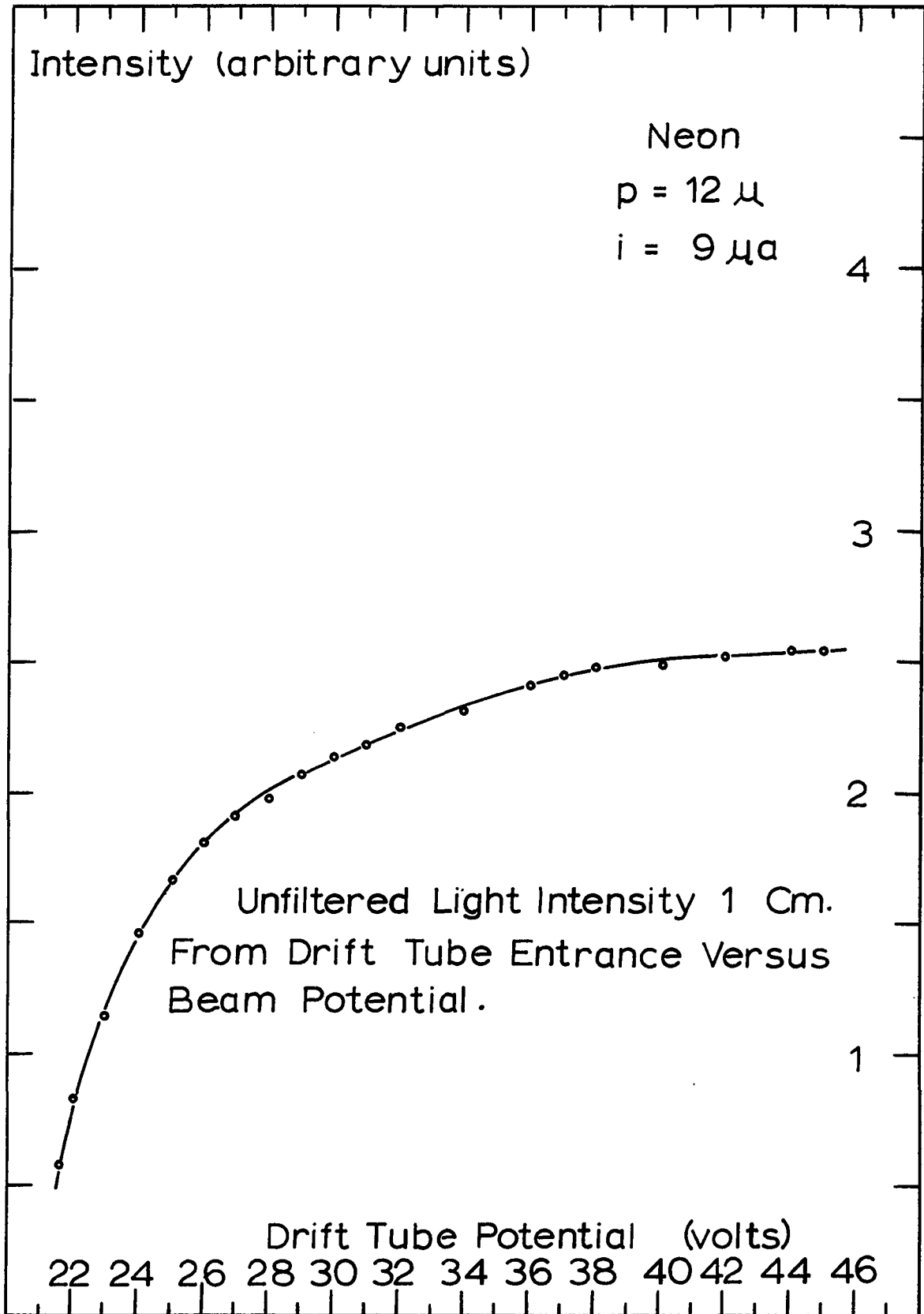


FIGURE 10.3.

16 centimeter length of beam at a voltage as high as 28 volts. At pressures of 17 and 19 millitorr the same length of beam was collimated at beam potentials above 27 volts. Beam broadening was observed in mercury at 3 microamperes current, pressure corresponding to a reservoir temperature of 26°C, for beam potentials a few tenths of a volt below the ionization potential. Ende²⁰ has observed and photographed beam bursting of a two hundred volt beam in hydrogen at one millitorr pressure. The phenomenon appears to be due to insufficient ion production along the beam to provide a net positive space charge in the beam.

The Beam in Helium

Measurements of light intensity of unfiltered helium light versus distance along the beam are shown in Figures 11.8 and 11.9. These measurements were made at a temperature of 24°C (uncorrected), a pressure of 16.6 millitorr and a beam current of 14 microamperes. The effective cross section of the gas to produce the decays observed, is plotted in Figure 12. Measurements of luminosity decay versus distance along the beam, for spectrally filtered light are shown in Figures 15.1 through 15.6. (The curves in Figures 15.1 through 15.6 have not been normalized to one another and were taken at differing photomultiplier voltages. The scales have been shifted by an arbitrary multiplying factor to allow a comparison of the shapes of the decay curves on a common plot. The data is presented in appendix D.) Filters were available to isolate the 4713, 4922, 3889, 5016, 5876 Å helium lines. The 4460 filter transmitted both the 4471 and 4438 Å helium lines. At 28 and 35 volts the

spectral line decays appear exponential along the available beam length and appear to decay at the same rate as the unfiltered light. The decay of all lines observed is more rapid at 28 than at 35 volts. At 50 and 65 volts the decay of the 4713 and 4922 Å lines appear exponential along the available length of beam. The 4922 Å line, at a pressure of 17 millitorr, temperature 27°C, decays by a factor of 1.9 over a 10 centimeter beam path, leading to a cross section for decay of luminosity of that line of $1.1 \times 10^{-16} \text{ cm}^2$ at 65 electron volts beam energy. At 50 electron volts energy the luminosity of the 4922 Å line drops by a factor of 1.85 over a 9 centimeter beam path, leading to a cross section of $1.25 \times 10^{-16} \text{ cm}^2$ at the same pressure and temperature. The 4713 Å light intensity decays by a factor of 1.73 over a path of 8 centimeters at a pressure of 19 millitorr, temperature 29°C, leading to a cross section of $1.1 \times 10^{-16} \text{ cm}^2$ at 65 electron volts beam energy. The decay of the spectral lines 5016, 5876 Å and the mixture of 4471 and 4438 Å lines is not even approximately exponential at beam energies of 50 and 65 electron volts. The cross sections corresponding to the luminosity decays are computed from the relation

$$Q = \left(\frac{10^{-16}}{3.54} \right) \left(\frac{T + 273.2}{273.2} \right) \left(\frac{1000}{P} \right) \frac{\ln (U_{jk}(x) / U_{jk}(x+d))}{d} \quad (5.1)$$

where T is the centigrade gas temperature, P is the gas pressure in millitorr, $U_{jk}(x)$ is the light intensity at x per unit current as defined in equation (4.3), d is the scanned path length in centimeters and Q is the cross section in cm^2 .

The Beam in Mercury

Luminosity versus distance measurements of unfiltered light from a 3 microampere beam in mercury vapor, with the mercury reservoir at $26.5 \pm 1^\circ\text{C}$, are shown in Figure 16. These measurements were taken over a period of approximately eight hours. At the end of the measurement run a separate measurement was taken of the light transmitted through a filter versus distance, at a beam potential of 12.8 volts. The latter measurement agreed with the decay curve taken at the same voltage several hours earlier and indicates that no appreciable pressure change occurred during the measurements.

The decay curves taken at 10.6 and 11 volts beam potential show exponential decay with distance. The decay curves taken above 12 volt beam potential deviate from exponential decay, the deviation becoming more marked as beam potential increases. The lengths for luminosity to decrease by one e-fold are 4.0 centimeter at 10.6 volts and 4.9 centimeter at 11 volts. If the number density of mercury atoms is computed under the assumption that the mercury reservoir temperature determines the mercury pressure to be the equilibrium vapor pressure of mercury at that temperature and the mercury atom number density can be computed using the ideal gas law at this pressure, 2.1 millitorr, and temperature, a cross section for decay of luminosity of $37 \times 10^{-16} \text{ cm}^2$ is obtained at 10.6 volts and $30 \times 10^{-16} \text{ cm}^2$ is obtained at 11 volts. At 30 volts beam potential the decay is less rapid than would be caused by a cross section of $14 \times 10^{-16} \text{ cm}^2$, corresponding to the steepest rate of decay measured at 30 volts potential.

The decays in mercury at potentials near the ionization potential do not show the type of deviation from exponential decay that is observed in helium and neon. This may be due to the large ionic mass and ionization cross section of mercury giving rise to a larger transverse potential holding the beam together. The appearance of elbows in the decay curves above 12.8 volts potential and their absence below 12 volts suggest that stage excitations may be occurring. The elbows do not appear in low energy observations of the beam in neon or helium. Elastic scatter is strongly forward²⁴ in mercury near the ionization energy and elastic backscatter would not account for the elbows below 14 volts, though a backscattered component might be present at 30 volts. The rate of the decay with distance and the appearance of elbows in the decay curves taken together are in disagreement with the conclusions of Koppius and Duffendack. If stage excitation does not, in fact, occur much faster luminosity decay should appear than is actually observed at 30 volts beam potential, to account for the size of the cross section, $1.5 \times 10^{-14} \text{ cm}^2$ observed by them. If stagewise excitation does occur then the decay would not necessarily be as rapid as would be the case when no stage processes occurred but this would be in conflict with Koppius' probe measurements. In either case the present results are in disagreement with those of Koppius and Duffendack.

The Beam in Neon

Semilogarithmic plots of unfiltered light intensity versus distance along the beam are shown in Figures 11.1 through 11.7. Except for beam energies within three volts of the ionization energy

the initial decay appears to be exponential within one e-folding of intensity. At larger distances the decay steepens. Figure 14 is a photograph of the beam in neon at 3.8 millitorr pressure, 14 microampere current. The same exposure time was used at all voltages.

Light intensity is measured at 23 millitorr pressure for a 33 volt, 11 microampere beam, for filtered light and for light filtered through blue and orange transmitting wratten filters and through a red broadband interference filter. The blue, orange and red regions of the spectrum appear to decay at the same rate as the unfiltered light (weighted by photomultiplier spectral response) at this beam potential. The measurements are shown in Figure 11.

The cross section determined by the luminosity decay is plotted versus beam potential in Figure 13, for runs at 4.9, 12.1 and 23.2 millitorr.

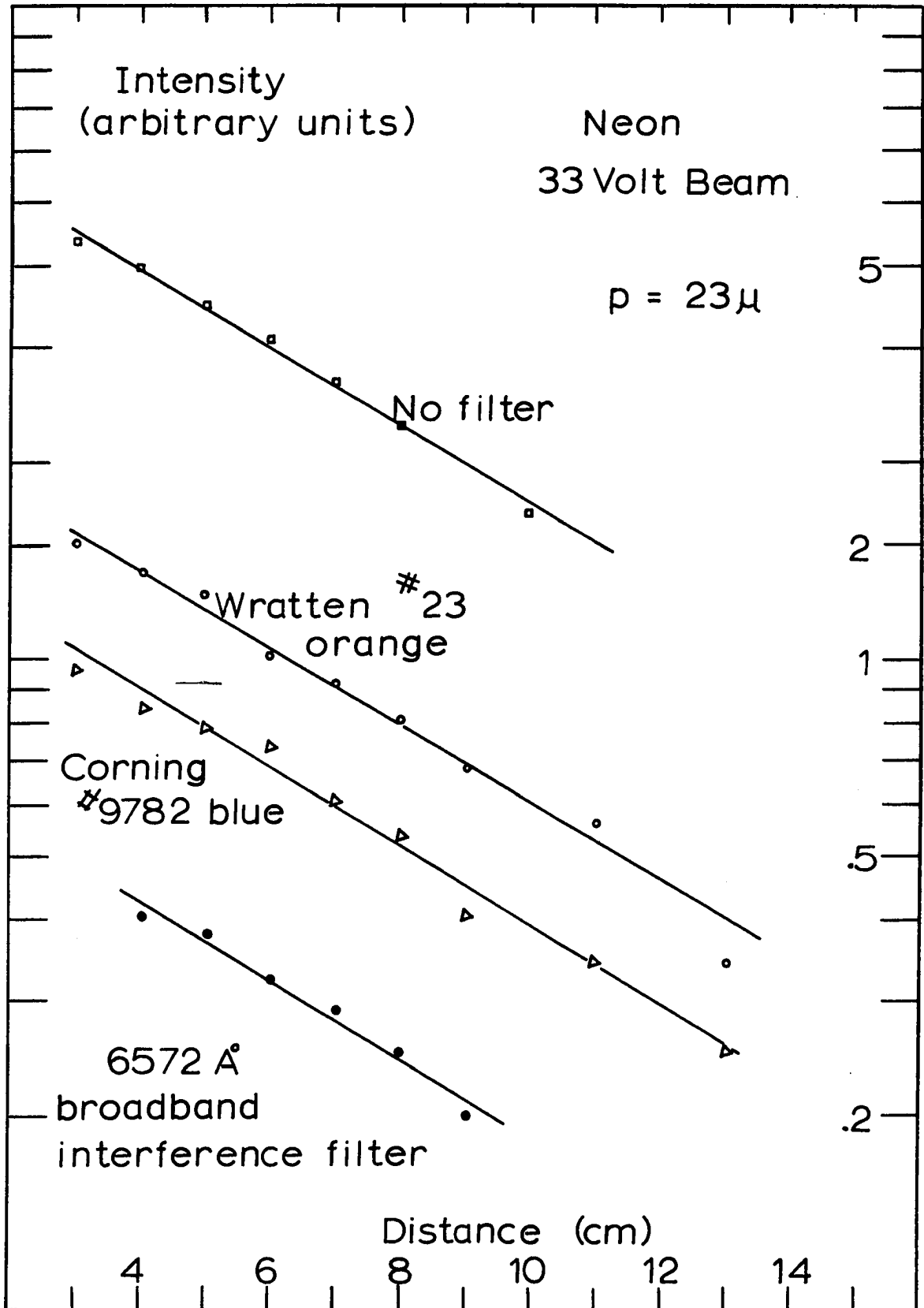


FIGURE 11.1.

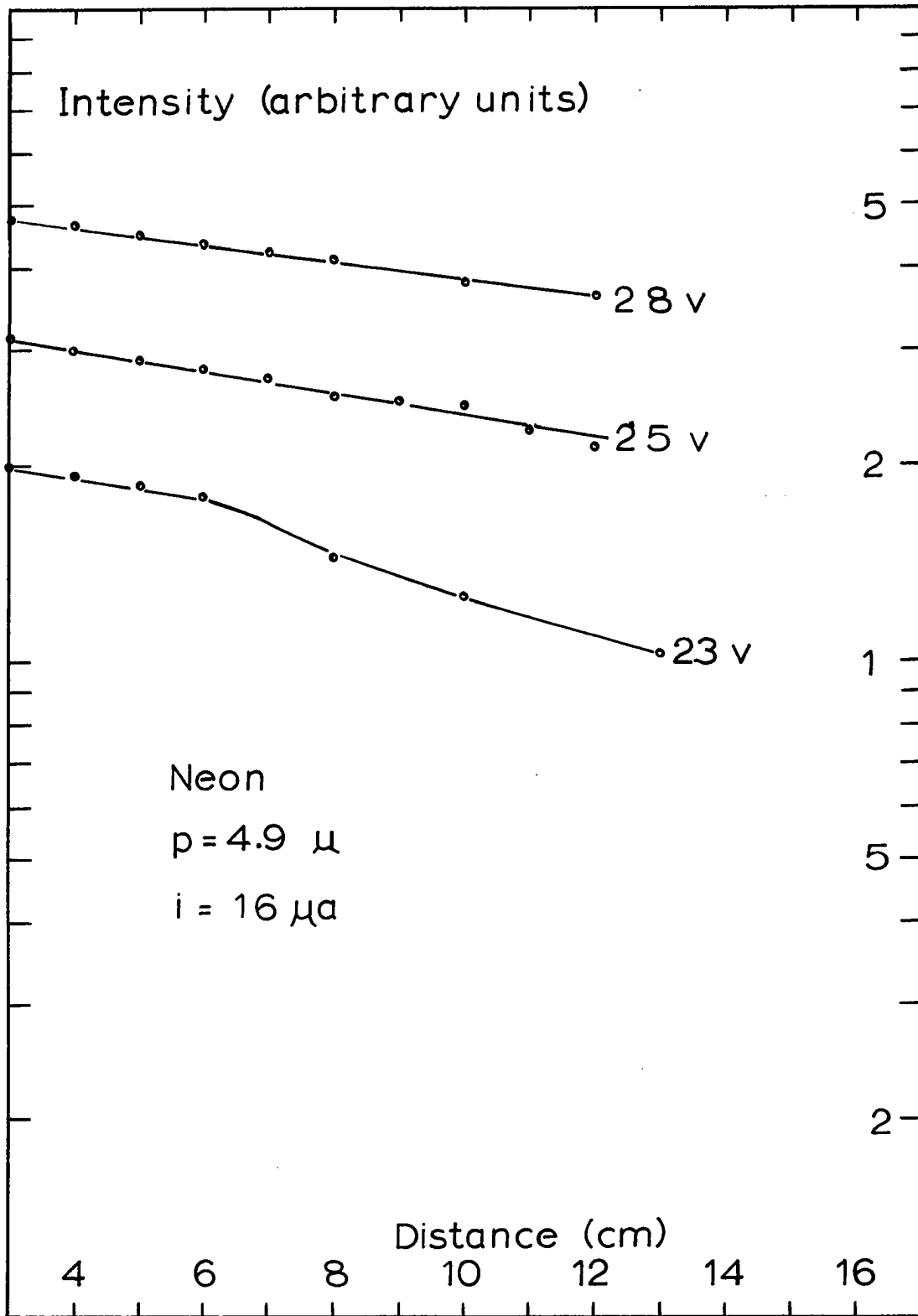


FIGURE 11.2.

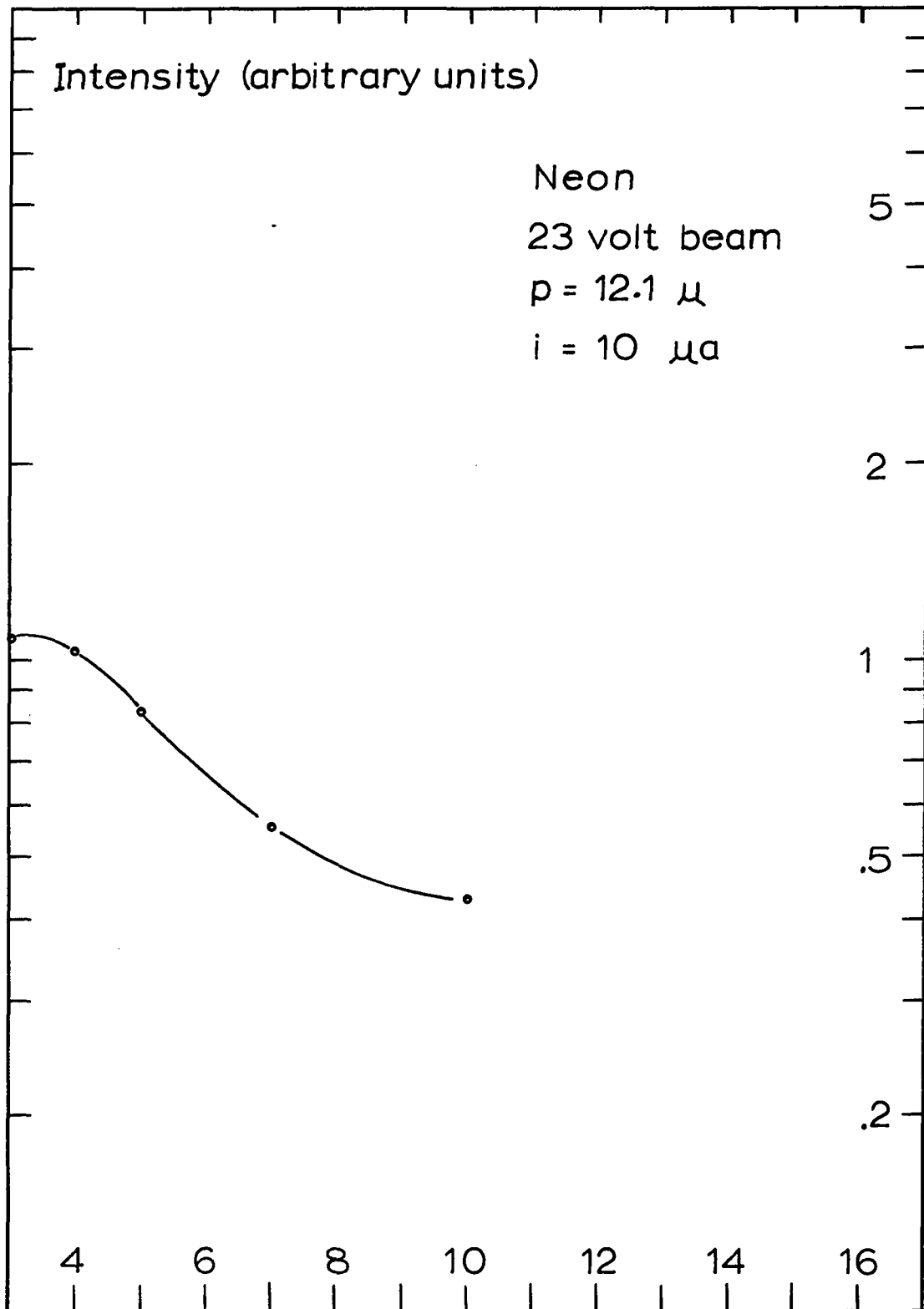


FIGURE 11.3.

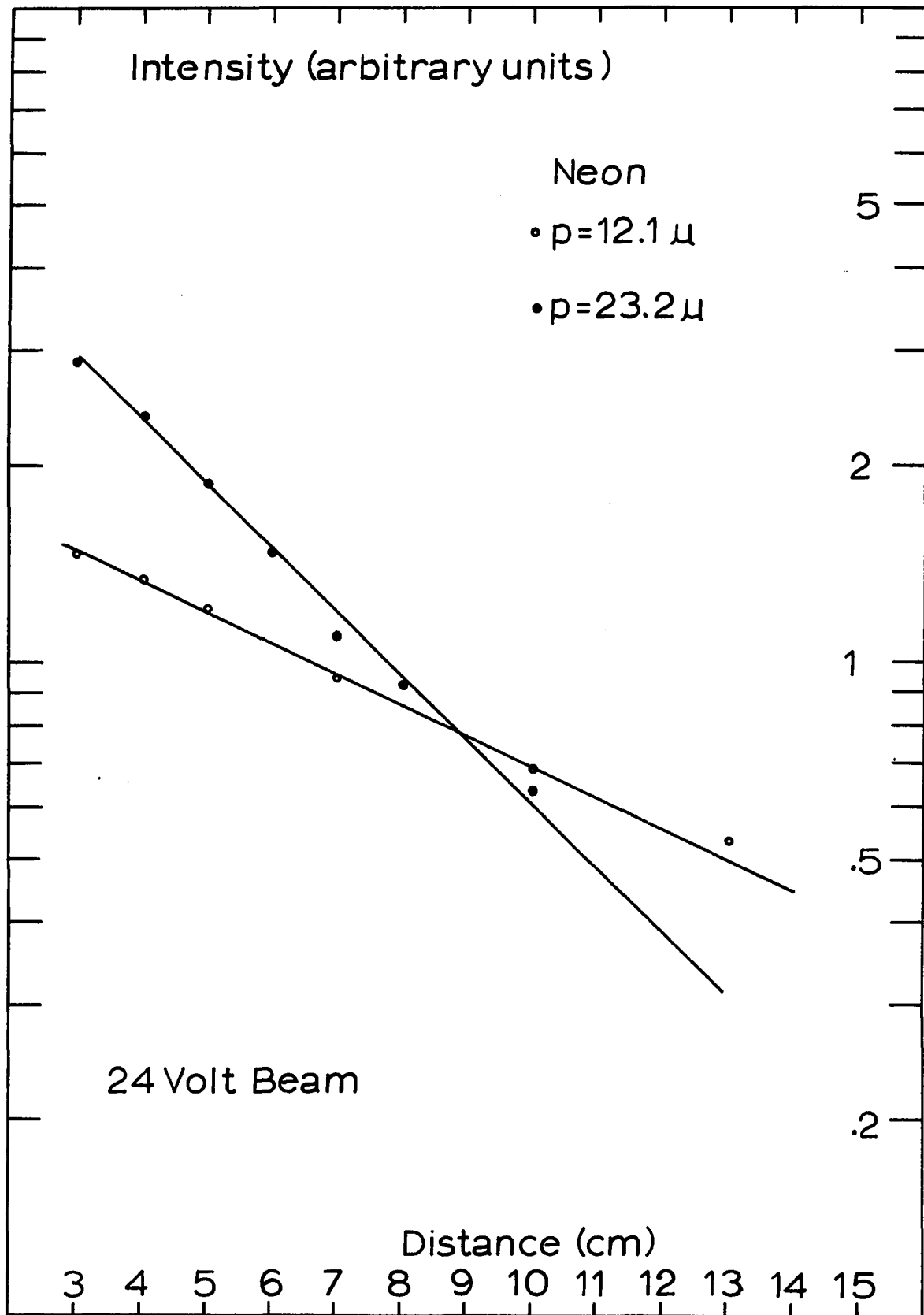


FIGURE 11.4.

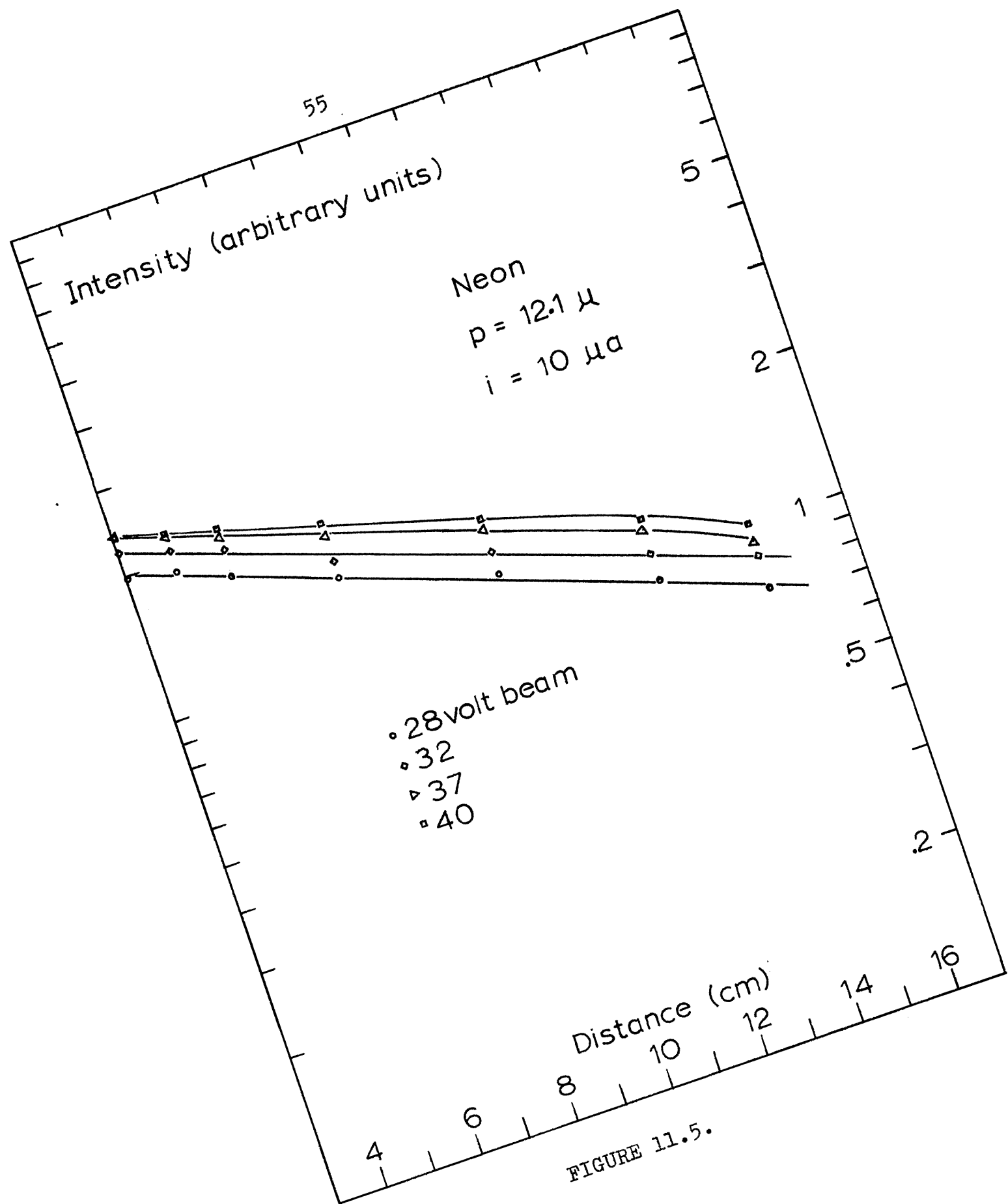


FIGURE 11.5.

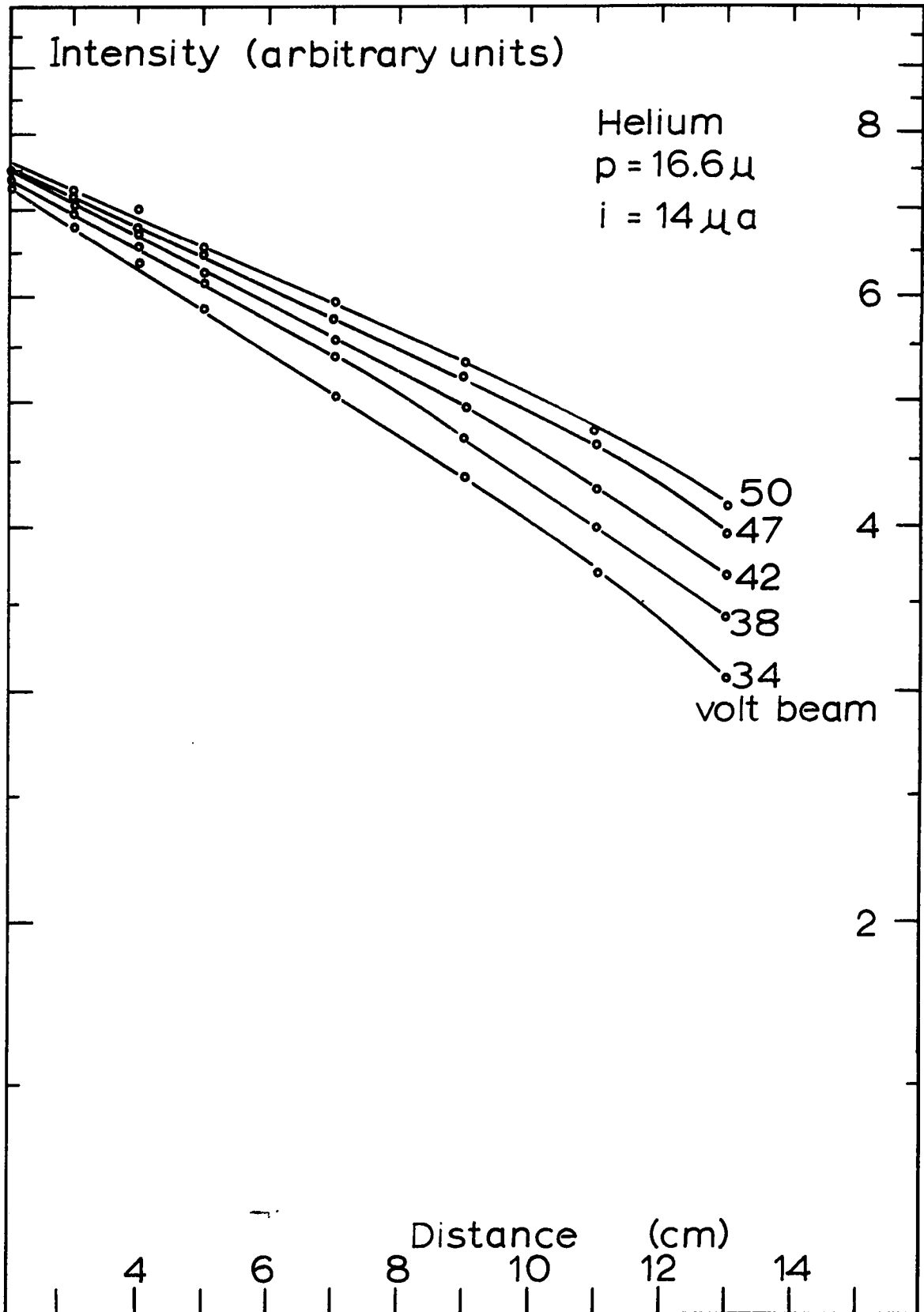


FIGURE 11.6.

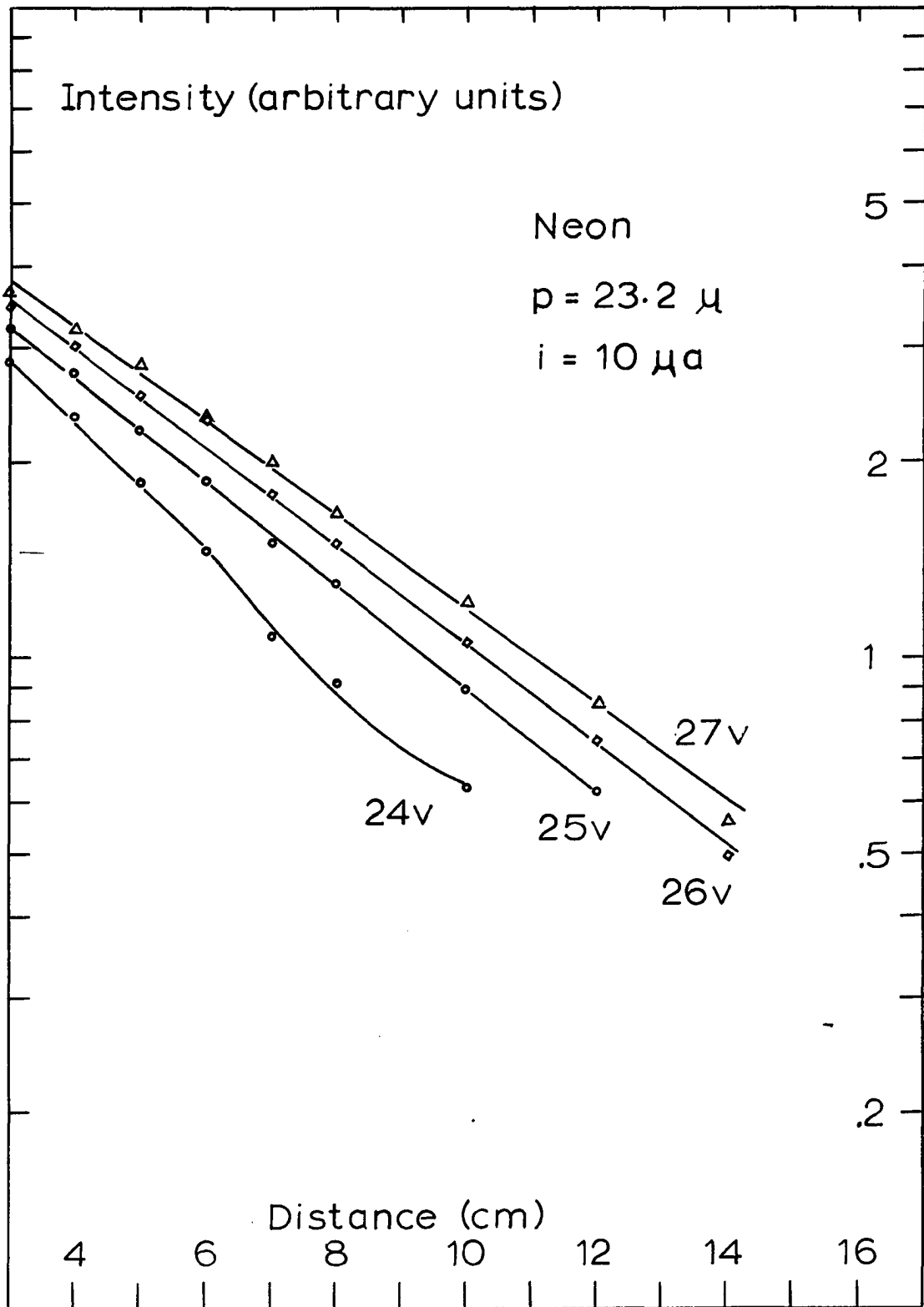


FIGURE 11.7.

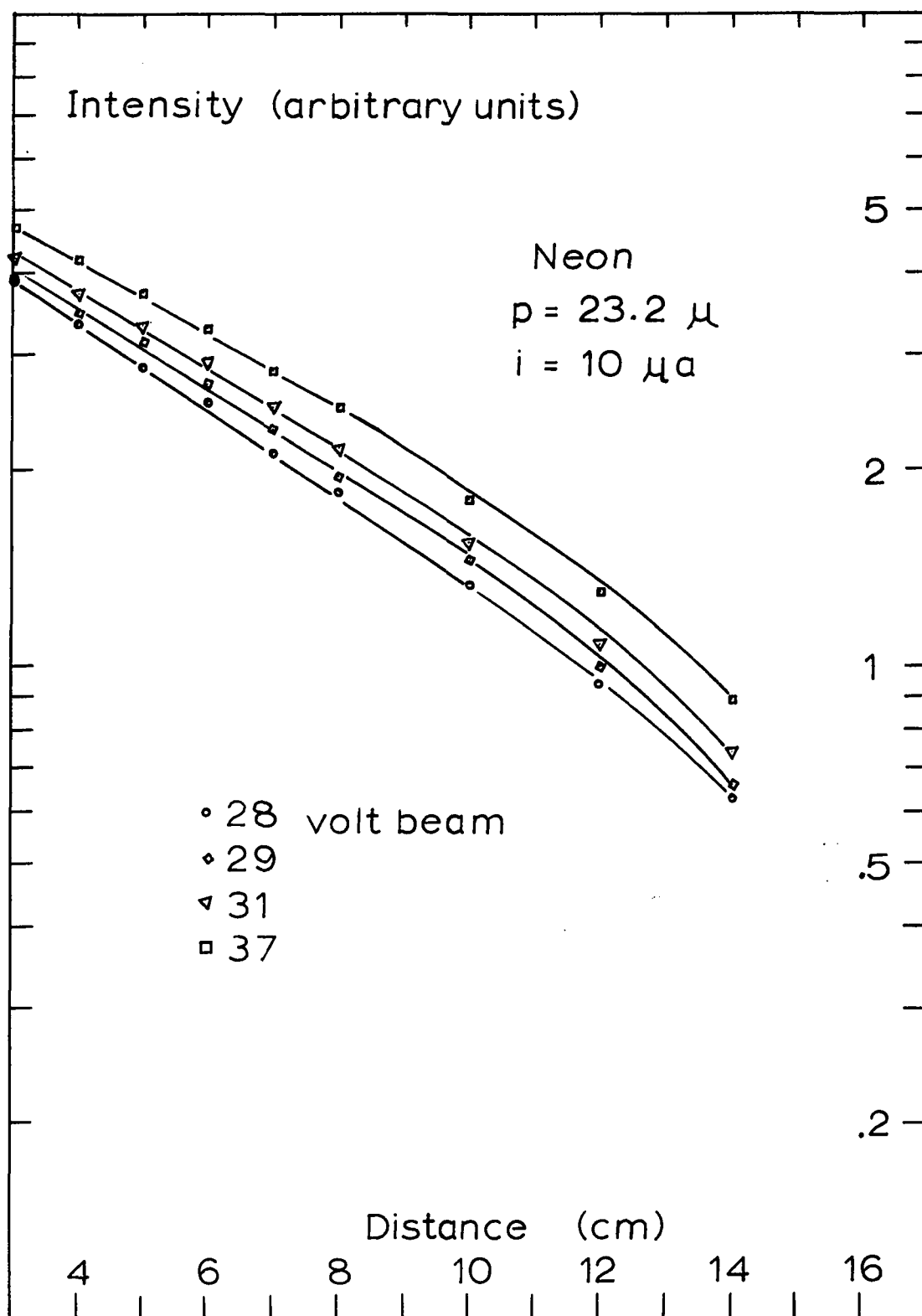


FIGURE 11.8.

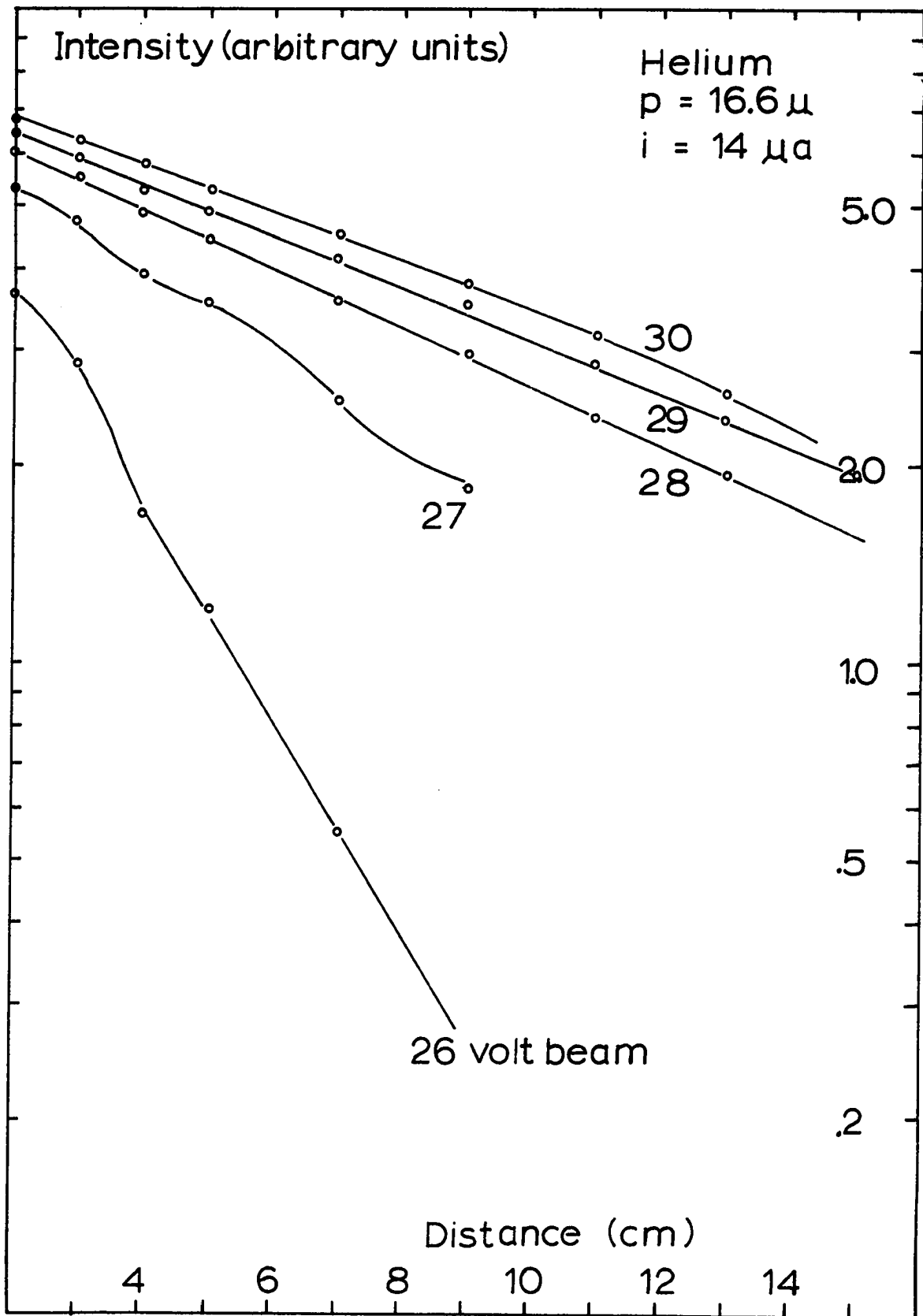


FIGURE 11.9.

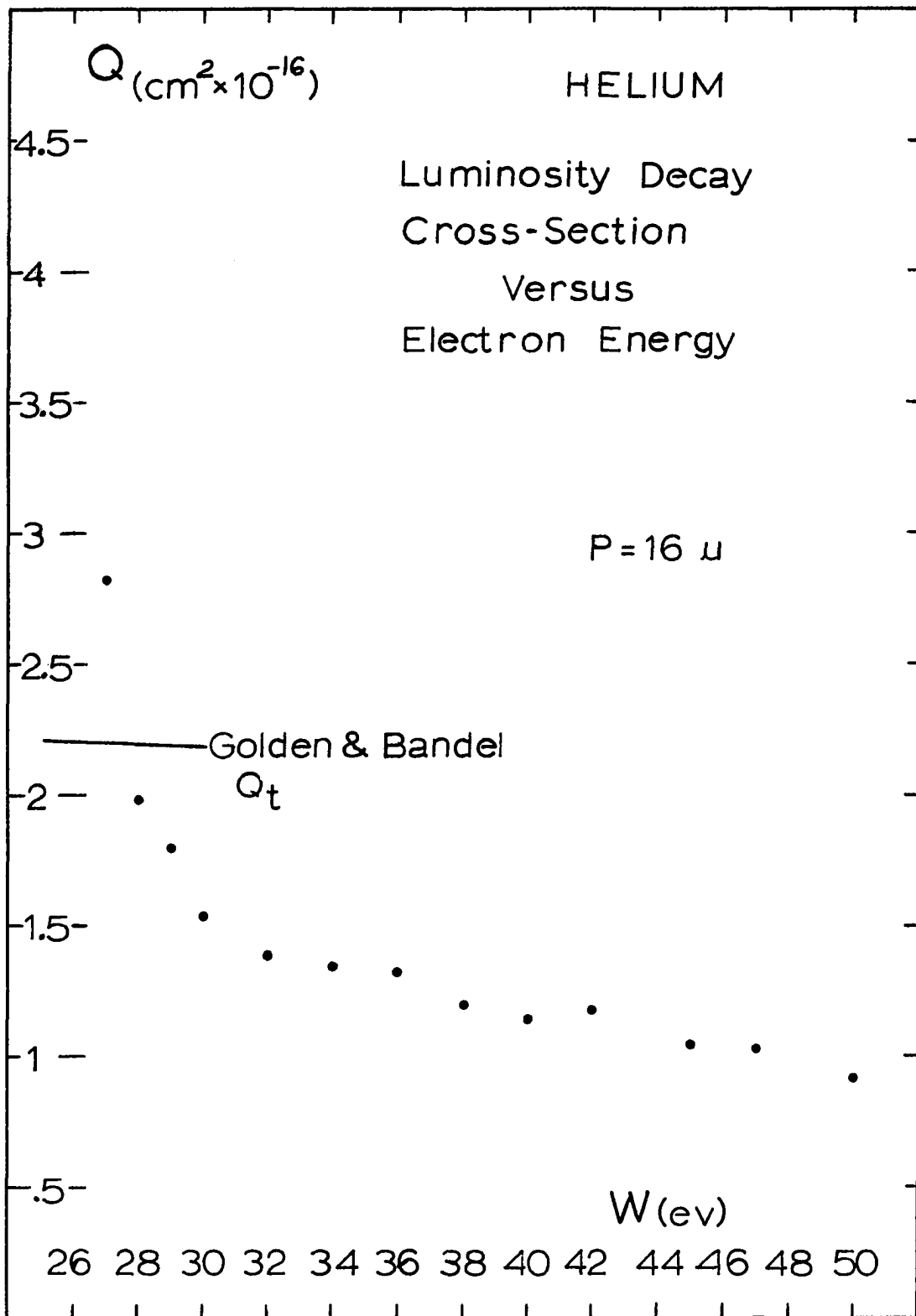


FIGURE 12.

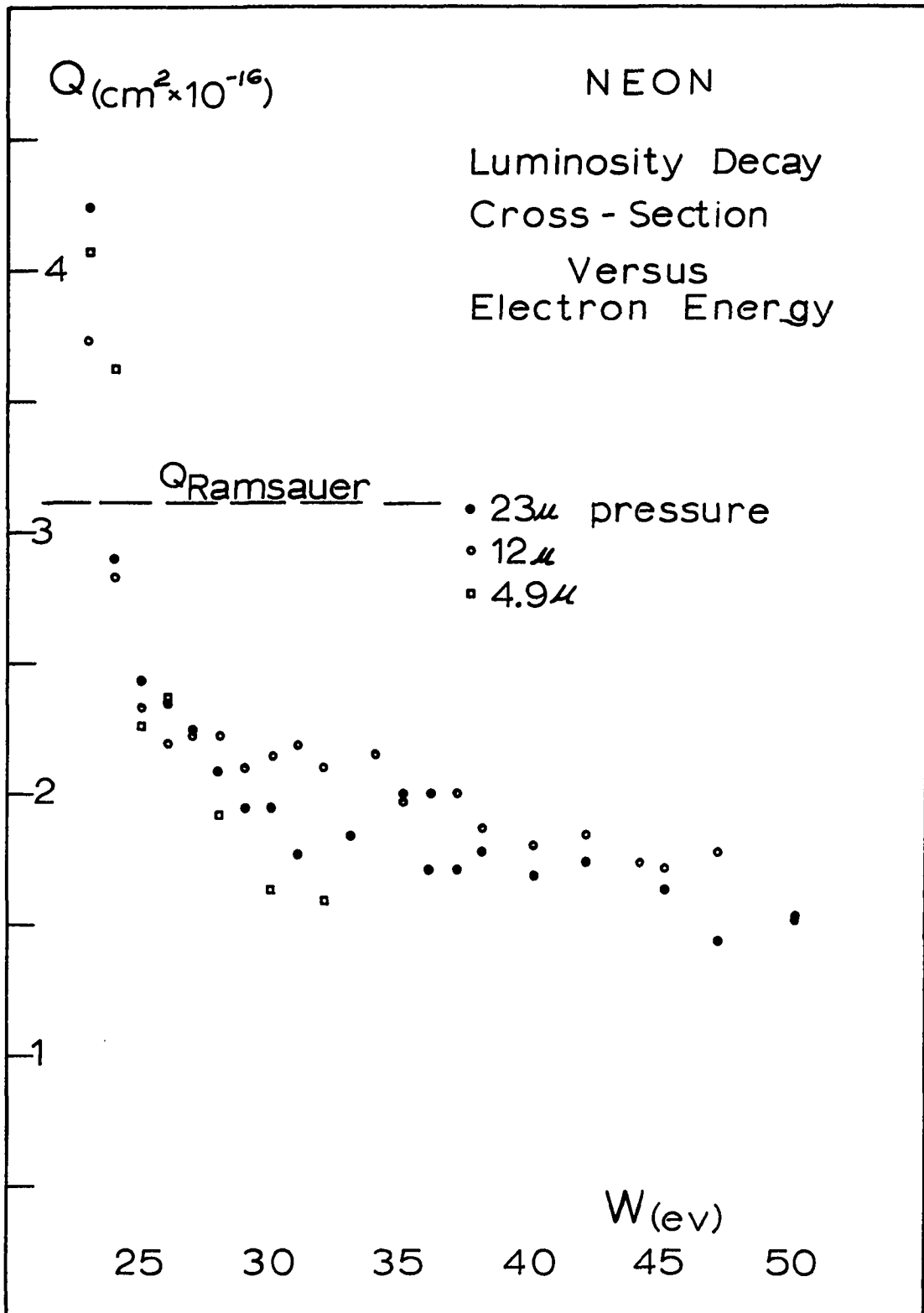
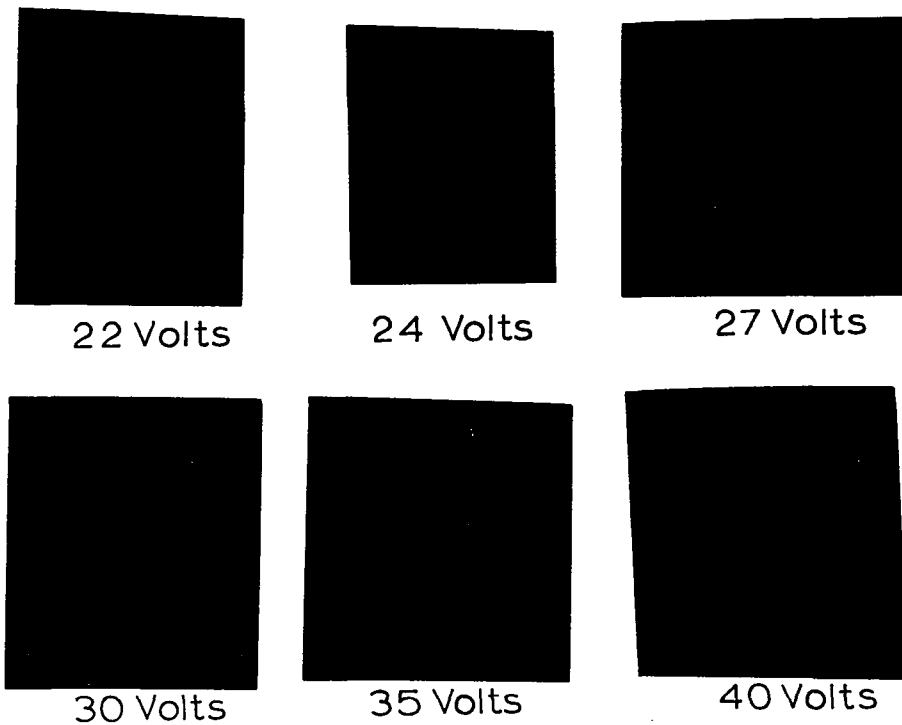


FIGURE 13.

FIGURE 14. THE ELECTRON BEAM IN NEON.



22 Volts

24 Volts

27 Volts

30 Volts

35 Volts

40 Volts

Electron Beam In Neon, $i=14 \mu\text{A}$, $p=3.8 \mu$

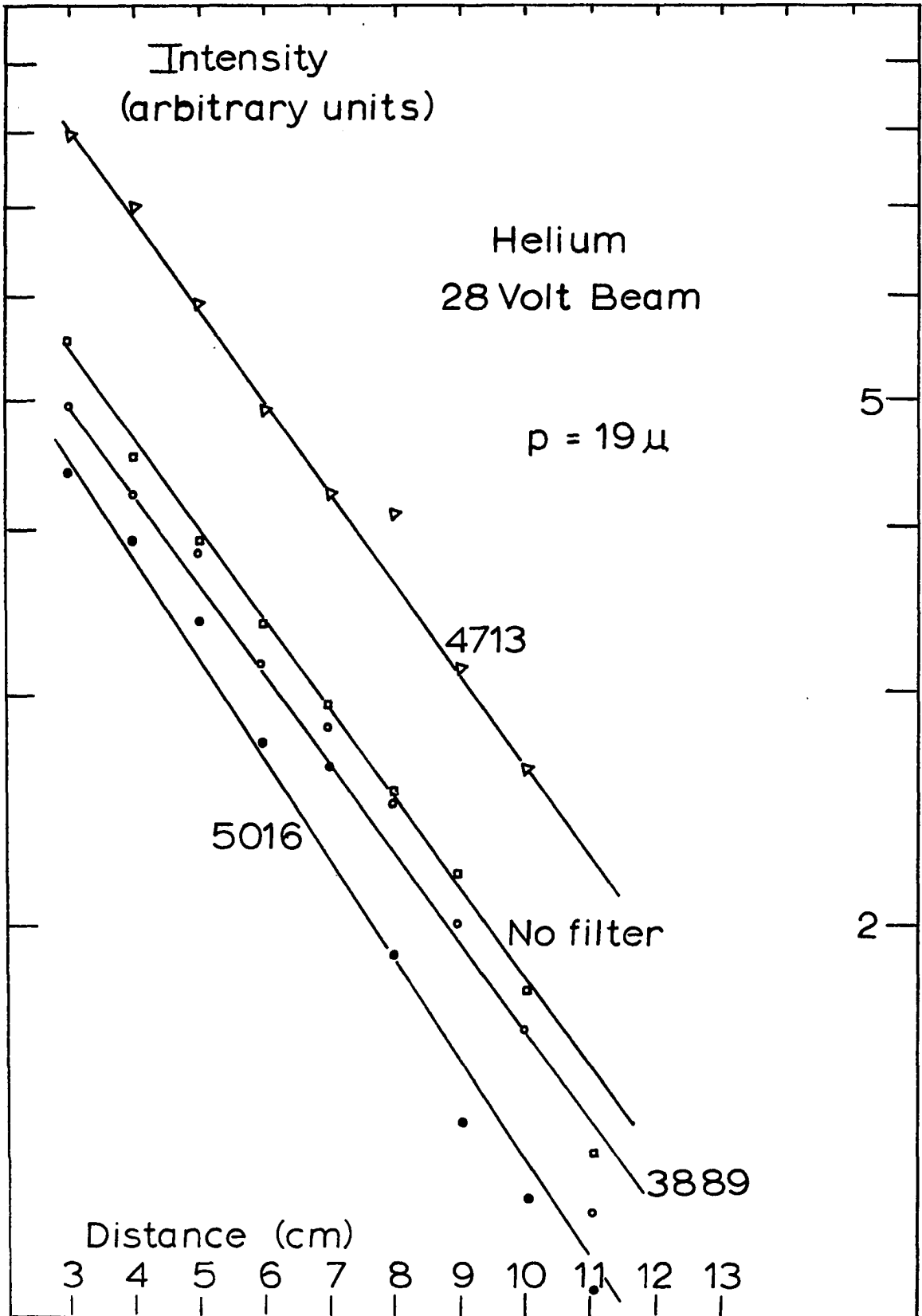


FIGURE 15.1.

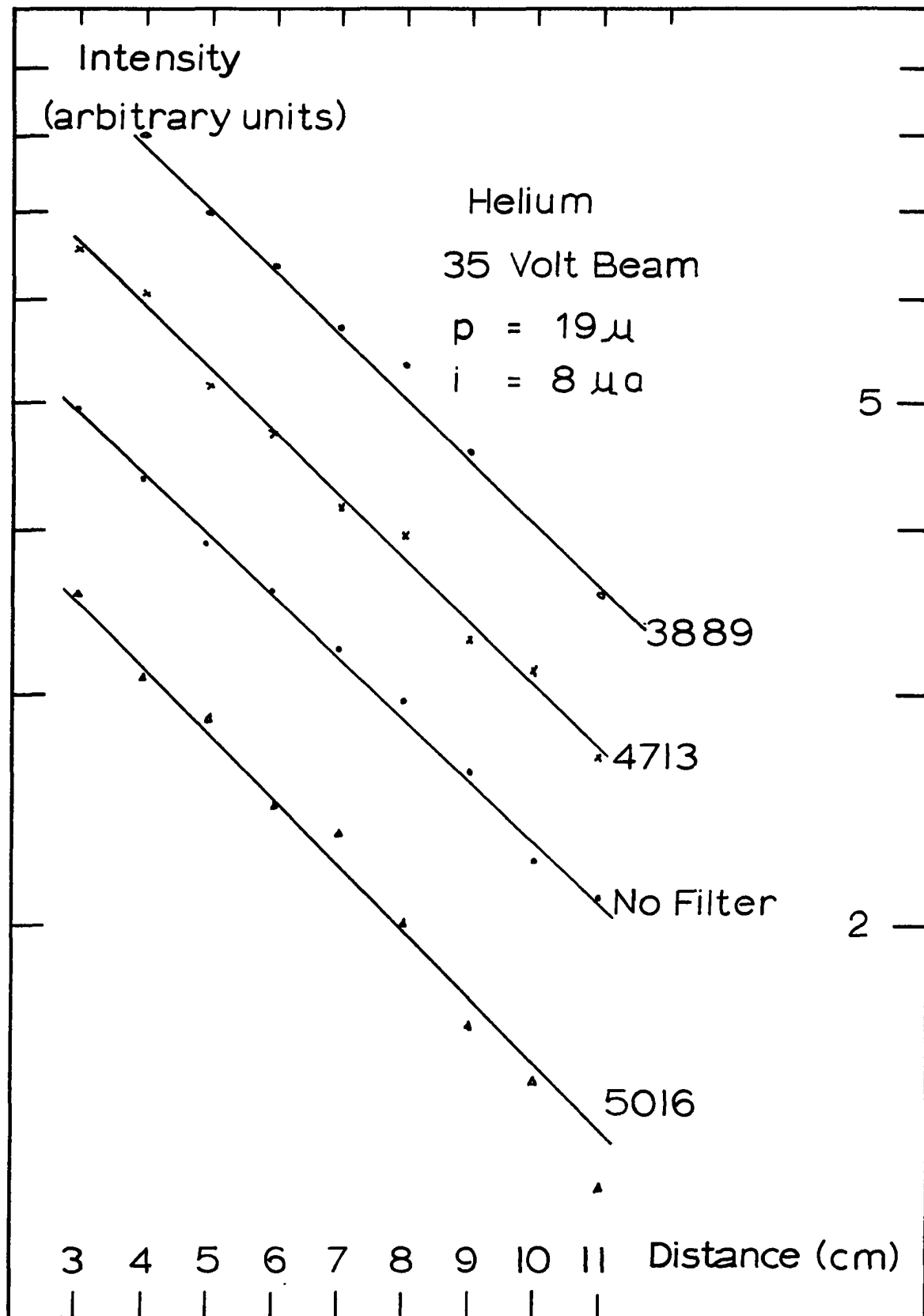


FIGURE 15.2.

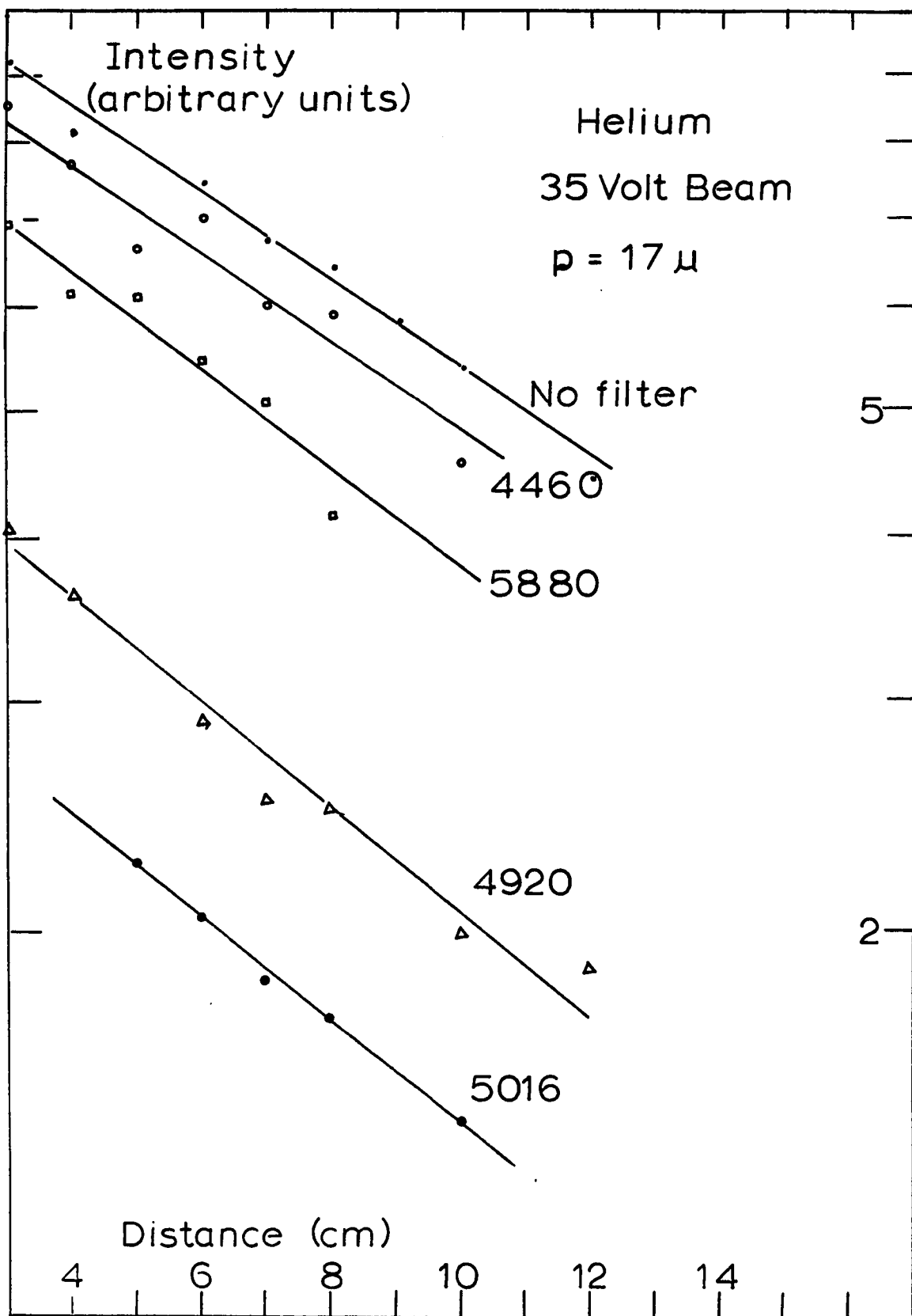


FIGURE 15.3.

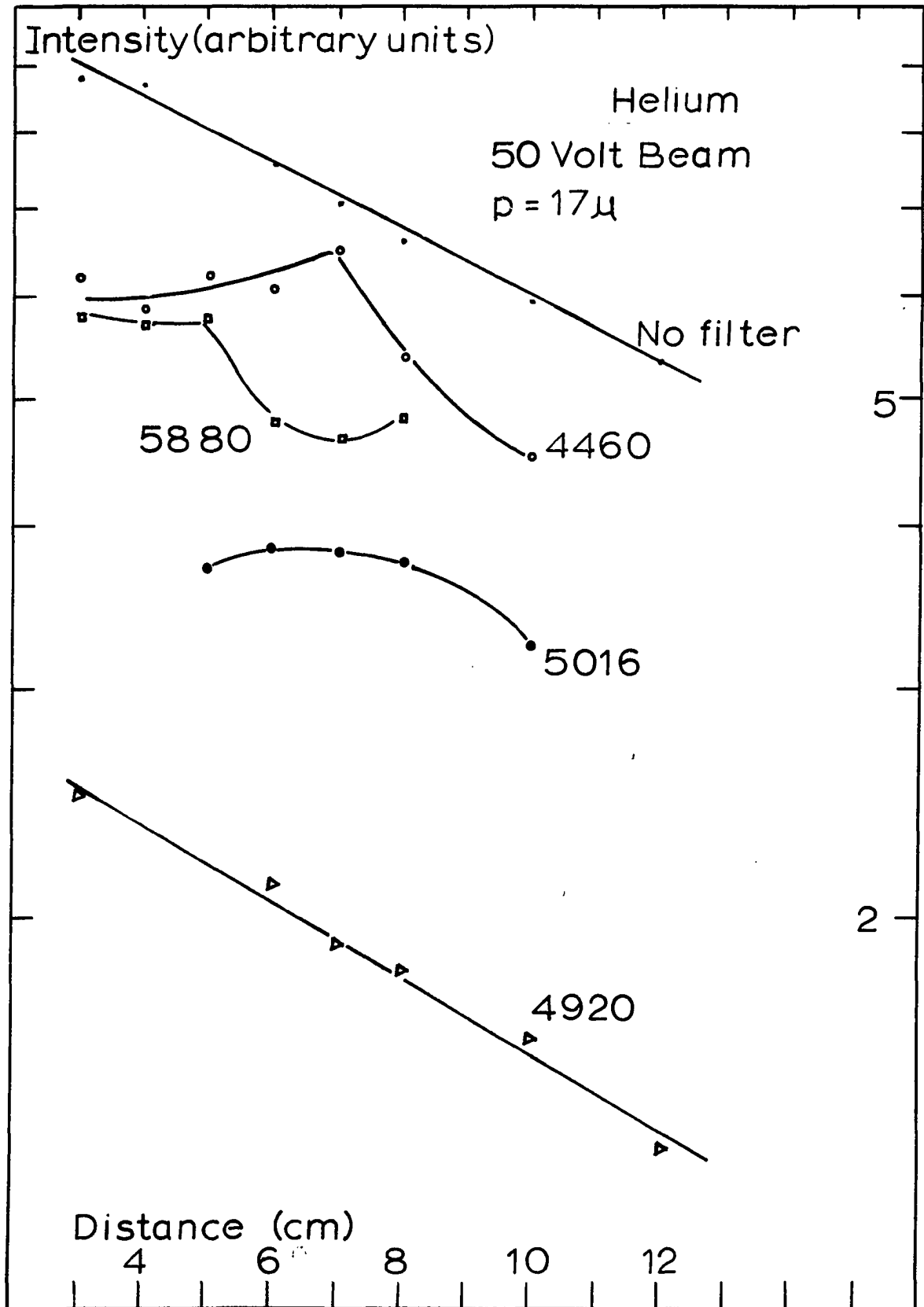


FIGURE 15.4.

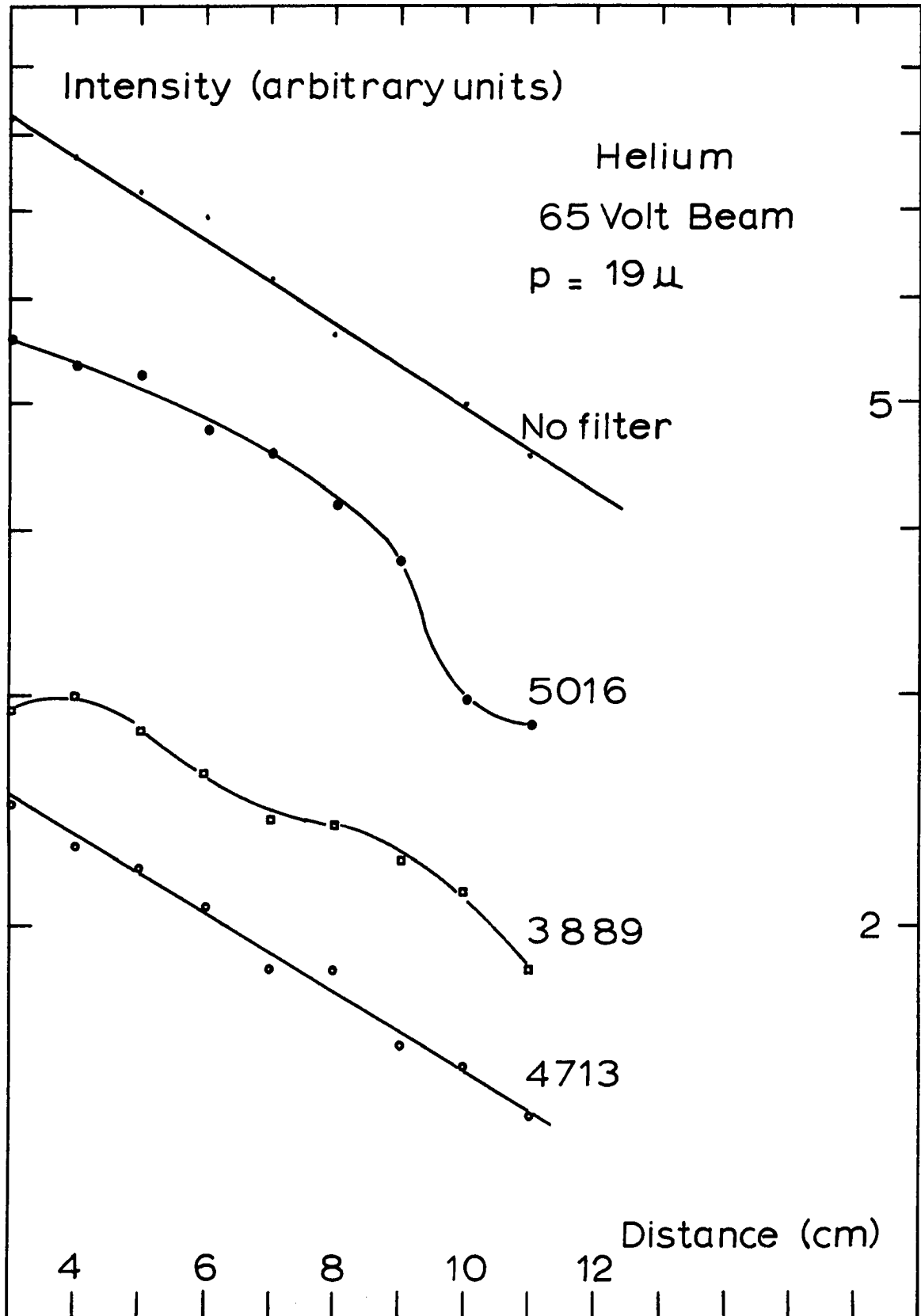


FIGURE 15.5.

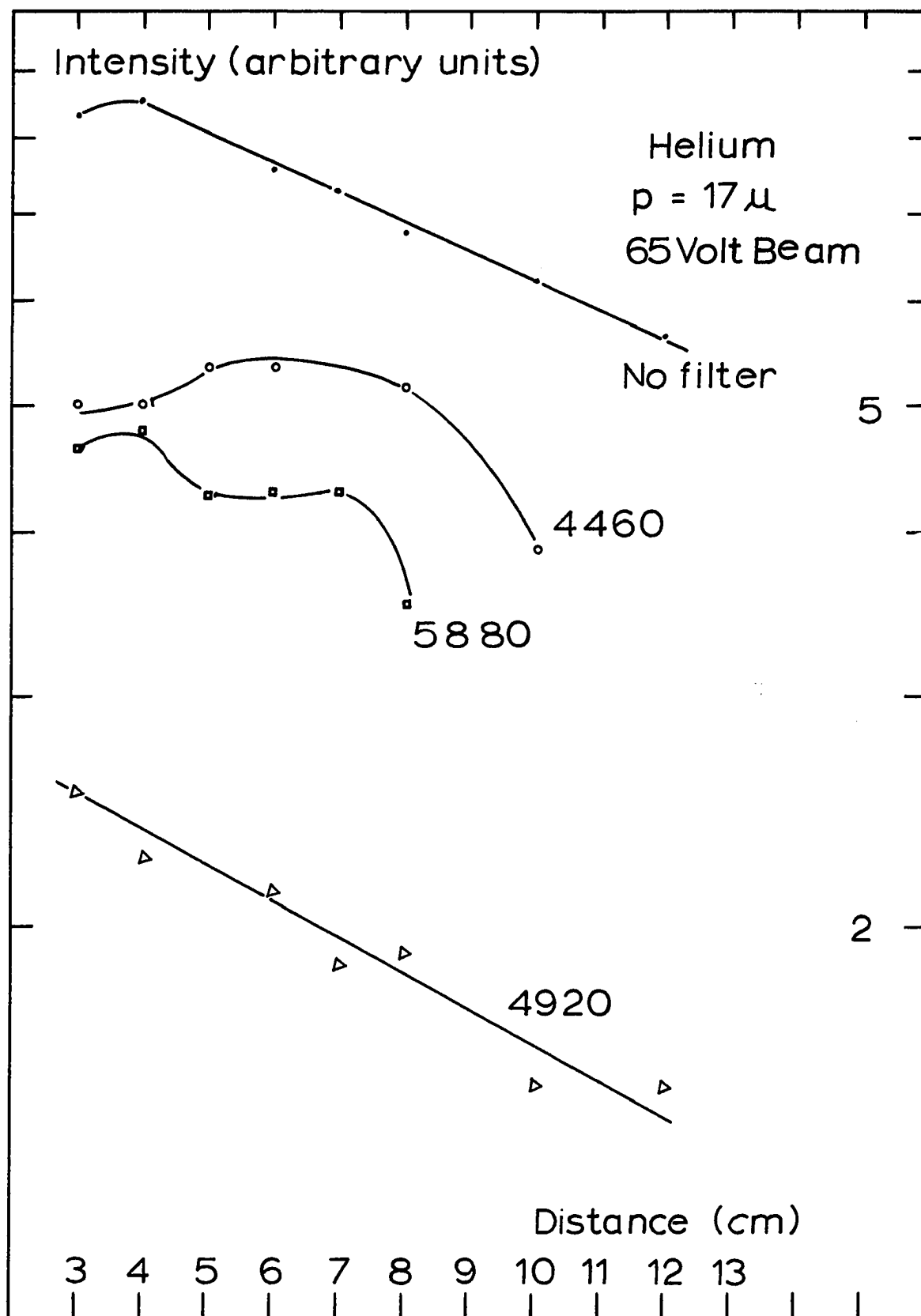


FIGURE 15.6.

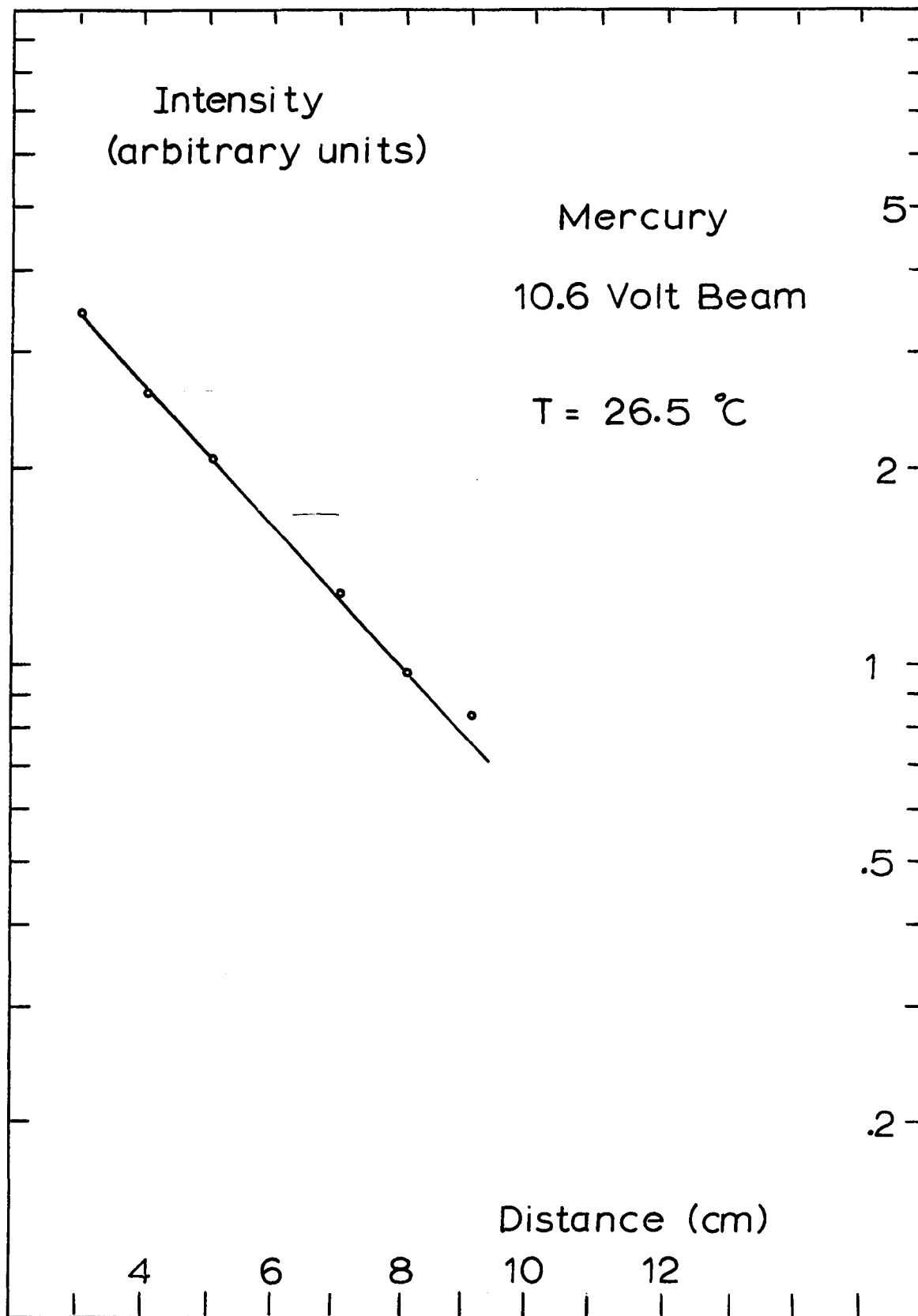


FIGURE 16.1.

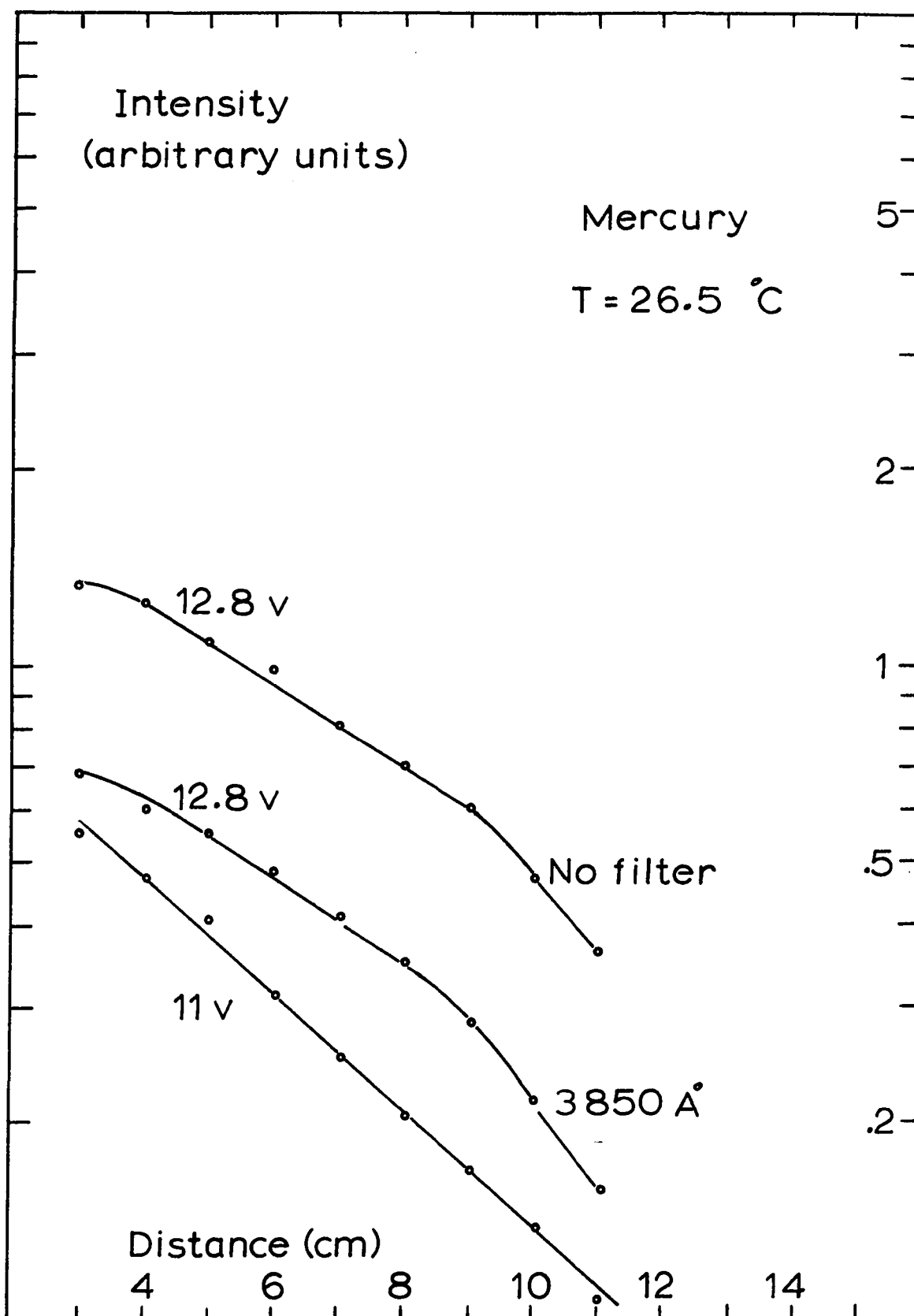


FIGURE 16.2.

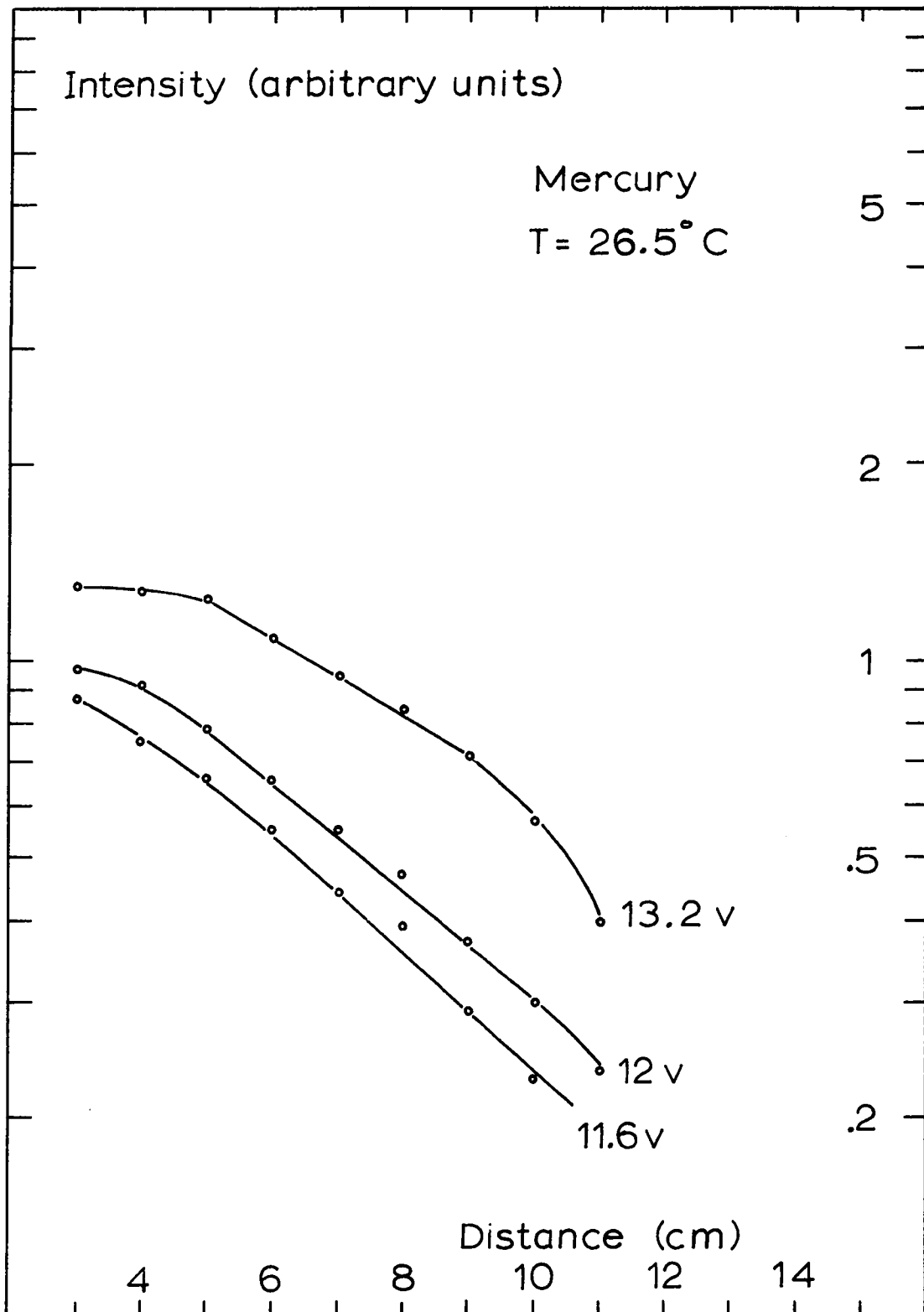


FIGURE 16.3.

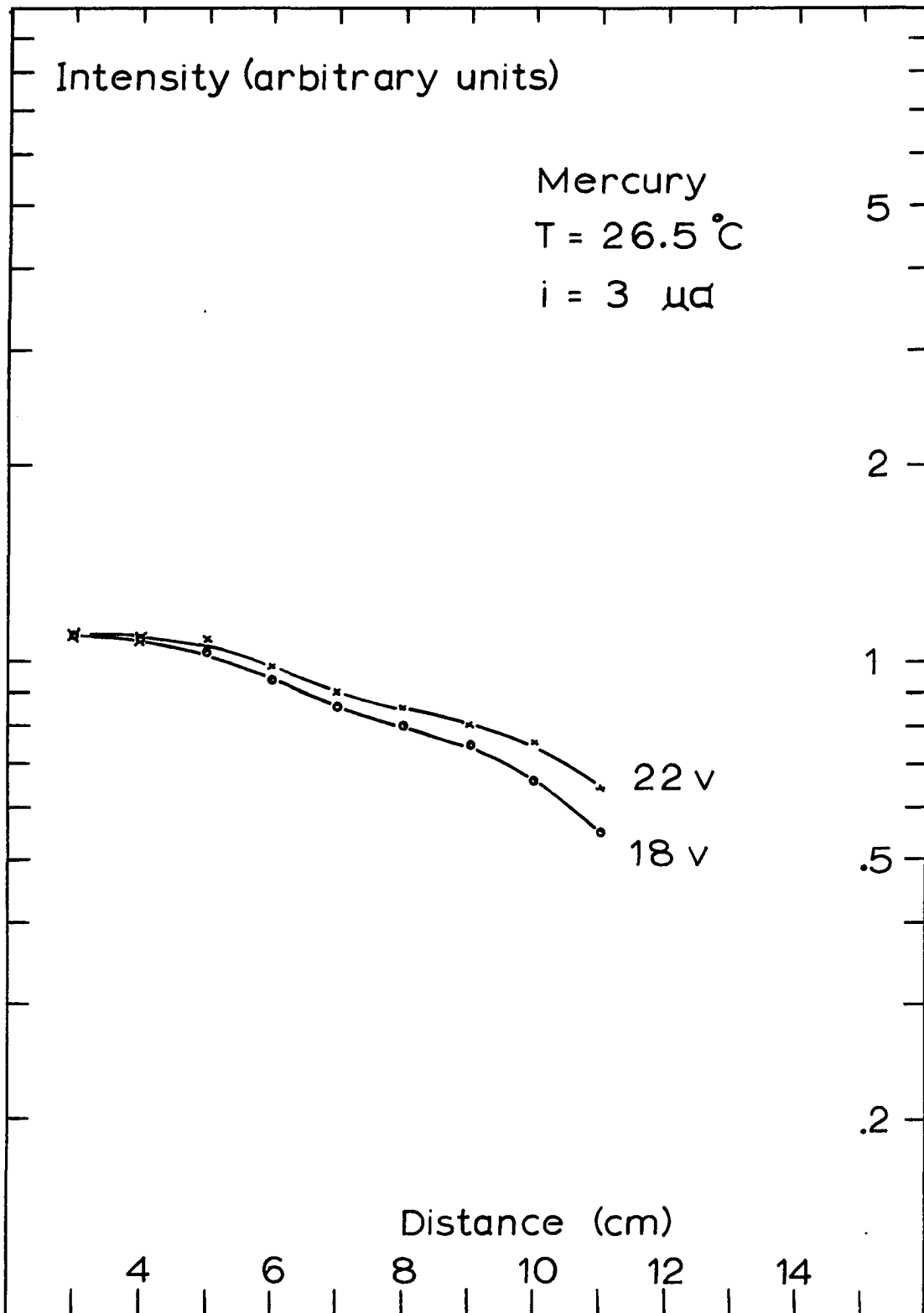


FIGURE 16.4.

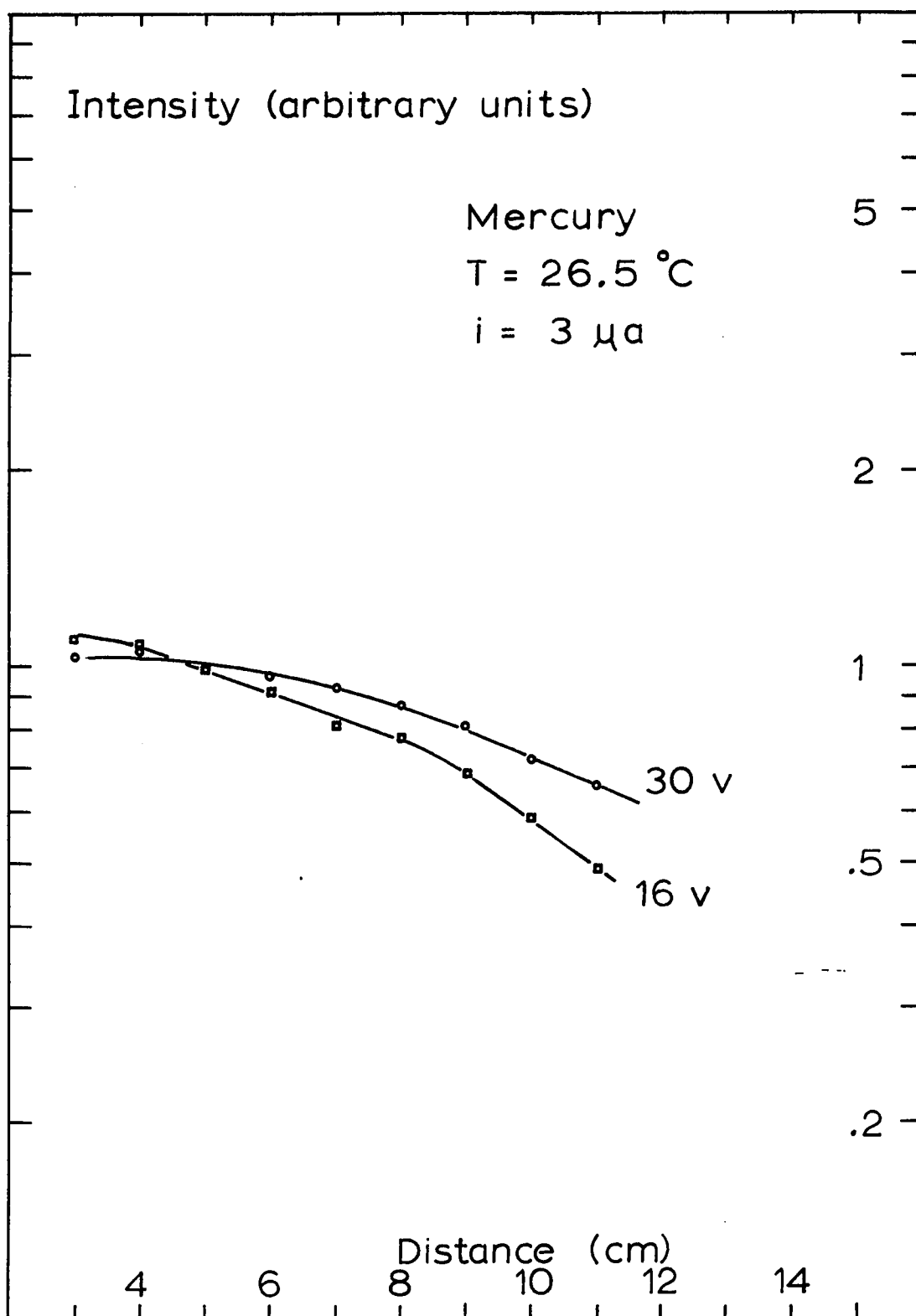


FIGURE 16.5.

CHAPTER IV
DISCUSSIONS OF OBSERVATIONS, CONCLUSIONS

The Beam in Neon and Helium

At beam energies more than two volts above the gas ionization energy the luminosity decays in helium and neon appear to be exponential near the cathode but show a greater steepening in decay rate, at distances greater than corresponds to an e-fold decrease of light intensity. With an electron energy within two volts of the gas ionization energy deviations from exponential decay appear. The cross sections as determined by decay of luminosity, shown in Figures 12 and 13 are, except within two electron volts of the ionization energy, smaller than the total cross sections for collision determined by Ramsauer type experiments and appear in general to decrease with increasing beam energy. The luminosity decay cross sections in the energy range 28 to 35 eV are $1.2 \times 10^{-16} \text{ cm}^2$ for helium and $1.8 \times 10^{-16} \text{ cm}^2$ for neon. These are large compared to the cross sections obtained by McClure¹¹ and by Maier-Leibnitz.⁹ The luminosity decay cross section of $1.2 \times 10^{-16} \text{ cm}^2$ in helium is one fourth that obtained by Ornstein and Elenbaas¹² in their measurements of luminosity decay, at 30 and 36 eV beam energy, 100 millitorr pressure. The cross sections obtained in helium are large compared to the sum of the peak cross sections for

excitation of low lying states plus ionization cross section plus an extrapolated cross section sum for excitation of high lying levels of $1S, 1P, 1D, 3S, 3P, 3D$ spectral series. The sum of the peak values of excitation cross sections of 2-5 $1S, 3-4 1P, 2-3 3P, 3-6 1D, 3-6 3D, 2-5 3S$ helium states at low pressure as obtained by St. John, Miller, Lin¹³ and Holt and Krotkov¹⁴ is $1.67 \times 10^{-17} \text{ cm}^2$. The excitation cross section for 2 P excitation at 35 eV energy is $.47 \times 10^{-17} \text{ cm}^2$ according to the calculation of Vainshtein and Dolgov on the basis of the strong coupling approximation neglecting exchange. For electron energies below 40 eV the cross section for ionization of helium by electron impact is less than $1.7 \times 10^{-17} \text{ cm}^2$. The sum of these values is $3.84 \times 10^{-17} \text{ cm}^2$. Contributions to excitation from levels of higher principal quantum number, of the series mentioned, will not appreciably increase this sum if peak cross sections for excitation to higher levels of a spectroscopic series vary with effective principal quantum number n^* as $(n^*)^{-3}$, where the energies of the series terms vary inversely with $(n^*)^2$. The value $3.84 \times 10^{-17} \text{ cm}^2$ should be greater than the elation cross section of helium in the energy range below 35 eV if excitation to higher levels does not appreciably contribute to the elation cross section. Nee²⁵ has computed the elation cross section of helium for electron energies below 450 eV by summing the measured excitation cross sections of St. John, Miller and Lin, the measured ionization cross section of Smith²⁶ and extrapolated cross sections of S, P, D states with principal quantum numbers $n = 2$ and $n > 6$. The extrapolation is made from the measured cross sections of St. John et. al.,

using the assumption of a power law variation of excitation cross section with principal quantum numbers. Nee computes an elation cross section of $3.2 \times 10^{-17} \text{ cm}^2$ at 35 eV, $3.7 \times 10^{-17} \text{ cm}^2$ at 40 eV, $4.9 \times 10^{-17} \text{ cm}^2$ at 65 eV. The elation cross section rises initially with increasing energy to a maximum value of $5.4 \times 10^{-17} \text{ cm}^2$ at 100 eV and then decreases with further increase of energy. The luminosity decay cross section measured in the 28-35 eV energy range is a factor of 3 to 4 larger than is indicated by these extrapolations and is a factor of 6 larger than the cross section of Maier-Leibnitz and 28 eV.

The common decay of the filtered light at 28 and 35 eV beam energy in helium and at 33 eV in neon appears to indicate that, at these energies in luminosity decay is due to a loss of primary electrons along the beam. These decays appear exponential, as do the observed decays of unfiltered light at energies from 28 to 35 eV and are consistent with this interpretation. Loss of primary electrons either by elastic scatter to the walls with no appreciable component of back-scatter or by inelastic collisions would be consistent with this interpretation.

The decays of the helium lines 4713 Å corresponding to the $4^3\text{S}-2^3\text{P}$ transition and 4922 Å corresponding to $4^1\text{D}-2^1\text{P}$ appear to be exponential at a beam energy of 65 eV and both appear to have the decay cross section $1.1 \times 10^{-16} \text{ cm}^2$. This suggests that the luminosity of these lines is proportional to the primary electron linear density along the beam at 65 eV. Fowler finds a value of $.8 \times 10^{-16} \text{ cm}^2$ at 70 eV by the density saturation method. The 5876 Å line corresponding to the

3^3D-2^3P transition, the 5016 Å line corresponding to 3^1P-2^1S , the 3889 Å line corresponding to 3^3P-2^3S and the 4471 Å line corresponding to 4^3D-2^3P do not show exponential decay at 65 or at 50 eV. At these energies the decay of these lines' intensities is not explained by mechanisms of cascade or elastic scatter. Both of these mechanisms would indicate a common variation of spectral intensity with distance. At 50 and 65 eV energy the elastic electron scatter is more strongly peaked in the forward direction than at 28 or 35 eV.²⁴ The transverse potential across the electron beam is expected to be greater at 65 and 50 eV than at 28 and 35 eV, according to the theory of Frenkel and Bobkovsky. The observed decay of intensity would appear to depend upon either excitation by radiative transport or collisional transfer of excitation or diffusion of long-lived excited species along the beam, at these energies and at pressures of 17 and 19 millitorr. Ostensibly the states feeding carriers of excitation transport would not be appreciably excited at the lower energies.

Focusing of the Beam

Sharp collimation of the beam and lack of a skirt of scattered electrons about the beam would appear to indicate a-priori that transverse elastic scatter is not important in contributing to decay of luminosity. This may however be illusory. It is possible that electrons scattered at small angles to the beam are trapped in the beam while electrons elastically scattered near 90° would be lost from the beam, due to the fact that an electron scattered near 90° would have sufficient energy transverse to the beam to overcome the potential energy well

across the beam, while an electron scattered at a small angle would have insufficient transverse energy to escape. The paths of large angle scattered electrons escaping to the drift tube wall would be short compared to either an elastic or an inelastic mean free collision path. The volume concentration of electrons outside the luminous beam would be much reduced from their concentration inside the beam, thus a skirt of scattered electrons would not necessarily be noticed even through primary electrons were escaping from the beam.

Assuming beam parameters used in the present experiment, the transverse beam potentials calculated from the theory of Frenkel and Bobkovsky are a few tenths of a volt in size. The transverse potential from beam center to drift tube wall ranges from a few tenths of a volt up to three volts. The calculations are presented in Appendix A. The transverse potential is small near gas ionization energy and increases with increasing beam energy at constant beam current and radius. The calculated potentials could hold electrons scattered elastically at small angles to the beam but are not sufficient to hold electrons scattered near 90° to the beam.

The increase of visible light intensity of the beam near beam entrance and concomitant decrease of luminosity decay cross section as beam energy increases, in helium and neon, does not appear consistent with an interpretation that the decay along the beam is due primarily to inelastic collisions. Equations (1.3) and (1.5) indicate that the intensity of light detected near beam entrance would indicate an average trend of the cross sections for excitation to states radiating

lines detected by the photosystem, so that increasing light intensity would be expected to be accompanied by increasing elation cross section, especially since the singlet P levels and ionization cross section are increasing with beam energy at low energies in helium. If a significant portion of the excitation were too long lived, high lying levels which did not radiate visible region spectral transitions would not be an objection to the assumption that inelastic collisions were responsible for luminosity decay through this assumption would be entirely ad hoc.

Luminosity Decay Near Ionization Threshold

In each of the gases studied the luminosity decay cross section increased markedly as the electron beam energy was lowered to within two volts of the gas ionization energy. The observed cross sections became larger than total collision cross sections measured in Ramsauer type experiments. This may well be due to the following modifications of the gas focusing mechanism when primary electron energies are near and above the gas ionization energy. As the primary electron energy is lowered to the ionization energy, the ionization cross section of the gas decreases rapidly and the net space charge along the beam becomes negative, producing a transverse depression rather than increase of potential across the tube, of a few tenths of a volt. This causes a net outward repulsion of the primary electrons from the beam to the wall of the drift tube, leading to a spurious large decay cross section. The beam would not necessarily diverge immediately upon entrance to the drift tube because some positive ions formed in the higher potential

region between the anode and focus ring may be injected into the drift tube with the beam; these ions would however be removed from the beam by collisions with neutral gas atoms and would not be replaced by ions formed by electron-atom impacts at energies near the ionization energy. The observed luminosity dependence on distance would be modified by this mechanism and would not necessarily be exponential near ionization threshold. The observed beam broadening near ionization threshold appears consistent with this picture. The rapid increase of rate of luminosity decay as the beam energy is lowered to ionization threshold is attributed to decrease in positive space charge in the beam, rather than to a property of the electron-atom excitation cross section.

Conclusions

The following conclusions are drawn from the present study. At low energies, 28 to 35 eV, in helium and neon the decay of luminosity along the beam appears to be caused by the loss of primary electrons from the beam, mainly by elastic scatter. The measured cross sections, $1.2 \times 10^{-16} \text{ cm}^2$ in helium and $1.8 \times 10^{-16} \text{ cm}^2$ in neon are large compared to elation cross sections measured electrically by Maier-Leibnitz and McClure. The present measurement does not distinguish whether the large decay is due to elastic scatter loss of primary electrons or is due to inelastic loss, possibly to long lived states not radiating in the visible spectral region. Separate determinations of the transmitted beam current and component scattered to the drift tube wall should have been made in the present experiment and were in fact contemplated. This

could not be carried out with the present apparatus, which was constructed with too great a length. Practical limitations and a misjudgment on the part of the experimenter prevented reconstruction of the experimental apparatus. A unique separation of the elastic and inelastic contributions to the decay was not obtained. This is a serious hindrance to a unique interpretation of the meaning of the cross sections obtained in helium and neon.

At energies above 50 eV, in helium transport of excitation along the beam is important in determining the dependence of intensity with distance.

The theory of Frenkel and Bobkovsky predicts potentials transverse to the beam which are too small to contain electrons elastically scattered at large angles to the beam within the beam, but which may trap electrons scattered at small angles (of order 10^0) to the beam. The theory is in general qualitative accord with observations made on the beam. If elastic scattering is actually responsible for the large component of primary electron loss from the beam it would then follow that the apparently sharply collimated beam, with sharply defined visible boundary, does not bound the trajectories of the primary electrons.

The observed decays in mercury are less rapid than suggested by the mechanism of Duffendack and Koppius, even though elastic scatter as well as inelastic loss could contribute to the decay of luminosity in the present experiment. An elastic cross section as large as $150 \times 10^{-16} \text{ cm}^2$ at a beam energy of 30 eV, would have produced far more

rapid decay than was observed, if only single inelastic impacts of electrons with mercury atoms had in fact occurred. The results of Koppius and Duffendack are in disagreement with the present measurements.

APPENDIX A

Transverse Variation of Potential Between the Electron Beam and Drift

Tube Wall

An upper bound to the transverse potential inside the drift tube may be estimated by the theory of Frenkel and Bobkovsky. The beam luminosity is observed to be within a distance R of the beam center. Assume the beam current to be carried by the primary electrons and to be uniformly distributed over the cross sectional area of the visible beam up to the luminosity radius, R , of the beam. Assume cylindrical symmetry of fields about the beam. Let

R = beam luminosity radius,

cR = inside radius of drift tube;

I = beam current,

E_r = radial component of the electric field at a distance r from the center of the beam,

V_w = potential of beam center relative to the conducting drift tube wall,

E_r^- = radial component of electric field at a distance r from the beam center, due to negative space charge of the primary beam electrons,

v = primary electron speed.

The space charge density due to primary beam electrons is taken as $-I/\pi R^2 v$ for $r < R$ and zero for $r > R$. Gauss' law gives

$$2\pi r E_r^- = \frac{\pi R^2}{\epsilon_0} \left(\frac{-I}{\pi R^2 v} \right), \quad r > R$$

and

$$2\pi r E_r^- = \frac{\pi r^2}{\epsilon_0} \left(\frac{-I}{\pi R^2 v} \right), \quad r < R$$

as the radial component of the electric field due to the primary electron space charge in the beam. Assuming that the total space charge in the beam is ρ/ρ_- times the magnitude of the negative space charge of the primary electrons, then

$$0 \leq |E_r| \leq \left(\frac{\rho}{\rho_-} \right) \frac{I}{2\pi\epsilon_0 v r}, \quad r > R$$

and

$$0 \leq |E_r| \leq \left(\frac{\rho}{\rho_-} \right) \frac{I r}{2\pi\epsilon_0 v R^2}, \quad r < R$$

giving

$$0 \leq |V_w| \leq \int_0^{cR} |E_r| dr \leq \left(\frac{\rho}{\rho_-} \right) \left(\frac{I}{2\pi\epsilon_0 v} \right) \left(\int_0^R \frac{r}{R^2} dr + \int_R^{cR} \frac{dr}{r} \right)$$

or

$$0 \leq |V_w| \leq \frac{I}{4\pi\epsilon_0 v} \left(\frac{\rho}{\rho_-} \right) (1 + 2 \ln c)$$

The potential variation across the luminosity radius of the beam is equal to $\frac{I}{4\pi\epsilon_0 v} \left(\frac{\rho}{\rho_-} \right)$ in the theory of Frenkel and Bobkovsky.

The ratio of charge density to primary electron charge density is computed from equations (3.2) and (3.3). The solutions of (3.2) are given in Table I following, computed transverse potentials are in Table II following.

Table I

Positive Real Solutions of $y^3 + 2y^2 + y - z = 0$

<u>z</u>	<u>y</u>	<u>z</u>	<u>y</u>
.001	.0010	80	3.67
.002	.0020	90	3.84
.010	.0010	100	4.00
.100	.077	120	4.29
.20	.151	140	4.55
.40	.254	160	4.78
.50	.297	180	5.00
.60	.336	200	5.20
.80	.405	300	6.04
1.0	.465 ¹	400	6.72
2.0	.695	500	7.28
3.0	.863	600	7.78
4.0	1.00	700	8.225
5.0	1.116	800	8.629
6.0	1.218	900	9.000
7.0	1.300	1200	9.97
8.0	1.395	1400	10.53
9.0	1.472	1600	11.04
10	1.545	1800	11.51
12	1.676	2000	11.94
14	1.793	2200	12.35
16	1.901	2400	12.73
18	2.00	3000	13.76
20	2.09	3500	14.52
30	2.48	4000	15.21
40	2.79	5000	16.44
50	3.05	5500	16.99
60	3.28	6000	17.51
70	3.48	6500	18.00

Table II

Transverse Potential Variation Across the Electron Beam Calculated from
the Theory of Frenkel and Bobkovsky

Neon:

Assumed Temperature 24°C

Beam Current Ampere x 10 ⁻⁶	Beam Radius Meter x 10 ⁻³	Beam Energy Electron Volts	Transverse Potential Across Beam Volts	Maximum Potential To Wall Volts
<u>I</u>	<u>R</u>	<u>φ</u>	<u>V</u>	<u>V_w</u>
10	.5	24	.031	.16
		26	.046	.34
		28	.068	.52
		30	.086	.66
		32	.10	.82
		36	.13	1.05
		40	.16	1.3
		45	.19	1.5
		50	.21	1.7
14	.5	24	.039	.20
		26	.057	.43
		28	.084	.71
		30	.11	.83
		32	.13	1.0
		36	.17	1.3
		40	.21	1.6
		45	.24	1.9
10	.3	24	.013	.12
		26	.028	.25
		28	.043	.39
		30	.057	.51
		32	.068	.60
		36	.089	.77
		40	.11	.99
		45	.13	1.1
		50	.15	1.3
	75	.21	1.9	

Table II (Continued)

Beam Current Ampere x 10 ⁻⁶	Beam Radius Meter x 10 ⁻³	Beam Energy Electron Volts	Transverse Potential Across Beam Volts	Maximum Potential To Wall Volts
<u>I</u>	<u>R</u>	<u>φ</u>	<u>V</u>	<u>V_w</u>
10	.1	30	.020	.22
	.2		.039	.36
	.3		.057	.51
	.5		.086	.66
	.7		.11	.79
	1.0		.15	.95
	1.2		.17	1.0
	1.5		.20	1.1
2 5 10 15 20 50 100 1000	.3	30	.021	.19
			.037	.33
			.056	.51
			.071	.63
			.083	.75
			.13	1.2
			.19	1.6
			.39	3.4

Helium:

Assumed Pressure 17 Millitorr

Assumed Temperature 24°C

<u>I</u>	<u>R</u>	<u>φ</u>	<u>V</u>	<u>V_w</u>
14	1	25	.0013	.0085
		26	.010	.070
		27	.022	.14
		28	.032	.21
		30	.052	.36
		36	.099	.62
		40	.12	.76
		45	.14	.90
		50	.16	1.04
		65	.19	1.2
70	.20	1.3		

Table II (Continued)

Mercury:

Assumed Pressure 2.1 Millitorr

Assumed Temperature 26.5°C

<u>I</u>	<u>R</u>	<u>φ</u>	<u>V</u>	<u>V_w</u>
3	.5	11.5	.027	.21
		15	.085	.67
		20	.16	1.3
		25	.21	1.65
		30	.23	1.8
3	.1	11.5	.047	.30
		15	.14	.90
		20	.27	1.75
		25	.33	2.1
		30	.37	2.4
3	1.5	11.5	.063	.37
		15	.19	1.0
		20	.35	1.9
		25	.44	2.4
		30	.49	2.7
3	2	11.5	.079	.40
		15	.24	1.2
		20	.42	2.1
		25	.53	2.7
		30	.59	3.0

APPENDIX B

The Equivalent Circuit of the Victoreen VTE-2 Electrometer

The VTE-2 electrometer functions as a zero impedance series connection between the drift tube voltage supply and the drift tube. The voltage developed across the electrometer terminals is zero while the electrometer provides a connection to complete the circuit between cathode, drift tube and drift tube voltage supply. The full supply voltage is across the drift tube and cathode.

The beam current metering circuit is shown in Figure 17. The electrometer is represented by the portion of the circuit between points labelled T_1 and T_2 , which represent the external electrometer terminals. Terminal T_1 leads to the grid of the 5889 electrometer vacuum tube which draws no current. This grid is biased by the input electron beam current, i_b , flowing through a large input resistor, R_{in} , internally connected in the instrument. The voltage $i_b R_{in}$ controls an amplifier providing current to drive the instrument's indicating panel meter. The panel meter is a milliammeter with a 1 milliamperes full scale current. It is connected in series with a resistor R_m between R_{in} and T_2 . The output current of the amplifier, $i_m + i_b$, is proportional to the voltage across R_{in} and in turn to i_b . The amplifier gain is such that $R_{in} i_b = i_m R_m$, where i_m is the meter current so that $R_{in} i_b - i_m R_m = 0$ and the voltage developed across the external terminals T_1 and T_2 vanishes.

The resistors R_{in} and R_m are adjusted separately for each range of the instrument to provide 100 per cent negative voltage feedback.

For the range having 10^{-5} amperes full scale current, for example,
 $R_{in} = 9 \times 10^5$ ohm, $R_m = 9 \times 10^3$ ohm; when $i_b = 10^{-5}$ ampere then
 $i_m = 10^{-3}$ ampere and $i_b R_{in} - i_m R_m = 0$.

During the running of the experiment the chassis of the electrometer is at a potential other than ground potential. To prevent current leakage paths to ground, the electrometer chassis is placed on an insulating baseboard.

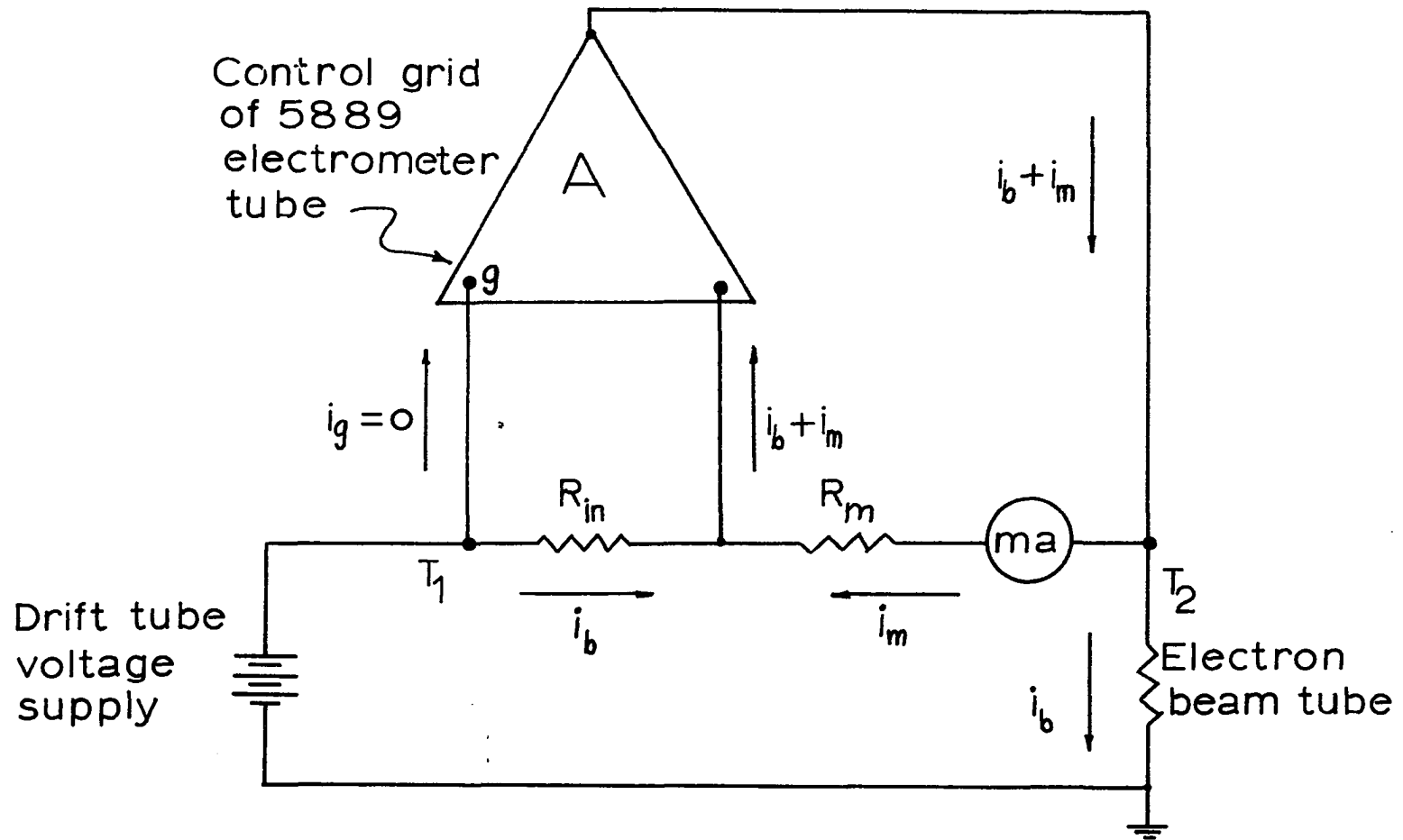


FIGURE 17. EQUIVALENT CIRCUIT OF THE VTE-2 ELECTROMETER.

APPENDIX C

Effect of Beam Width on Detected Signal Amplitude

Luminosity of the electron beam is detected by modulation of the optical signal with a chopping wheel and amplification of the first harmonic of the modulated signal. When no imaging lenses are used in the optical system, the signal entering the tuned amplifier is a trapezoidal wave whose shape is indicated in Figure 18.

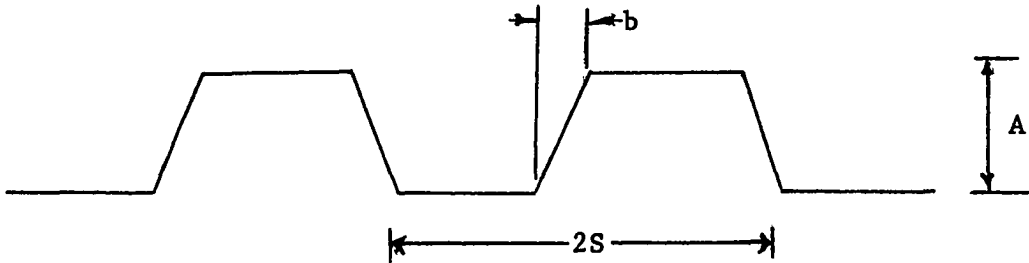


Figure 18

The ratio of the rise time of the signal, b , to the period of the signal, $2S$, is approximately equal to the ratio of electron beam width, $2R$, to twice the chopping wheel's slot width, assuming that the chopping wheel is located near the beam and the width of the teeth of the wheel is equal to the slot width in the wheel. The amplitude of the first harmonic of the trapezoidal wave is,

$$a_1 = \frac{4A}{\pi^2 \left(1 - \frac{S-b}{S}\right)} \cos \left[\left(\frac{\pi}{2}\right) \left(\frac{S-b}{S}\right) \right] .$$

When $b \ll S$,

$$a_1 \approx \frac{2A}{\pi} \left(1 - \frac{\pi^2 b^2}{24 S^2} \right) .$$

Should the beam width double, assuming luminosity of the beam remaining the same, $b \ll S$ and no convergent optics between the beam and the photocathode, the fractional change in the first harmonic is

$$\frac{\Delta a_1}{a_1} = - \frac{\pi^2 b^2}{8 S^2} .$$

For a beam of width 1 millimeter and a chopping wheel slot width of 28 millimeters, $b/S = 1/28$ and the change in amplitude of the first harmonic signal is of order 1/4 per cent, should the radius of the beam double, total beam luminosity being unchanged. This is a small correction.

APPENDIX D

Intensity Versus Distance Along the Beam, Data

Table III

Helium:

P = 19 millitorr

4713 filter

$t_N = 52.6$ seconds

Z = .40 volts x .02

ϕ volts	x cm	S(x) volts x .02	t seconds	I ampere x 10^{-5}
65	3	3.65	57.7	.75
	4	3.57	59.6	.757
	5	3.55	60.5	.762
	6	3.4	58.7	.805
	7	3.75	70.7	.810
	8	3.55	64.6	.845
	9	3.40	69.7	.847
	10	3.50	70.7	.890
	11	3.40	72.6	.905
35	3	3.7	36.7	.747
	4	3.8	40.3	.747
	5	4.1	41.8	.760
	6	3.6	44.7	.802
	7	3.8	52.5	.813
	8	4.0	56.1	.827
	9	3.5	61.3	.855
	10	3.63	59.8	.912
	28	3	3.85	37.5
4		3.8	41.3	.745
5		4.0	49.6	.765
6		3.2	46.5	.775
7		3.65	57.5	.815
8		3.7	59.0	.830
9		3.6	70.7	.857
10		3.6	81.7	.865
11		3.15	91.9	.900

Helium:

P = 19 millitorr

3880 filter

$t_N = 77.3$ seconds

Z = .50 volts x .02

ϕ volts	x cm	S(x) volts x .02	t seconds	I ampere x 10^{-5}
65	3	3.73	40.7	.85
	4	3.6	37.2	.88
	5	3.6	39.7	.875
	6	3.53	41.3	.88
	7	3.38	43.2	.875
	8	3.3	42	.885
	9	3.35	44.9	.893
	10	3.23	45.5	.895
	11	3.0	47.9	.905

Helium:

P = 17 millitorr

4920 filter

$t_N = 30.6$ seconds

Z = .3 volts x .02

ϕ volts	x cm	S(x) volts x .02	t seconds	I ampere x 10^{-5}
65	3	3.85	37.6	.655
	4	3.8	42.4	.635
	6	3.46	40.5	.638
	7	3.7	50.4	.615
	8	4.0	53.1	.615
	10	4.2	69.0	.608
	12	4.0	65.0	.610
50	3	3.8	42.5	.642
	6	3.8	49.2	.635
	7	4.4	63.8	.620
	8	3.4	51.4	.620
	10	3.8	64.4	.608
	12	3.9	76.7	.612

35	3	3.5	47.2	.638
	4	3.6	54.4	.630
	6	3.0	54.7	.630
	7	3.85	78.6	.622
	8	3.6	74.9	.620
	10	3.5	87.5	.608
	12	3.4	88.6	.610
28	3	3.0	60.4	.620
	4	3.3	78.0	.623
	6	3.3	95.2	.630
	7	3.65	108.9	.630
	8	3.1	112.9	.618
	10	2.4	101.0	.610
	12	2.0	99.4	.610

Helium:

P = 19 millitorr

5016 filter

$t_N = 66.3$ seconds

Z = .45 volts x .02

ϕ volts	x cm	S(x) Volts x .05	t seconds	I amperes x 10^{-5}	
65	3	3.80	26.6	.884	
	4	3.80	27.5	.895	
	5	3.95	28.9	.900	
	6	3.90	31.7	.890	
	7	3.80	31.3	.910	
	8	3.60	32.3	.915	
	9	3.52	34.1	.932	
	10	3.30	35.0	.940	
	11	3.0	40.3	.890	
	35	3	2.87	43.3	.890
		4	2.60	45.0	.895
5		1.44	26.6	.895	
6		1.46	30.9	.905	
7		1.52	33.4	.905	
8		1.52	38.4	.920	
9		1.36	40.0	.937	
10		1.52	49.2	.930	
11		1.56	59.3	.946	

28	3	1.26	42.3	.895
	4	1.44	53.4	.895
	5	1.44	61.5	.887
	6	1.28	64.6	.905
	7	1.20	62.4	.907
	8	1.00	68.0	.922
	9	.80	68.4	.925
	10	.76	71.8	.928
	11	.68	72.1	.935

Helium:

P = 17 millitorr

4460 filter

$t_N = 89.9$ seconds

Z = .45 volts x .02

ϕ volts	x cm	S(x) volts x .02	t seconds	I amperes x 10^{-5}
65	3	2.6	74.8	.900
	4	3.3	93.4	.930
	5	3.2	86.0	.930
	6	3.0	83.7	.890
	7	3.2	98.2	.885
	8	3.4	98.6	.905
	10	2.8	95.6	.915
50	3	4.0	106.7	.905
	4	3.25	89.0	.927
	5	3.2	83.0	.930
	6	3.2	87.5	.890
	7	3.6	93.9	.885
	8	3.2	94.5	.905
	10	2.8	93.1	.915
35	3	4.0	83.5	.908
	4	3.9	87.3	.920
	5	3.5	87.9	.925
	6	3.4	81.1	.938
	7	3.4	94.6	.887
	8	3.6	100.1	.900
	10	2.8	92.8	.913
28	3	3.25	80.6	.908
	4	3.1	86.3	.910
	5	3.05	93.7	.930
	6	2.8	99.3	.932
	7	2.8	110.8	.890
	8	2.4	116.8	.895
	10	1.8	100.6	.912

LIST OF REFERENCES

1. O. Koppius, Ph.D. Dissertation, University of Michigan, Ann Arbor (1938).
2. O. Koppius and O. Duffendack, Phys. Rev. 55, 1199 (1939).
3. R. G. Fowler and O. Duffendack, Phys. Rev. 76, 81 (1949).
4. R. G. Fowler, Handbuch der Physik XXII, Springer Verl., Berlin, 1956, pp. 209-253.
5. R. G. Fowler, Ph.D. Dissertation, University of Michigan, Ann Arbor (1949).
6. R. B. Brode, Proc. Roy. Soc. A125, 135 (1929).
7. C. Ramsauer, Ann. Physik 66, 545 (1921).
8. D. E. Golden and H. W. Bandel, Phys. Rev. A138, 14 (1965).
9. H. Maier-Leibnitz, A. Physik 95, 499 (1935).
10. P. J. Chantry, A. V. Phelps and G. J. Schulz, Phys. Rev. 152, 81 (1966).
11. B. T. McClure, unpublished, reported in program of 16th Annual Gaseous Electronics Conference, Pittsburgh, October 1963.
12. L. S. Ornstein and W. Elenbaas, Zeitschr. f. Physik 59, 306 (1930).
13. R. M. St. John, F. L. Miller and C. C. Lin, Phys. Rev. A134, 888 (1964).
14. H. K. Holt and R. Krotkov, Phys. Rev. 144, 82 (1966).
15. L. J. Kieffer and G. H. Dunn, Rev's. Mod. Phys. 38, 1 (1966).
16. L. A. Vainshtein and G. Dolgov, Optics and Spectroscopy 7, 1 (1961).
17. R. G. Fowler, Electrically Energized Shock Tubes, University of Oklahoma Research Institute, Norman, 1963, p. 130.

18. J. B. Johnson, J. O. S. and R. S. I. 6, 701 (1922).
19. J. W. Buchta, J. O. S. and R. S. I. 10, 581 (1925).
20. W. Ende, Phys. Zeitschr. 32, 942 (1931).
21. J. Frenkel and S. Bobkovsky, Physikalische Zeitschr. der Sov-
jetunion 5, 464 (1934).
22. H. Ishii and K. Nakayama, Vacuum Symposium Trans. 8(I), 519 (1961).
23. C. Meineke and G. Reich, Vacuum 13, 579 (1963)
24. H.S.W. Massey and E.H.S. Burhop, Electronic and Ionic Impact
Phenomena, Oxford Univ. Press, Oxford, 1952.
25. T. W. Nee, Master's Thesis, University of Oklahoma, (1965).
26. P. T. Smith, Phys. Rev. 36, 1293 (1930).